タテハチョウの翅における生体内リアルタイム・イメ ージングと鱗粉分布様式の分析

博士（理学）学位論文

Doctoral Dissertation of Science

タテハチョウの翅における生体内リアルタイム・イメージングと鱗粉分布様式の分析

Real-Time *In Vivo* Imaging and Scale Distribution Analysis in Nymphalid Butterfly Wings

２０１６年９月

September 2016

岩田　大生

Masaki Iwata

琉球大学
大学院理工学研究科
海洋環境学専攻

Marine and Environmental Science
Graduate School of Engineering and Science
University of the Ryukyus

指導教員：准教授　大瀧丈二

Supervisor: Associate Prof. Joji Otaki

本論文は、博士(理学)の学位論文として適切であると認める。

論　文　審　査　会

大瀧丈二　印
(主　　査) 大瀧　丈二

中村宗一　印
(副　　査) 中村　宗一

池田譲　印
(副　　査) 池田　譲

Abstract

Butterfly wings are covered with regularly arranged single-colored scales that are formed at the pupal stage. Understanding pupal wing development is therefore crucial to understand wing color pattern formation. Chapter 1 in this thesis describes a new method for observing living pupal wings for a long time in real time, revealing the dynamics of wing development. I successfully applied the real-time *in vivo* imaging technique to pupal hindwings of the blue pansy butterfly, *Junonia orithya*. A transparent sheet of epithelial cells that were not yet regularly arranged was observed immediately after pupation. Bright-field imaging and autofluorescent imaging revealed free-moving hemocytes and tracheal branches of a crinoid-like structure underneath the epithelium. The wing tissue gradually became gray-white, epithelial cells were arranged regularly, and hemocytes disappeared, except in the bordering lacuna, after which scales grew. The dynamics of the epithelial cells and scale growth were also confirmed by fluorescent imaging. Fluorescent *in vivo* staining further revealed that these cells harbored many mitochondria at the surface of the epithelium. Organizing centers for the border symmetry system were apparent immediately after pupation, exhibiting a relatively dark optical character following treatment with fluorescent dyes, as well as in autofluorescent images. The wing tissue exhibited slow and low-frequency contraction pulses with a cycle of approximately 10 to 20 minutes, mainly occurring at 2 to 3 days postpupation. The pulses gradually became slower and weaker and eventually stopped. The wing tissue area became larger after contraction, which also coincided with an increase in the autofluorescence intensity that might have been caused by scale growth. Examination of the pattern of color development revealed that the black pigment was first deposited in patches in the central areas of an eyespot black ring and a parafocal element. These results of live *in vivo* imaging that covered wide wing area for a long time can serve as a foundation for studying the cellular dynamics of living wing tissues in butterflies.

Chapter 2 in this thesis describes spatial patterns of scale size in relation to color pattern elements in butterfly wings. A reasonable level of correspondence between the

color pattern element and scale size in *Junonia orithya* and *Junonia oenone* have indicated that a single morphogenic signal contain positional information for both color and size, but this color–size relationship has not been demonstrated in other species of the family Nymphalidae. For this reason, we investigated the distribution patterns of scale size in relation to color pattern elements on the hindwings of the peacock pansy butterfly *Junonia almana*, together with other nymphalid butterflies, *Vanessa indica* and *Danaus chrysippus*. In these species, we observed a general decrease in scale size from the basal to the distal areas, although the size gradient was small in *D. chrysippus*. Scales of dark color in color pattern elements, including eyespot black rings, parafocal elements, and submarginal bands, were larger than those of their surroundings. Within an eyespot, the largest scales were found at the focal white area, although there were exceptional cases. Similarly, ectopic eyespots that were induced by physical damage on the *J. almana* background area had larger scales than in the surrounding area. These results are consistent with the previous finding that scale color and size coordinate to form color pattern elements. We propose a ploidy hypothesis to explain the color–size relationship in which the putative morphogenic signal induces the polyploidization (genome amplification) of immature scale cells and that the degrees of ploidy (gene dosage) determine scale color and scale size simultaneously in butterfly wings.

Finally, Chapter 3 in this thesis presents comparative morphological analysis between an eyespot and a focus in butterfly wing color patterns. A typical eyespot (such as that of *Bicyclus anynana*) has a few concentric rings of dark and light colors and a white spot (called a focus) at the center. The prospective eyespot center during the early pupal stage is known to act as an organizing center. It has often been assumed, according to gradient models for positional information, that a white spot in adult wings corresponds to an organizing center and that the size of the white spot indicates how active that organizing center was. However, there is no supporting evidence for these assumptions. To evaluate the feasibility of these assumptions in nymphalid butterflies, we studied the unique color patterns of *Calisto tasajera* (Nymphalidae, Satyrinae), which have not been analyzed before in the literature. In the anterior forewing, one white spot was located at the center of

an eyespot, but another white spot associated with either no or only a small eyespot was present in the adjacent compartment. The anterior hindwing contained two adjacent white spots not associated with eyespots, one of which showed a sparse pattern. The posterior hindwing contained two adjacent pear-shaped eyespots, and the white spots were located at the proximal side or even outside the eyespot bodies (defined as all the eyespot portions except a white focal area). The successive white spots within a single compartment along the midline in the posterior hindwing showed a possible trajectory of a positional determination process for the white spots. Several cases of focus-less eyespots in other nymphalid butterflies were also presented. These results argue for the uncoupling of white spots from eyespot bodies, suggesting that an eyespot organizing center does not necessarily differentiate into a white spot and that a prospective white spot does not necessarily signify organizing activity for an eyespot. Incorporation of these results in future models for butterfly wing color pattern formation is encouraged.

概要

蝶の鱗粉は一枚につき一色を呈しており、それらが規則的に配列されることによって、翅の色模様はモザイク画のように彩られている。こうした色模様形成は蛹の時期に行われている。そのため蝶の翅の色模様形成の仕組みを解明するには、蛹の中で行われている翅組織の発生過程の徹底的な観察と、それによる理解が必要である。この博士論文の第 1 章では、生きた蛹の翅組織の発生過程をリアルタイムで長期間観察するための新しい手法を報告するとともに、生きた翅組織の発生動態についても述べていく。第 1 章の実験では、アオタテハモドキ *Junonia orithya*（鱗翅目、タテハチョウ科）と呼ばれる蝶の蛹を用いた *in vivo* でのリアルタイム・イメージングに成功した。蛹化後 0 時間では、翅の表皮細胞は規則的に並んでおらず、このような表皮細胞によって構成されている翅組織は透明であった。明視野と自家蛍光でのイメージングによって、血球とウミユリのような形状をした蛹気管小枝が自由に動く様子が翅表皮の下で観察された。蛹化後 20–23 時間では、翅組織が徐々に白くなりはじめると同時に、翅組織を構成する表皮細胞が規則的に並びはじめた。またこの時期には、翅の縁に存在するラクナ(bordering lacuna)を除き、翅全体において血球細胞の消失も観察された。そしてこれらの現象が観察された後に、鱗粉の成長が観察された。このような鱗粉細胞の動態と鱗粉の成長は、自家蛍光イメージングによっても観察された。さらに、*in vivo* 蛍光染色によって、これらの表皮細胞の表面付近にミトコンドリアが数多く存在することが判明した。自家蛍光でのイメージングの時と同様に、染色色素を用いた際のイメージングでも、辺縁部対称系（border symmetry system）の形成中心（眼状紋の焦点出現予定地）が他の部位と比べて比較的暗くなるという特徴が得られた。蛹化後 2–3 日の間、ゆっくりとした拍動が翅において観察された。この拍動が一回行われるのには 10–20 分ほどを要し、一回の拍動ごとに翅組織は大きくなっていったが、拍動は時間とともに次第に弱くなっていき最終的には停止した。この拍動と翅の拡大が起きている時期と同じ時期に、自家蛍光の強度が増大しており、これは鱗粉の成長によって引き起こされていたものと考えられる。これらの実験に加え、翅面上に色模様が現れるパターンを調査した結果、眼状紋の黒いリングとパラフォーカルエレメントの色素（黒）の沈着は、リン

グとエレメントの中心部からはじまっており、その沈着の仕方はパッチ状であった。翅全体におけるこれらの生体内長期ライブイメージングの結果より、生きた蝶の翅組織における細胞動態の研究をするための基盤を、本研究によって構築できたといえる。

さらに、この博士論文の第２章においては、蝶の翅の色模様に関連した鱗粉サイズの空間分布様式について述べる。以前の実験でアオタテハモドキ *J. orithya* とアフリカタテハモドキ *Junonia oenone* の後翅において、翅面上の色模様要素と鱗粉サイズとの間に明らかな相関関係が見られており、この結果は単一のモルフォゲンが鱗粉の色とサイズの両方に影響を与える可能性を示していたが、この現象がタテハチョウ科の他の種において成り立つかどうかは不明であった。こうした理由により、前回の実験とは異なる３種類のタテハチョウ科（タテハモドキ *Junonia almana*、アカタテハ *Vanessa indica*、カバマダラ *Danaus chrysippus*）の後翅を用いて、その翅面上の鱗粉サイズと色模様との間に相関関係がみられるかどうかについて調べた。これら３種において、基部から外縁に向けての鱗粉サイズの減少が全体的な傾向として得られた。眼状紋の黒色リング、パラフォーカルエレメント、サブマージナルバンドといった色模様要素にみられる黒色鱗粉のサイズは、周りの鱗粉よりも大きかった。眼状紋の鱗粉サイズにおいては、わずかな例外はあったが、焦点（眼状紋の中心にある白色領域）を構成する鱗粉のサイズは周りの鱗粉よりも大きかった。同様に、タテハモドキの翅において、色模様要素のない領域（背景色）に物理的な損傷を与え、人為的に翅面上に生み出した異所的眼状紋の中心の鱗粉も周りの鱗粉よりも大きかった。これらの結果は、アオタテハモドキにおいて得られていた鱗粉の色模様とサイズに関するこれまでの研究結果と一致する。そこで、鱗粉の色とサイズに関するこれらの相関関係を説明するために、推定上のモルフォゲン・シグナルによって、倍数化（ゲノムの増加）が未成熟の鱗粉細胞によって引き起こされ、この倍数化（ゲノムの量）の程度によって鱗粉の色とサイズが決定されるという倍数化仮説を提案した。

最後に、この博士論文の第３章では、蝶の翅の色模様のうち、眼状紋と焦点との比較形態学的研究について述べる。典型的な眼状紋（ジャノメチョウの一種である *Bicyclus anynana* のような眼状紋）は、３つほどの同心円状のリング（明るいリング

と暗いリング）とその円の中心にある白点（焦点）で構成されている。また、将来的に眼状紋の中心となる部位が形成体（オーガナイザー）として、蛹期間の初期に働いていることが知られている。さらに、位置情報を与えるとされる濃度勾配モデルによると、成虫の翅の焦点は眼状紋の形成体に対応していると考えられているとともに、焦点のサイズが形成体の活性の程度を示しているとも考えられている。しかし、これらの仮説を支持する証拠はない。そこで、これらの仮説がどれほど正しいかをタテハチョウ科のチョウで評価するため、これまで調査されてこなかった *Calisto tasajera* (Nymphalidae, Satyrinae)の色模様について、形態学的比較に基づいて調査を行った。前翅前縁において、ある焦点は眼状紋の中心に位置していたが、別の焦点（小さな眼状紋の形成にのみに関連のある焦点、あるいは眼状紋の形成とは関連のない焦点）は隣の翅室に存在していた。後翅前縁では、隣接する２つの焦点は眼状紋形成とは関係なく存在し、この２つの焦点のうち１つは、まばらな模様を示していた。後翅後縁には、隣接する２つの眼状紋（梨のような形の眼状紋）があり、それらの焦点は基部側に位置しているだけでなく、眼状紋本体（眼状紋とは区別して、焦点を除く眼状紋の領域をこう定義する）の外側に位置しているものさえ存在した。また、この翅室内において正中線に沿って連続して続く焦点も見られ、それは、焦点の位置決定過程の軌跡を表している可能性を示していた。加えて、この実験では、焦点のない眼状紋の事例をタテハチョウ科の他の種を用いて紹介した。これらの結果に基づいて、焦点と眼状紋本体との関係性（焦点が眼状紋本体から独立している可能性）について議論した。その結果、眼状紋の中心に位置する形成体は必ずしも焦点に分化するわけではないこと、また、将来的に焦点になる部位が、必ずしも眼状紋の形成体の活性レベルを意味しているわけではないことが示された。言い換えると、焦点が眼状紋本体から独立的あるいは半独立的に形成される可能性が示された。

Author's publication list

Iwata, M., Ohno, Y., Otaki, J.M., 2014. **Real-time *in vivo* imaging of butterfly wing development: revealing the cellular dynamics of the pupal wing tissue.** PLoS ONE 9, e89500. DOI: 10.1371/journal.pone.0089500.

Iwata, M., Otaki, J.M., 2016. **Spatial patterns of correlated scale size and scale color in relation to color pattern elements in butterfly wings.** J. Insect Physiol. 85, 32-45. DOI: 10.1016/j.jinsphys.2015.11.013.

Iwata, M., Otaki, J.M., 2016. **Focusing on butterfly eyespot focus: uncoupling of white spots from eyespot bodies in nymphalid butterflies.** SpringerPlus 5, 1287. DOI: 10.1186/s40064-016-2969-8.

Acknowledgements

First of all, I would like to thank my supervisor, Associate Professor J.M. Otaki, for supporting my research and helping me to write my thesis. I would also like to thank my committee members, Professor S. Nakamura and Professor Y. Ikeda for valuable suggestions and informative comments. Many thanks go to J.M. Otaki, S. Nakamura, M. Tsutsumi, K. Motomura, Y. Ohno, M. Iwasaki, A. Hiyama, B. Dhungel, W. Taira, K. Nakajima, and other members of the BCPH Unit of Molecular Physiology for technical assistance and discussion. Especially, I would like to thank Y. Ohno for the autofluorescent imaging and the fluorescent staining experiment in Chapter 1, M. Iwasaki for the damage experiment in Chapter 2, and N. Yamada, H. Takizawa and J.M. Otaki for specimens used in Chapter 3. I am also very thankful to the staff of Keyence Corporation, Osaka, Japan, for helping us to obtain bright-field images with the VHX-1000 and VHX-2000 digital microscopes, and the staff of Hamamatsu Photonics, Hamamatsu, Japan, for helping us to obtain autofluorescent images and fluorescent images using the real-time confocal microscope.

Table of Contents

Chapter 3

General discussion

List of Figures and Tables

General Introduction

General Introduction

In a process of morphogenesis and pattern formation of complex multicellular organisms, immature cells are thought to obtain positional information to determine their own developmental fate. Wolpert (1969) proposed that a substance called morphogen that is secreted from particular source cells forms a concentration gradient toward the periphery in target tissues. Cell-fate determination is achieved based on both morphogen concentration at a given cell and thresholds for morphogen concentration that are inherently set in cells. That is, according to the morphogen concentration, cells recognize their own positions and differentiate into specific cell types. A localized source for morphogens was discovered based on transplantation experiments with salamander eggs (Spemann and Mangold, 1924) and known as the Spemann organizer (the Spemann-Mangold organizer).

A spatial patterning mechanism based on morphogens and organizers has attracted many biologists (especially evolutionists and embryologists), chemists and mathematicians, and has been studied using various animals such as mice (Satre and Kochhar, 1989; Towers and Tickle, 2009; Litingtung et al., 2002), frogs (*Xenopus*) (Kiecker and Niehrs, 2001; Kim et al., 2011; Smith et al., 2008; Watabe et al., 1995), fruit flies (*Drosophila*) (Driever and Nüsslein-Volhard, 1988a,b; Ephrussi and St Johnston, 2004; Nüsslein-Volhard and Wieschaus, 1980; Frohnhöfer and Nüsslein-Volhard, 1986; Nüsslein-Volhard et al., 1987) and butterflies (Nijhout, 1980, 1985, 1991). In butterflies, both wing physical damage experiments and transplantation experiments in pupae of *Junonia coenia* have supported that an organizer for eye-like patterns called an eyespot is located at the center (focus) of an eyespot on butterfly wings (Nijhout, 1980, 1985, 1991). Butterfly wing color patterns are organized as a two-dimensional pattern that makes their developmental dissection much simpler than three-dimensional morphological patterns and structures such as the limbs of terapods

and the appendages of insects (Nijhout, 1991). In addition, a *Hox* gene, *Distal-less* (*Dll*), which is best known to be involved in development of appendage in insects (Cohen et al., 1989; Panganiban et al. 1994), is expressed at the center of eyespots in butterflies such as *J. coenia* (Carroll et al., 1994) and *Bicyclus anynana* (Monteiro et al., 2006; Shirai et al., 2012). The *Dll* expression level during the pupal stage is correlated with the size of eyespots between seasonal phenotypes in the *B. anynana* butterflies (Brakefield et al., 1996**)**. Regardless of seasonal phenotypes, the level of *Dll* expression during the pupal stage contributes to eyespot size determination in *Juonia orithya* females (Adhikari and Otaki, 2016) and in *B. anyana* (Monteiro et al., 2013). In addition, misexpression of *Dll* protein fused with green fluorescent protein (GFP) has induced ectopic elemental color patterns (Dhungel et al., 2016).

Surgical experiments and physiological experiments have demonstrated that the wing color patterns are organized during the early pupal stages (Nijhout, 1980, 1985, 1991; Otaki, 2008). However, morphogens and their organizers for the color pattern formation are not well understood, and no one knows chemical identity of morphogens. Because morphogens for eyespot formation may be proteins such as Wingless and TGF-β ligands (Monteiro et al., 2006), it is possible to observe the dynamics of such molecules that are fused with GFP during the critical period of color pattern formation. To this end, it is necessary to establish the method for observing pupal wing development for a long time in the details. Thus, in Chapter 1, I report a technique to take real-time *in vivo* images of wing tissue development over time in the *J. orithya* pupae.

On the other hand, Kusaba and Otaki (2009) has shown the correlation between scale size and scale color in adult butterfly wings of *J. orithya* (Nymphalinae) and *Junonia oenone* (Nymphalinae). This size information might be useful to discover an unknown organizer and understand the feature of signals for butterfly wing color pattern formation. In Chapter 2, we report the scale measurement experiment using three species of nymphalid butterflies, *Junonia almana* (Nymphalinae), *Vanessa indica*

(Nymphalinae), and *Danaus chrysippus* (Danainae) to examine whether the size-color correlation is applicable to other species of Nymphalidae.

Previous studies on formation of scales in Lepidopteran wings have shown the following two points. First, undifferentiated epithelial cells become differentiated into scale-building cells during the pupal stage in the flour moth *Ephestia kühniella* (Stossberg, 1938; Henke and Pohley, 1952). Second, the larger a scale is, the larger the number of ploidy in scale-building cells is (Henke, 1946; Henke and Pohley, 1952). Interestingly, in *J. orithya*, focal scales in the eyespot centers, which are believed to be an organizing center for eyespot formation (Nijhout, 1980, 1985, 1991), are much larger than their surrounding scales (Kusaba and Otaki, 2009). Although these results indicate a possibility that scale-building cells that function as an organizer for eyespot formation are large polyploid cells, there is no direct evidence. Examination of spatial relationship between nuclear size in scale-building cells and color pattern will lead us to an understanding of the mechanisms of butterfly wing color pattern formation in depth. Chapter 1 and 2 of my thesis are an attempt toward addressing such a relationship. To explain this relationship, we propose the ploidy (gene dosage or genome amplification) hypothesis at the end of Chapter 2.

In addiotion to these experiments, to test an assumption that a white focal area (called a focus or a white spot) in adult butterfly wings corresponds to an organizing center for an eyespot (Nijhout, 1980, 1991; French and Brakefield, 1995; Brakefield et al., 1996), and an inference that the size of a white focal area indicates the activity levels of an organizing center for eyespot during the pupal stage (Beldade and Brakefield, 2002), in Chapter 3, we examined the relationship between an eyespot body (defined as all the eyespot portions except a white focal area) and a white focal area in butterfly wing color patterns using several Nymphalidae butterflies.

References

Adhikari, K., and Otaki J.M., 2016. A Single-Wing Removal Method to Assess Correspondence Between Gene Expression and Phenotype in Butterflies: The Case of *Distal-less.* Zool. Sci. 33, 13-20.

Beldade, P., Brakefield, P.M., 2002. The genetics and evo-devo of butterfly wing patterns. Nat. Rev. Genet. 3, 442-452.

Brakefield, P.M., Gates, J., Keys, D., Kesbeke, F., Wijngaarden, P.J., Monteiro, A., French, V., Carroll, S.B., 1996. Development, plasticity and evolution of butterfly eyespot patterns. Nature 384, 236–242.

Carroll, S.B., Gates, J., Keys, D.N., Paddock, S.W., Panganiban, G.E., et al., 1994. Pattern formation and eyespot determination in butterfly wings. Science 265, 109–114.

Cohen, S.M., Brönner, G., Küttner, F., Jürgens, G., Jäckle, H., 1989. *Distal-less* encodes a homoeodomain protein required for limb development in *Drosophila*. Nature 338, 432–434.

Dhungel, B., Ohno, Y., Matayoshi, R., Iwasaki, M., Taira, W., Adhikari, K., Grung, R., Otaki, J.M., 2016. *Distal-less* induces elemental color patterns in Junonia butterfly wings. Zool. Lett. 2, 4.

Driever, W., Nüsslein-Volhard C., 1988a. The *bicoid* protein determines position in the *Drosophila* embryo in a concentration-dependent manner. Cell 54, 95–104.

Driever, W., Nüsslein-Volhard, C., 1988b. A gradient of *bicoid* protein in *Drosophila* embryos. Cell 54, 83–93.

Ephrussi, A., St Johnston, D., 2004. Seeing is believing: The Bicoid morphogen gradient matures. Cell 116, 143–152.

French, V., Brakefield, P.M., 1995. Eyespot development on butterfly wings: the focal signal. Dev. Biol. 168, 112-123.

Frohnhöfer, H.G., Nüsslein-Volhard, C., 1986. Organisation of the anterior pattern in the *Drosophila* embryo by the maternal gene *bicoid*. Nature 324, 120–125.

Henke, K., 1946. Über die verschiedenen Zellteilungsvorgange in der Entwicklung des beschuppten Flügelepithels der Mehlmotte *Ephestia kühniella* Z. Biol. Zentralbl. 65, 120–135. (In German).

Henke, K., Pohley, H.J., 1952. Differentielle Zellteilungen und Polyploedie bei der Schuppenbildung der Mehlmotte *Ephestia kühniella*. Z. Z. Naturforsch. B 7, 65–79. (In German).

Kiecker, C., Niehrs, C., 2001. A morphogen gradient of Wnt/β-catenin signalling regulates anteroposterior neural patterning in *Xenopus*. Dev. 128, 4189-4201.

Kim Y., Joshi S. D., Messner W.C., LeDuc P. R., Davidson L.A., 2011. Detection of dynamic spatiotemporal response to periodic chemical stimulation in a *Xenopus* embryonic tissue. PloS ONE. 6, e14624.

Kusaba, K., Otaki, J.M., 2009. Positional dependence of scale size and shape in butterfly wings: wing-wide phenotypic coordination of color-pattern elements and background. J. Insect. Physiol. 55, 174–182.

Litingtung, Y., Dahn, R.D., Li, Y., Fallon, J.F., Chiang, C., 2002. Shh and Gli3 are dispensable for limb skeleton formation but regulate digit number and identity. Nature 418, 979-983.

Monteiro, A., Glaser, G., Stockslager, S., Glansdrop, N., Ramos, D., 2006. Comparative insights into questions of lepidopteran wing pattern homology. BMC. Dev. Biol. 6, 52.

Monteiro, A., Chen, B., Ramos, D.M., Oliver, J.C., Tong, X., Guo, M., Wang, W.K., Fazzino, L., Kamal, F., 2013. *Distal-Less* regulates eyespot patterns and melanization in *Bicyclus* butterflies. J. Exp. Zool. 320B: 321–331.

Nijhout, H.F., 1980. Pattern formation on lepidopteran wings: determination of an eyespot. Dev. Biol. 80, 267–274.

Nijhout, H.F., 1985. Cautery-induced colour patterns in *Precis coenia* (Lepidoptera: Nymphalidae). J. Embryol. Exp. Morphol. 86, 191–203.

Nijhout, H.F., 1991. The Development and Evolution of Butterfly Wing Patterns. Smithsonian Institution Press, Washington, DC.

Nüsslein-Volhard, C., Wieschaus, E., 1980. Mutations affecting segment number and polarity in *Drosophila*. Nature 287, 795–801.

Nüsslein-Volhard, C., Frohnhöfer, H.G., Lehmann, R., 1987. Determination of anteroposterior polarity in *Drosophila*. Science 238, 1675–1681.

Otaki, J.M., 2008. Physiologically induced color-pattern changes in butterfly wings: mechanistic and evolutionary implications. J. Insect Physiol. 55, 174–182.

Panganiban, G., Nagy, L., Carroll, S.B., 1994. The role of the *Distal-less* gene in the development and evolution of insect limbs. Curr. Biol. 4, 671–675.

Satre, M.A., Kochhar, D.M., 1989. Elevations in the endogenous levels of the putative morphogen retinoic acid in embryonic mouse limb-buds associated with limb dysmorphogenesis. Dev. Biol. 133, 529-536.

Shirai, L.T., Saenko, S.V., Keller, R.A., Jerónimo, M.A., Brakefield, P.M., Descimon, H., Wahlberg, N., Beldade, P., 2012. Evolutionary history of the recruitment of conserved developmental genes in association to the formation and diversification of a novel trait. BMC. Evol. Biol. 12, 21.

Smith, J.C., Hagemann, A., Saka, Y., Williams, P.H., 2008. Understanding how morphogens work. Philos. Trans. Roy. Soc. Lond. 363, 1387–1392.

Spemann, H., Mangold, H., 1924. Über Induktion von Embryonalanlagen durch, Implantation artfremder Organisatoren. Arch. mikrosk. Anat. EntwMech. 100, 599–638.

Stossberg, M., 1938. Die Zellvorgänge bei der Entwicklung der Flügelschuppen von *Ephestia kühniella* Z. Z. Morph. und Ökol.Tiere 34, 173-206. (In German).

Towers, M., Tickle, C., 2009. Growing models of vertebrate limb development. Dev. 136, 179-190.

Watabe, T., Kim, S., Candia, A., Rothbacher, U., Hashimoto, C., Inoue, K., Cho, K.W., 1995. Molecular mechanisms of Spemann's organizer formation: conserved growth factor synergy between *Xenopus* and mouse. Genes Dev. 9, 3038–3050.

Wolpert, L., 1969. Positional information and the spatial pattern of cellular differentiation. J. Theor. Biol. 25, 1–47.

Chapter 1: Real-time *in vivo* imaging of butterfly wing

1.1. Introduction

Introduction

The spectacular diversity of butterfly wing color patterns has fascinated many evolutionary biologists throughout the history of biological research, but it was only after the seminal work of Nijhout (1991) that biologists began to discuss evolutionary developmental aspects of butterfly wing color pattern formation. Despite their diversity, the color patterns of nymphalid butterfly wings appear to be constructed according to the nymphalid groundplan (Nijhout, 1991, 2001; Otaki, 2012a), which is a general rule underlying color pattern development and evolution. The nymphalid groundplan is the scheme in which color pattern elements are placed in a plain background. The groundplan is basically composed of three major symmetry systems (the basal, central, and border symmetry systems) and two peripheral systems (the wing root band system and the marginal band system) (Otaki, 2012a). At least the major symmetry systems are composed of a core element and a pair of paracore elements that surround the core (Otaki, 2012a). In addition to these color pattern elements, there are venous stripes, intervenous striples, ripple patterns, and background coloration, which are not understood within the scheme of the nymphalid groundplan (Nijhout, 1991).

These various color patterns are composed of the scales that cover the surface of butterfly wings. Each scale is produced by a single scale cell and exhibits a single distinct color (Ghiradella, 1998; Kristensen and Simonsen, 2003; Nijhout, 1991) which may be dubbed the “one cell, one scale, and one color” rule. Furthermore, scales are arranged regularly in anteroposterior rows, in parallel to one another and to the outer wing margin (Kristensen and Simonsen, 2003; Nijhout, 1991; Yoshida, 1988; Yoshida and Aoki, 1989a; Yoshida et al., 1983). Two types of scales usually alternate in a row:

cover and ground scales (Kristensen and Simonsen, 2003; Nijhout, 1991; Yoshida, 1988; Yoshida and Aoki, 1989a; Yoshida et al., 1983). The arrangement of rows occurs at the pupal stage, and it does not appear to contribute to the determination of color pattern elements (Kristensen and Simonsen, 2003; Yoshida, 1988; Yoshida and Aoki, 1989a; Yoshida et al., 1983).

Among the color pattern elements that constitute the overall wing color pattern, the most conspicuous are likely eyespots, which belong to the border symmetry system. A species of butterfly that has been used to study eyespot formation, especially in early research, is the American buckeye butterfly, *Junonia coenia* (Nijhout, 1980a,b, 1985), which is distributed in North America. Since the 1990s, many studies on the development of butterfly wing color patterns have focused on the eyespot structure of the African satyrine butterfly, *Bicyclus anynana* (Brakefield and French, 1995; French and Brakefield, 1992; Saenko et al., 2010). Additionally, we have been using several species of *Junonia* and other butterflies to study the mechanistic basis of color pattern diversity, such as the blue pansy, *J. orithya* (Dhungel and Otaki; 2013a; Mahdi et al., 2010; Otaki et al., 2005a), and the peacock pansy, *J. almana* (Otaki, 2007, 2011a, 2012b), both of which are distributed widely in Southeast Asia, including on the Ryukyu Archipelago of Japan. These species display large eyespots on their wings, which facilitate color pattern analysis.

Surgical studies have demonstrated that the prospective eyespot focus functions as an organizing center for an eyespot (Nijhout, 1991; Nijhout, 1980b; Nijhout, 1985; French and Brakefield, 1992; Otaki, 2011a; Otaki et al., 2005b). It is likely that the same organizing center is responsible for the entire border symmetry system, including an eyespot (i.e., the core element) and parafocal elements (i.e., paracore elements), despite their partial independence (Otaki, 2009, 2011b, 2012a; Otaki et al., 2005b; Dhungel and Otaki, 2009). Because of the developmental function of the prospective eyespot focus as an organizing center, many studies in butterflies have focused on putative molecular mechanisms underlying eyespot development.

These studies have identified several candidate genes, such as *Distal-less*, that may be responsible for color pattern formation (Brakefield et al., 1996; Beldade et al., 2002; Carroll et al., 1994; Monteiro et al., 2006, 2013; Reed and Serfas, 2004; Shirai et al., 2012). Although sequence variation in *Distal-less* is reported to be correlated with size variation in eyespots (Beldade et al., 2002), the functional status of *Distal-less* is not yet fully understood due to a lack of sufficient molecular evidence of its organizing activities despite a considerable effort to produce transgenic butterflies (Monteiro et al., 2013).

In contrast to these molecular approaches, we have been studying morphological and physiological aspects of butterfly wing development and color pattern determination (Otaki, 2008; Otaki and Yamamoto, 2004; Hiyama et al., 2012). We have proposed that in addition to the organizing centers for eyespots (i.e., the border symmetry system), organizing centers for other symmetry systems also exist on the surface of a developing wing (Otaki et al., 2005b). Interestingly, it appears that these organizing centers can be identified based on the presence of pupal cuticle spots in many nymphalid butterflies (Otaki et al., 2005b). For example, one of the groups of pupal cuticle spots, referred to as edge spots, are found along the outer margin (Otaki, 2012a; Otaki et al., 2005b). The edge-spot cells may function as organizing centers for the marginal band system (Otaki, 2012a; Otaki et al., 2005b).

To understand the physiological aspects of color pattern development at the cellular and tissue levels, basic descriptive records of normally developing pupal wings are necessary as a foundation for interpreting any experimental data. We know how the development of butterfly wings occurs in the larval and pupal stages based on morphological and histochemical studies (Kühn, 1954; Nijhout, 1991; Kuntze, 1935). First, in larvae, epidermal cells form the wing imaginal discs, which then form a sac-like structure consisting of a single cellular sheet (Kuntze, 1935). This sac-like structure is flattened but leaves gaps as lacunae. Tracheae then elongate into lacunae. At the time of pupation, the larval wings (i.e., the wing imaginal discs) expand

extensively, and the pupal wings already display the primary tracheal system that later merges with the wing veins. At this point, although the sheet of epithelial cells consists of a monolayer, they are not arranged regularly. These epithelial cells undergo cell division, forming one daughter precursor that gives rise to scale and socket cells and another daughter cell that undergoes programmed cell death (Greenstein, 1972; Kühn, 1954). The precursor cells then undergo another cell division, horizontally in this case, producing scale and socket cells (Greenstein, 1972; Kühn, 1954). At this point, the scale and socket cells are arranged regularly in rows (Yoshida, 1988; Yoshida and Aoki, 1989a; Yoshida et al., 1983). Scale cells are likely organized via Notch-mediated lateral inhibition process, similarly to bristles in other insects (Galant et al., 1998; Reed, 2004). The wing boundary is determined by the bordering lacuna, and the peripheral tissue outside the bordering lacuna degenerates (Dohrmann and Nijhout, 1990; Kodama et al., 1995; Macdonald et al., 2010; Süffert, 1929; Yoshida and Aoki, 1989b).

While we can reconstruct these developmental sequences, the previous studies on lepidopteran wings were performed using fixed tissues at given time points. Partly to compensate for this approach, we have previously analyzed the scale number, size, shape, and arrangement in adult wings to infer developmental changes that might have occurred at the pupal stage (Dhungel and Otaki, 2013b; Kusaba and Otaki, 2009). Although these morphometric studies are important, it is desirable to directly record the dynamic cellular changes occurring in the rapidly developing wing tissues *in vivo*. For this purpose, we previously developed a simple surgical (but non-invasive) method to expose a developing hindwing inside a pupal case to allow real-time *in vivo* observations to be made (Kusaba and Otaki, 2009). We reported the developmental sequences of single individuals by presenting images obtained at approximately one-hour intervals (Kusaba and Otaki, 2009).

The present study is a systems biology approach to the butterfly wing system, which aims at the comprehensive description of components and dynamics of the

system. Here, to understand the pupal wings as a biological system, we employed state-of-the-art digital imaging technologies to record real-time *in vivo* images of wing tissue development over time in pupae using *J. orithya*. We employed three different imaging systems, depending on the magnification and optical conditions: a digital single-lens reflex camera system to obtain macroscopic whole-wing images, a high-resolution high-depth digital microscope system to record bright-field images at the compartmental level, and a real-time confocal microscope system for fluorescent imaging at the compartmental and cellular levels. These methods allowed us to observe various characteristics of developing pupal wings in real-time *in vivo* images. In addition to confirming previously known phenomena, we discovered dynamic movements of the wing system that could not be inferred from fixed specimens. Our results build a foundation for in-depth analyses of the developing wing systems in butterflies.

1.2. Materials and methods

Butterflies

The blue pansy butterfly, *J. orithya* (Lepidoptera, Nymphalidae, Nymphalinae), was used throughout this study. Adult females were caught on Okinawa-jima Island and Ishigaki-jima Island, from which eggs were collected. Additionally, larvae were collected from fields. Larvae were reared at ambient temperatures, approximately 27 °C, using a natural host plant, *Plantago major* or *P. asiatica*.

Operation for Hindwing Exposure

The surgical method that exposes the surfaces of the dorsal hindwing and the ventral forewing for real-time observations was performed as follows. Immediately after pupation (within 1 h after pupation), a pupae was laid down with wing side up, and the tip of a right or left pupal forewing was picked up using forceps. The right or left pupal forewing was then lifted up slowly from the wing tip to the wing base. It is important not to lift up both the forewing and hindwing together and not to physically damage the wings. The exposed hindwing and forewing surfaces were immediately covered with a sheet of transparent plastic wrap or with a piece of cover glass to avoid evaporation of fluid. The operated pupae were allowed to develop into adults at ambient temperatures (approximately 27 °C). The entire operation took less than 10 minutes, which made it possible to record images of pupae at 0 h postpupation. Most of the operated pupae developed normal color patterns in the pupal case and then eclosed, although their wings could not expand normally.

Whole-wing Bright-field Imaging

For whole-wing bright-field macroscopic imaging, a Canon EOS 40D digital single-lens reflex camera with a Canon EF-S 60 mm macrolens was utilized, which was controlled with Canon ZoomBrowser EX and EOS Utility software (Tokyo, Japan),

installed in a Fujitsu FM V-Biblo NF/A50 personal computer with the Windows Vista operating system. Automatic shuttering was set to obtain images at 1-min intervals at ISO800, a shutter speed of 1/5, and a diaphragm setting of F10. The focus was adjusted manually.

Static images were compiled as a movie. First, the images were converted from jpeg (1,936×1,288 pixels) to bmp (720×480 pixels) files using the free software JTrim. The converted bmp images were compiled as an avi movie using the free software AviUtl. The avi movie was then compressed and converted into an mp4 using Windows Movie Maker. One of the movies made in this manner is shown as Movie S1 in the present study. The frame rate (frames per second; fps) of this movie is 29.97 fps. Because images were captured at 1-min intervals, 1 sec of the playing movie corresponds to 0.5 h of the real time span. For Movie S1, see Movie Information in 2.2 Materials and Methods.

Compartmental Bright-field Imaging

High-resolution high-depth wing images at the compartmental level were obtained using a high-resolution high-depth Keyence VHX-1000 and VHX-2000 digital microscopes (Osaka, Japan). Following the operation for hindwing exposure, a pupa was physically fixed in a Petri dish, using double-sided adhesive tape if necessary. To avoid optical reflection from the wing surface, a polarized illumination adaptor was employed, and the dark-field command built into the machine was used. Images were obtained in 2-min or 5-min intervals, focusing on the compartments CuA_1 (150×) and $Sc+R_1$ (400×).

Static images were compiled as a movie. First, the images were converted from jpeg (1,600×1,200 pixels) to bmp (720×480 pixels) files using the free software JTrim or IrfanView. The converted bmp images were then compiled as an avi movie using the free software AviUtl and then converted into an mp4 using Windows Movie Maker. Three of the movies made in this manner are shown as Movies S2, S4, and S6 in the

present study. The frame rate of these movies is 29.97 fps. Because the images in Movies S2 and S4 were captured every 5 or 2 min, respectively, 1 sec of the playing movie corresponds to 2.5 or 1 h of the real time span, respectively. Movie S6 was made in the same way as Movie S4, except that the images were obtained from different compartments (Movie S4 from Sc+R_1 and Movie S6 from CuA_1). For Movies S2, S4 and S6, see Movie Information in 2.2 Materials and Methods.

Compartmental Autofluorescent Images

Higher magnification compartmental and cellular images were collected using a real-time confocal microscope imaging system including a Nikon Eclipse Ti-U inverted epifluorescence microscope (Tokyo, Japan), a Yokogawa laser-scanning unit CSU-X1 (Tokyo, Japan), a Hamamatsu Photonics ImagEM C9100-13 electron-multiplying charge-couple device (EM-CCD) camera (Hamamatsu, Japan), and the Hamamatsu Photonics AQUACOSMOS/RATIO system (Hamamatsu, Japan). The hindwing was exposed within 0.5 h postpupation. The exposed hindwing was placed on a piece of cover glass (0.12–0.17 mm in thickness; Muto Pure Chemicals, Tokyo, Japan) and subjected to real-time time-lapse confocal imaging. The exposure time was set to 10 sec (14 mW, EM gain 255) with autofluorescent signals being recorded at 1-min intervals using a 488 nm excitation light and a 520/25 nm bandpass filter.

Static images were acquired using AQUACOSMOS 2.6 as naf images (512×512 pixel), which were converted to avi files with the same software. These images were then converted and compressed into mp4 files using the free software Freemake Video Converter. One of the movies made in this way is shown as Movie S3 in the present study. Images were captured at 1-min intervals, but only images collected every 20 min were incorporated into the movie. The frame rate of this movie was set to 12 fps, and 1 sec of this movie therefore corresponds to 240 min (4 h). For Movie S3, see Movie Information in 2.2 Materials and Methods.

Compartmental and Cellular Fluorescent Images

CFSE (5- or 6-(*N*-Succinimidyloxycarbonyl)-fluorescein 3′, 6′-diacetate) was purchased from Dojindo Molecular Technologies (Kumamoto, Japan). CFSE is useful for tracing cellular dynamics over a relatively long period of time because it remains inside the cell for days. CFSE was dissolved in DMSO (dimethyl sulfoxide) and then in Insect Ringer's solution (NaCl 10.93 g, KCl 1.57 g, $CaCl_2 \cdot 2H_2O$ 0.83 g, and $MgCl_2 \cdot 6H_2O$ 0.83 g per liter) to obtain a final concentration of 10 µM. The pupal operation was performed similarly as described above, but to load CFSE (and the other fluorescent dyes indicated below), the loading solution (40 µL) was sandwiched between the fore- and hindwings in a similar manner to the previous method for loading various chemicals (Dhungel and Otaki, 2009). The sandwiched state was maintained in a humidified chamber for 30 min to allow loading at ambient temperatures (approximately 27 °C). After this step, the loading solution was washed off with Insect Ringer's solution. The forewing was then curled up again, and the hindwing was placed on a cover glass (0.12–0.17 mm in thickness; Muto Pure Chemicals).

Real-time *in vivo* confocal images of wing compartments following CFSE loading were obtained using the imaging system described above, with a 488 nm excitation light and a bandpass filter of 520/25 nm. We first obtained *Z*-axis scanning images at 5.0-µm sectioning steps (11 images per sampling time point) using a Physik Instrumente P721 PIFCO Piezo Flexure Objective Scanner (Karlsruhe, Germany), which controlled the *Z*-axis position of the objective lens (Nikon CFI S Fluor 10×, [NA]=0.5). The exposure time for capturing each optical slice was set at 300 msec (6 mW, EM gain 180). One well-focused image per time point was selected out of 11 images. These images were collected at 10-min intervals. The same image depth (*Z*-axis position) and fluorescent intensity were employed at 50 time points (500 min). That is, the depth and intensity were adjusted in every group of 50 time points, so that

well-focused images with a reasonable fluorescence intensity could be obtained. These selected images were connected and converted into a movie as described above. One of the movies made in this way is shown as Movie S5 of the present work. The frame rate of this movie was 30 fps. Because images were taken every 10 min, 1 sec of this movie corresponds to 300 min (5 h). For Movie S5, see Movie Information in 2.2 Materials and Methods.

Other fluorescent images were acquired similarly. The final concentrations of the fluorescent dyes were as follows: 100 μM MitoTracker Orange CMTMRos (Life Technologies, Carlsbad, CA, USA), 5× SYBR Green-1 (2,000-fold dilution from the original 10,000× stock solution) (Life Technologies), and 10 μM $DiBAC_4(3)$ (Bis(1,3-dibutylbarbituric acid)trimethine oxonol, sodium salt) (Dojindo Molecular Technologies). MitoTracker Orange and SYBR Green-1 stain mitochondria and nuclei, respectively. $DiBAC_4(3)$ is generally used as a membrane potential-sensitive dye. To load $DiBAC_4(3)$, the curled wing tissue was floated in the solution in a 35-mm glass-base Petri dish with a bottom consisting of a glass plate with a thickness of 0.16–0.19 mm and a diameter of 12 mm (Iwaki, AGC Techno Glass, Tokyo, Japan). Live images of the floating wings were obtained. The excitation and emission wavelengths used to obtain these confocal images were 561 nm and 617/73 nm for MitoTracker Orange and 488 nm and 520/25 nm for SYBR Green-1 and $DiBAC_4(3)$, respectively.

Area and Distance Measurements

The relative areas of the compartments and the relative distances between wing veins were measured from acquired images using the free software ImageJ. For these measurements, one movie consisting of whole-wing bright-field images was used to obtain area values (Movie S1), while one consisting of autofluorescent images (Movie S3) and one consisting of compartmental bright-field images (Movie S6) were used to acquire distance values. Reference values were set to indicate the relative values of

compartmental changes over time. During these measurements, image distortions were ignored, which were unavoidable due to the expansion of the wing tissue. For Movie S1, S2 and S6, see Movie Information in 2.2 Materials and Methods.

Movie Information

For all movies (Movies S1-S6) in this study, see Movies S1-S6 at this site (http://journals.plos.org/plosone/article?id=10.1371/journal.pone.0089500) of a journal called PLoS ONE. The movies are freely downloadable at the site.

1.3. Results

Whole-wing Development over Time

We first recorded macroscopic live wing images in a developing pupa from the early pupal stage to eclosion using a time-lapse image-capturing method ($n=3$) (Fig. 1-1; Movie S1). As reported previously (Kusaba and Otaki, 2009), the wing tissue was transparent, and the major wing-vein-associated tracheae had already been established at 0 h postpupation (Fig. 1-1A, B). The wing tissue then gradually became gray-white (Movie S1), likely suggesting scale growth. We were able to observe the completed adult wings inside the pupal case prior to eclosion (Fig. 1-1C, D; Movie S1), demonstrating that the normal developmental processes took place throughout the imaging period following the wing-curling operation (Kusaba and Otaki, 2009). We will discuss the developmental changes in color pigment deposition in the scales later in this paper.

We discovered that the wing tissue exhibited contraction pulses from 20 to 80 h postpupation, with a contraction cycle of approximately 10–20 min (Movie S1). The forewing and hindwing contracted synchronously (Movie S1). These slow contraction pulses gradually became weak and finally ceased, and the tissue became almost completely gray-white. These contraction pulses will be examined later in this paper.

Dynamics at the Compartmental Level over the First Two Days

At the compartmental level, we focused on the CuA_1 ($n=5$) and $Sc+R_1$ ($n=4$) compartments using a bright-field digital microscope (Fig. 1-2A; Movie S2). The two compartments showed similar (if not identical) features. The elaboration and movement of numerous tracheal branches were notable, and numerous free-moving hemocytes (Dohrmann and Nijhout, 1990) were observed underneath the epithelial sheet (Movies S2 and S4), as revealed in the autofluorescent images obtained using the confocal microscope as well ($n=3$) (Movie S3). Regular arrays of epithelial cells were

being generated when the entire hindwing became slightly gray-white at 20–33 h postpupation (Fig. 1-2A–C). Array formation was completed by 48 h postpupation (Fig. 1-2B, C). Then, the contraction pulses became more frequent, and the tracheal branches became less mobile (Movies S2 and S3). Together with the contraction pulses, a possible front of appression that may induce a seal between the dorsal and ventral epithelia moved from the basal to the distal region (Fig. 1-2B), which likely accompanied the decrease of hemolymph space within the pupal wing (Dohrmann and Nijhout, 1990). It appeared that the compartment area became larger following the contraction pulses, which will be examined later in this paper.

In the autofluorescent images ($n=3$), a possible organizing center for the marginal band system (Otaki, 2012a; Otaki et al., 2005b) was observed immediately after pupation (0 h) in the form of a dark region at the prospective wing margin compared to other regions (Movie S3). This dark region corresponds to the marginal focus, which is specified by the edge spot of the pupal cuticle spots in a forewing (Otaki et al., 2005b). A prospective eyespot focus, which corresponds to the organizing center for the border symmetry system, was similarly observed as a dark region almost immediately after pupation (0 h), and it appeared to be connected to more tracheal branches than other regions, which was observed beginning at 15 h postpupation (Fig. 1-2C). After the movement of the tracheal branches gradually disappeared from the proximal to distal region, the prospective eyespot focus was observed more clearly as a dark region at 48 h postpupation (Fig. 1-2C). At this point, the tracheal system could not be detected as non-fluorescent objects.

Interestingly, the major wing-vein-associated tracheae passed through the wing edge and the bordering lacuna at 0 h postpupation (Fig. 1-2C). The extra portion was not eliminated (Movies S2 and S3). At the same time, the peripheral tissue appeared to begin degenerating, as demonstrated by previous studies (Dohrmann and Nijhout, 1990; Kodama et al., 1995; Macdonald et al., 2010; Süffert, 1929; Yoshida and Aoki, 1989b). However, in our images, the degeneration appeared to occur at the margin of

the pupal wing proper at 35 h postpupation. Most likely due to the degeneration of the wing margin, the bordering lacuna expanded, and the marginal scales grew into the bordering lacuna. In the pupal wing proper, free-moving hemocytes were already observed at 0 h postpupation, then increased in number, peaking at 20–30 h postpupation. The hemocytes then gradually disappeared by 48 h postpupation, but they were still active in peripheral tissues that were degenerating (Fig. 1-2C, Movie S3), which may simply be because hemolymph space was available only in the peripheral region at that time. This finding could suggest that some of the hematocytes may play a role in sequestering cell debris.

Regular arrangement of the epithelial cells occurred at approximately 32 h postpupation (Movies S2 and S3). The row-arrangement front moved from the proximal to the distal region. Following the arrangement, scale growth and expansion of the compartment area occurred. The growth of the marginal scales was notable. Furthermore, contraction pulses and folding of wing tissue took place at 75 h postpupation, which may be due to the growth of the tissue. The bordering lacuna disappeared due to the expansion of the pupal wing proper.

Cellular Arrangement, Scale Growth, Tracheal Branches, and Hematocytes

Similar observations were made in the Sc+R_1 and CuA_1 compartments at higher magnifications using a bright-field digital microscope ($n=9$) (Fig. 1-3 and 1-4; Movie S4). A transparent cellular sheet of wing epithelium was observed immediately after pupation (Fig. 1-3A, B). The cellular diameter was approximately 10 μm. At 15–20 h postpupation, the epithelial cells started to be regularly arranged (Fig. 1-3C, D), and we successfully recorded growing scales at approximately 33 h postpupation afterwards (Fig. 1-3E). The scales subsequently increased in size, while the wing area increased dramatically (Fig. 1-3F).

Free-moving hemocytes were clearly observed underneath the epithelial sheet at approximately 1 d (23 h) after pupation (Fig. 1-4). Tracheal branches were also

present immediately after pupation, but they were not yet well elaborated (Figs. 1-3 and 1-4). The tracheal branches were numerous and moved briskly (Figs. 1-3 and 1-4). A single branch from the major trachea exhibited a crinoid-like structure, consisting of a stalk with a knob from which tracheoles radiate. These knobs and tracheoles appeared to be attached to the epithelial sheet from inside, but their columnar stalk did not. The knobs became less obvious as the epithelial cells were arranged.

Cellular Flourescent Staining of Wing Tissues

To confirm the dynamics of cellular arrangement using fluorescent images, we performed CFSE staining of wing tissues ($n=2$) (Fig. 1-5; Movie S5). The organizing center for the border symmetry system (i.e., eyespots and their associated elements) in the CuA_1 compartment did not stain well. The adjacent compartment (compartment M_3), which does not contain an eyespot, was relatively evenly stained, and we therefore focused on this compartment. Immediately after pupation, epithelial cells were observed, which were not yet arranged and were loosely distributed. At approximately 6 h postpupation, black patches appeared randomly, which may indicate cellular gaps due to cellular mobility or division. By 16 h postpupation, the black patches had disappeared, and cells were packed relatively tightly. These cells appeared to be smaller than those at 0–6 h, suggesting that cell division occurred. Gradually, cellular arrangement occurred, beginning at approximately 24 h postpupation, after which scales appeared to develop. By approximately 54 h postpupation, many fluorescent dots emerged, which indicated growing scales. Careful examination of the movie indicated that the arrangement and scale development occurred from the proximal to distal region (from the top to the bottom in Fig. 1-5 and Movie S5).

To confirm the identity of the epithelial cells and their relationship with the tracheal branches, we performed double staining of living tissues using two fluorescent dyes, MitoTracker Orange for mitochondria and SYBR Green-1 for nuclei ($n=7$). We

observed developing cells in the compartment CuA_1 at 0.5 h postpupation (Fig. 1-6A–C). The cellular diameter was approximately 10 μm, which was consistent with the above results obtained using the bright-field digital microscope. Interestingly, the organizing center was resistant to staining. Stacking of the *Z*-axis images revealed that the dorsal surface of the epithelial cells was rich in mitochondria above a relatively large nucleus (Fig. 1-6C). We also found that $DiBAC_4(3)$ strongly stained the major wing-vein-associated tracheae and tracheal branches and weakly stained epithelial cells ($n=4$) (Fig. 1-6D, E).

Contraction Pulses of the Developing Hindwing

Low-frequency slow contraction pulses were observed prior to the epithelial cellular differentiation indicated by the gray-white coloration of the wing tissue. Although the mechanism underlying these contraction pulses is unknown, it appeared that they were either tissue autonomous or driven by thoracic flight muscle. We found that both the fore- and hindwings showed synchronized pulses (Movie S1).

Because the contraction pulses appeared to be associated with the wing-tissue expansion, we quantitatively examined whether the wing area values changed before and after the contraction pulses using the bright-field whole-wing images. During a contraction, the areas of compartments M_1, M_2, and CuA_1 decreased and then increased back to similar or slightly greater areas (Fig. 1-7). However, because there were slight increases in area observed without contraction, we do not know whether the size increase following a contraction was directly due to the contraction.

Similar results were obtained using autofluorescent images of developing wings. We measured the distances between two wing veins and found that the distance decreased during a contraction and then increased back to the original or a slightly greater distance (Fig. 1-8A, B). When the distances were compared between 0 and 80 h postpupation, the latter distance was greater (Fig. 1-8C, D).

To examine the relationship between the contraction pulses and the increase in

vein distances, we recorded the frequency of contractions (the number of contractions within a 10-h period) and the wing-vein distances every 10 h. The contraction frequency was generally low, but it was highest (17 times) in the 40–50 h period, which coincided with the period of a marked increase in vein distance (Fig. 1-8E). This period also coincided with the period of increasing scale size. Furthermore, the period during which the vein distance increase occurred coincided with the period of increased autofluorescence (Fig. 1-8F).

Color Pigment Deposition in Scales

We analyzed the time course of pigment deposition in a single wing of a given individual in whole-wing images ($n=3$) (Fig. 1-9; Movie S1). Color patterns (including eyespots and parafocal and submarginal bands) were already recognizable approximately 2 d before eclosion (approximately 5 d after pupation), but pigments were clearly deposited approximately 1.5 d before eclosion. This pigment deposition process continued until the point immediately prior to eclosion.

Coloration appeared in the following order: eyespot red rings, black/brown background (from the discal spot or its proximity to the peripheral area), eyespot black rings, and black peripheral elements (the parafocal and submarginal bands). However, the black rings and the black peripheral elements were detected as early as the red rings. The background black/brown coloration extended from a discal spot or its proximity toward the distal and proximal regions, and this expansion appeared to be blocked by the eyespots and the parafocal elements. The black ring first emerged at a single location and expanded along the red ring. Later, the width of the black ring expanded considerably. This sequence of events was not observed clearly in the red ring.

We further analyzed the pigment deposition sequence using the compartmental images ($n=5$) (Fig. 1-10; Movie S6), which revealed that within a prospective width of the black ring, the black pigment was first deposited in patches as

fragments in the central areas of the width. The pigmented regions of the black ring then expanded not only along the red ring but also outside and inside the eyespot (Fig. 1-10A, B). Similarly, within a prospective parafocal element, the black pigment was first deposited at the center, and it expanded laterally (Fig. 1-10A, C). The red ring that appeared first was invaded by the black ring that developed subsequently. This superimposition process reduced the transient width of the red ring considerably.

1.4. Discussion

Discussion

In this study, we obtained real-time *in vivo* images of butterfly wing tissue development. The developmental time-course that was observed in this study is largely consistent with and complementary to those found in previous histological and morphometric studies on lepidopteran wings (Dhungel and Otaki, 2013b; Dohrmann and Nijhout, 1990; Galant et al., 1998; Ghiradella, 1998; Greenstein, 1972; Kodama, 1995; Kristensen and Simonsen, 2003; Koch et al., 2003; Kühn, 1954; Kuntze, 1935; Kusaba and Otaki, 2009; Macdonald et al., 2010; Nijhout, 1991; Reed, 2004; Süffert, 1929; Yoshida, 1988; Yoshida and Aoki, 1989a; Yoshida et al., 1983). We recorded time course of developing epithelial cells, including the arrangement of rows and scale growth. We also described images of epithelial cells that are rich in mitochondria at the dorsal surface of the cell. Mitochondria may be functionally important in these actively growing and differentiating epithelial cells to supply ATP as a free energy source. The mitochondrial distribution pattern at the surface of epithelial cells may suggest a high metabolic activity for producing scales at the surface of the epithelium.

Consistent with the observed richness of mitochondria, we found briskly moving tracheal branches originating from the major tracheae, which supply oxygen to epithelial cells from inside the tissue. The structure of a single tracheal branch is crinoid-like, similar to a sea lily, exhibiting a white knob from which many tracheoles radiate. Interestingly, the prospective eyespot focus is likely to be connected to more tracheal braches than other regions, and its autofluorescent character and sensitivity to fluorescent dyes are different from other regions, as observed in the putative marginal focus (edge-spot) organizing centers. The optical character of the organizing centers may be due to high density of cells that formed a non-flat structure in wings (i.e., an elevation or dent of wing surface), which is consistent with the previous report (Koch et al., 2003). These unique features of the organizing centers may indicate their high

metabolic activity related to signaling.

In addition to the highly mobile tracheal branches, we discovered cellular dynamics that may be difficult to detect using fixed histological samples, including free-moving hemocytes; slow, low-frequency contraction pulses; movement of the possible appression front in the early pupal stage; and dynamic coloration processes a few days prior to eclosion. Within one day after pupation, moving hemocytes were observed underneath the epithelial sheet. Initially, the hemocytes were seen throughout a compartment and were not confined to the lacunae along tracheae, indicating the existence of a hemolymph space between the two epithelia at this point. Later, the hemocytes were confined to the bordering lacuna. Some of these hemocytes may be macrophages and may be responsible for eliminating apoptotic cells from the wing tissue and for degradation of the peripheral region outside the pupal wing proper. Interestingly, we observed similar macrophage-like cells during the damage-induced regeneration of fish skin (Ohno and Otaki, 2012). In our images, degradation of the margin of the pupal wing proper widened the bordering lacuna.

We discovered contraction pulses in the wing tissue. A single pulse cycle required 10–20 min, and the highest frequency recorded was 17 pulses within a 10-hour period, meaning that one contraction occurred every 35 min on average. Because such slow, low-frequency contractions are difficult to detect in fixed histological samples, the present study is likely the first report of these contraction pulses. These contractions are too slow and too rare in frequency to be caused by the heart or accessory pulsatile organs. Thoracic flight muscles may be involved in the contraction process. However, because the contraction is very slow and because it is coupled with the wing area increase and with the scale development, there is a possibility that the wing contraction may be autonomous. Although the functional importance of the contraction pulses is unclear, they appeared to be coupled to increases in the wing area and autofluorescence intensity. This wing-area increase may have been achieved through increases in cell size and by the growth of scales on the

surface of the wing, as cell division likely ceased prior to the arrangement of rows (Greenstein, 1972; Kühn, 1954). Further physiological characterization of these contractions can be expected in the future.

Butterfly wings are a two-dimensional system on which scales (and hence scale and socket cells) are regularly arranged in anteroposterior rows at regular intervals (Dhungel and Otaki, 2013b; Ghiradella, 1998; Kristensen and Siomonsen, 2003; Kusaba and Otaki, 2009; Nijhout, 1991). In the present study, we found that the arrangement of the cellular rows began at approximately 20 h postpupation. Almost simultaneously, scales began to grow. Initially, the scales were colorless and were observed as white or fluorescing objects. At this point, it is likely that positional information has already been supplied from organizing centers and that the scale-forming cells have committed to their fate regarding scale coloration, size, and shape (Dhungel and Otaki, 2013b; Kusaba and Otaki, 2009). Scale size likely reflects the degree of polyploidy in the scale cells of butterflies (Cho and Nijhout, 2012; Henke, 1946; Henke and Pophley, 1952; Nijhout, 1991). Cell size and shape may be determined by positional information, which may be supplied as a ploidy signal (Dhungel and Otaki, 2013b). Unfortunately, the present study did not have a sufficient resolving power to detect changes in cell size.

Nevertheless, we present a detailed time course of color pigment deposition in the scales of a single individual. As indicated in a previous study (Kusaba and Otaki, 2009), the background coloration of this species shows similar behavior to an enlarged element, as it originates from the discal spot or its proximity, which is the center of the central symmetry system. Furthermore, the peripheral region is not invaded by this black/brown coloration, most likely because the pigmentation front is blocked by the eyespots and parafocal elements. These phenomena are reminiscent of elemental interactions between an eyespot and a parafocal element (Dhungel and Otaki, 2009) and between two eyespots (Otaki, 2011a).

An alternative explanation is that the pigment deposition order and pigment

intensity simply reflect either the distribution pattern of pigment synthesizing enzymes or the availability of pigment precursors provided via hemolymph. However, it appears that the black pigment was first deposited at the place where the primary organizing center is located, namely, the discal spot. Furthermore, the distribution pattern of pigment synthesizing enzymes is likely what positional information for color patterns determines. The availability of pigment precursors would be basically uniform throughout a wing, and it is difficult to think that the prospective discal spot organizing center is more accessible to pigment precursors than other portions of a wing.

In the whole-wing images, the black ring appeared at the single location first and then expanded along the red ring. The black ring further expanded in width. In the case of the red ring, such a sequence of events was less apparent. The expansion of the black ring was further observed in the compartmental images, which revealed the fragmental or patchy deposition and expansion. That is, the black fragments emerged first and then expanded laterally, distally and proximally to complete a ring. The outer parts of the red ring were subsequently invaded by the expanding black ring, indicating that the red signal and the black signal overlap in the boundary area. In other words, the two signals in a given eyespot are different from each other. The development of the parafocal element followed a similar sequence, although only a single fragment emerged first at the center of the parafocal element and expanded laterally.

We believe that these detailed analyses of the pigment deposition process are insightful for understanding the nature of positional information. The process of determination of positional information (i.e., pre-patterning) occurs immediately after pupation, and the process of pigment deposition occurs immediately before pupation. Therefore, these two processes are different. However, the latter must be executed according to the former. In this sense, these two processes are closely related. We believe that increased enzymatic activity related to pigment synthesis may be indicated by the timing of the appearance of coloration during development, and we can further

assume that this difference in activity reflects the difference in positional information, i.e., different levels of morphogenic signals.

We have proposed the induction model as a mechanism for specifying positional information (Iwata et al., 2013; Otaki, 2011a-c, 2012b), which is more widely applicable to various color patterns than the classical morphogen gradient model. The induction model states that a pulse-like signal for a dark eyespot ring (a dark signal) is emitted from the prospective focus. The velocity of the signal decreases as it goes further. Cells that are located in positions where the dark signal settles can serve as a secondary organizing center by amplifying the signal itself. This nested dark signal also induces a different signal for a light eyespot ring (a light signal) adjacent to it. This light signal is inhibitory to the dark signal. Dynamic interactions among these dark and light signals determine the final eyespot morphology. We were able to observe the time course of pigment deposition in a wing from a given individual, and if the pigment deposition process reflects the distribution pattern of positional information, our observations support the induction model of positional information, which predicts central-to-peripheral deposition (due to independent nested signaling from the center of a width of a black ring or from the center of a parafocal element) that can be executed in a patchy manner. Our observations are not consistent with the gradient model of positional information because it predicts even deposition (due to an even threshold-like response within a width of a black ring or within a parafocal element). It is plausible that a parafocal element is equivalent to an isolated black ring of an eyespot, as predicted by the previous analyses (Dhungel and Otaki, 2009; Dhungel and Otaki, 2013b; Kusaba and Otaki, 2009; Otaki, 2008, 2011b, 2012a,b). Furthermore, the superimposition of a part of a black ring on a red ring cannot be supported by the gradient model, because redundant information for a single position cannot theoretically be supplied by the gradient model. However, if the pigment deposition process does not reflect the distribution pattern of positional information at all, these observations support neither the induction model nor the gradient model. It is

interesting to note that a recent study showed that morphogen molecules do not have to form concentration gradients to function (Alexander et al., 2014).

Technically, real-time *in vivo* imaging is an entirely new approach for investigating butterfly biology. In the present study, we employed several techniques, including three different optical systems, and took advantage of inherent characters of butterflies, such as their resistance to surgical operation, the autofluorescence of developing cells, and the penetration of fluorescent dyes. The time points detected using the different systems are slightly different but largely consistent. Each system exhibits advantages and disadvantages. Although we utilized only a handful of fluorescent dyes in this study, we believe that the application of other dyes may increase our observational range. Genetically engineered fluorescent proteins may also be employed, as a gene transfer method is now established (Dhungel et al., 2013). In the future, we may be able to trace molecular movements in real time in a developing wing using this system, which may provide us with conclusive evidence of how morphogens determine eyespots and other color pattern elements in butterfly wings.

1.5. References

Alexandre, C., Baena-Lopez, A., Vincent. J.P., 2014. Patterning and growth control by membrane-tethered Wingless. Nature 505, 180–185.

Beldade, P., Brakefield, P.M., Long, A.D., 2002. Contribution of *Distal-less* to quantitative variation in butterfly eyespots. Nature 415, 315–318.

Brakefield, P.M., French, V., 1995. Eyespot development on butterfly wings: the epidermal response to damage. Dev. Biol. 168, 98–111.

Brakefield, P.M., Gates, J., Keys, D., Kesbeke, F., Wijngaarden, P.J., Monteiro, A., French, V., Carroll, S.B., 1996. Development, plasticity and evolution of butterfly eyespot patterns. Nature 384, 236–242.

Carroll, S.B., Gates, J., Keys, D.N., Paddock, S.W., Panganiban, G.E., et al., 1994. Pattern formation and eyespot determination in butterfly wings. Science 265, 109–114.

Cho, E.H., Nijhout, H.F., 2012. Development of polyploidy of scale-building cells in the wings of *Manduca sexta*. Arthropod Struct. Dev. 42, 37–46.

Dhungel, B., Otaki, J.M., 2009. Local pharmacological effects of tungstate on the color-pattern determination of butterfly wings: a possible relationship between the eyespot and parafocal element. Zool. Sci. 26, 758–764.

Dhungel, B., Otaki, J.M., 2013a. Larval temperature experience determines sensitivity to cold-shock-induced wing color pattern changes in the blue pansy butterfly *Junonia orithya*. J. Therm. Biol. 38, 427–433.

Dhungel, B., Otaki, J.M., 2013b. Morphometric analysis of nymphalid butterfly wings: number, size and arrangement of scales, and their implications for tissue-size determination. Entomol. Sci. 17, 207-218.

Dhungel, B., Ohno, Y., Matayoshi, R., Otaki, J.M., 2013. Baculovirus-mediated gene transfer in butterfly wings *in vivo*: an efficient expression system with an anti-gp64 antibody. BMC Biotechnol. 13, 27.

Dohrmann, C.E., Nijhout, H.F., 1990. Development of the wing margin in *Precis coenia* (Lepidoptera: Nymphalidae). J. Res. Lepidoptera 27, 151–159.

French, V., Brakefield, P.M., 1992. The development of eyespot patterns on butterfly wings: morphogen sources or sinks? Development 116, 103–109.

Galant, R., Skeath, J.B., Passock, S., Lewis, D.L., Carroll, S.B., 1998. Expression pattern of a butterfly *achaete-scute* homolog reveals the homology of butterfly wing scales and insect sensory bristles. Curr. Biol. 8, 807–813.

Ghiradella, H., 1998. Hairs, bristles and scales. In: Harrison, F.W., Locke, M. (Eds.), Microscopic Anatomy of Invertebrates: Insecta, vol. 11, John Wiley & Sons, New York, pp. 257–287.

Greenstein, M.E., 1972. The ultrastructure of developing wings in the giant silkmoth,*Hyalophora cecropia*. II. Scale-forming and socket-forming cells. J. Morphol. 136, 23–52.

Henke, K., 1946. Über die verschiedenen Zellteilungsvorgange in der Entwicklung des beschuppten Flügelepithels der Mehlmotte *Ephestia kühniella* Z. Biol. Zentralbl. 65, 120–135. (In German).

Henke, K., Pohley, H.J., 1952. Differentielle Zellteilungen und Polyploedie bei der Schuppenbildung der Mehlmotte *Ephestia kühniella*. Z. Z. Naturforsch. B 7, 65–79. (In German).

Hiyama, A., Taira, W., Otaki, J.M., 2012. Color-pattern evolution in response to environmental stress in butterflies. Front. Genet. 3, 15.

Iwata, M., Hiyama, A., Otaki, J.M., 2013. System-dependent regulations of colour-pattern development: a mutagenesis study of the pale grass blue butterfly *Zizeeria maha*. Sci. Rep. 3, 2379.

Koch, P.B., Merk, R., Reinhardt, R., Weber, P., 2003. Localization of ecdysone receptor protein during colour pattern formation in wings of the butterfly *Precis coenia*(Lepidoptera: Nymphalidae) and co-expression with Distal-less protein. Dev. Gene. Evol. 212, 571–584.

Kodama, R., Yoshida, A., Mitsui, T., 1995. Programmed cell death at the periphery of the pupal wing of the butterfly, *Pieris rapae*. Roux Arch. Dev. Biol. 20, 418–426.

Kristensen, N.P., Simonsen, T.J., 2003. Hairs and scales. In: Kristensen, N.P. (Ed.). Lepidoptera, Moths and Butterflies: Morphology, Physiology, and Development. Handbook of Zoology, Anthoporda: Insecta, vol. IV, Walter de Gruyter, Berlin, pp. 9–22.

Kühn, A., 1954. Vorlesungen unber Entwicklungsphysiologie. Springer-Verlag, Berlin. (In German).

Kuntze, H., 1935. Die Flügelentwicklung bei *Philosamia cynthia* Drury, mit besonderer Berücksichtigung des Geäders der Lakunen und der Tracheensysteme. Z. Morphol. Ökol. Tiere 30, 544–572 (In German).

Kusaba, K., Otaki, J.M., 2009. Positional dependence of scale size and shape in butterfly wings: wing-wide phenotypic coordination of color-pattern elements and background. J. Insect Physiol. 55, 174–182.

Macdonald, W.P., Martin, A., Reed, R.D., 2010. Butterfly wings shaped by a molecular cookie cutter: evolutionary radiation of lepidopteran wing shapes associated with a derived Cut/wingless wing margin boundary system. Evol. Dev. 12, 296–304.

Mahdi, S.H., Gima, S., Tomita, Y., Yamasaki, H., Otaki, J.M., 2010. Physiological characterization of the cold-shock-induced humoral factor for wing color-pattern changes in butterflies. J. Insect Physiol. 56, 1022–1031.

Monteiro, A., Glaser, G., Stockslager, S., Glansdrop, N., Ramos, D., 2006. Comparative insights into questions of lepidopteran wing pattern homology. BMC. Dev. Biol. 6, 52.

Monteiro, A., Chen, B., Ramos, D.M., Oliver, J.C., Tong, X., Guo, M., Wang, W.K., Fazzino, L., Kamal, F., 2013. *Distal-Less* regulates eyespot patterns and melanization in *Bicyclus* butterflies. J. Exp. Zool. 320B: 321–331.

Nijhout, H.F., 1980a. Ontogeny of the color pattern on the wings of *Precis coenia*. Dev. Biol. 80, 275–288.

Nijhout, H.F., 1980b. Pattern formation on lepidopteran wings: determination of an eyespot. Dev. Biol. 80, 267–274.

Nijhout, H.F., 1985. Cautery-induced colour patterns in *Precis coenia* (Lepidoptera: Nymphalidae). J. Embryol. Exp. Morphol. 86, 191–203.

Nijhout, H.F., 1991. The development and evolution of butterfly wing patterns. Smithsonian Institution Press, Washington, DC.

Nijhout, H.F., 2001. Elements of butterfly wing patterns. J. Exp. Zool. 291, 213–225.

Reed, R.D., 2004. Evidence for Notch-mediated lateral inhibition in organizing butterfly wing scales. Dev. Genes Evol. 214, 43–46.

Reed, R.D., Serfas, M.S., 2004. Butterfly wing pattern evolution is associated with changes in a Notch/Distal-less temporal pattern formation process. Curr. Biol. 14, 1159–1166.

Saenko, S.V., Brakefield, P.M., Beldade, P., 2010. Single locus affects embryonic segment polarity and multiple aspects of an adult evolutionary novelty. BMC. Biol. 8, 111.

Shirai, L.T., Saenko, S.V., Keller, R.A., Jerónimo, M.A., Brakefield, P.M., Descimon, H., Wahlberg, N., Beldade, P., 2012. Evolutionary history of the recruitment of conserved developmental genes in association to the formation and diversification of a novel trait. BMC. Evol. Biol. 12, 21.

Süffert, F., 1929. Die Ausbildung des imaginalen Flügelschnittes in der Schmetterlingspuppe. Z. Morphol. Ökol. Tiere 14, 338–359.

Ohno, Y., Otaki, J.M., 2012. Eyespot colour pattern determination by serial induction in fish: Mechanistic convergence with butterfly eyespots. Sci. Rep. 2, 290.

Otaki, J.M., 2007. Reversed type of color-pattern modifications of butterfly wings: a physiological mechanism of wing-wide color-pattern determination. J. Insect Physiol. 53, 526–537.

Otaki, J.M., 2008. Physiologically induced color-pattern changes in butterfly wings: mechanistic and evolutionary implications. J. Insect Physiol. 55, 174–182.

Otaki, J.M., 2009. Color-pattern analysis of parafocal elements in butterfly wings. Entomol. Sci. 12, 74–83.

Otaki, J.M., 2011a. Artificially induced colour-pattern changes in butterflies: dynamic signal interactions. Sci. Rep. 1, 111.

Otaki, J.M., 2011b. Generation of butterfly wing eyespot patterns: a model for morphological determination of eyespot and parafocal element. Zool. Sci. 28, 817–827.

Otaki, J.M., 2011c. Color-pattern analysis of eyespots in butterfly wings: a critical examination of morphogen gradient models. Zool. Sci. 28, 403–413.

Otaki, J.M., 2012a. Color pattern analysis of nymphalid butterfly wings: Revision of the nymphalid groundplan. Zool. Sci. 29, 568–576.

Otaki, J.M., 2012b. Structural analysis of eyespots: dynamics of morphogenic signals that govern elemental positions in butterfly wings. BMC Syst. Biol. 6, 17.

Otaki, J.M., Yamamoto, H., 2004. Species-specific color-pattern modifications of butterfly wings. Dev. Growth Differ. 46, 1–14.

Otaki, J.M., Ogasawara, T., Yamamoto, H., 2005a. Tungstate-induced color-pattern modifications of butterfly wings are independent of stress response and ecdysteroid effect. Zool. Sci. 22, 635–644.

Otaki, J.M., Ogasawara, T., Yamamoto, H., 2005b. Morphological comparison of pupal wing cuticle patterns in butterflies. Zool. Sci. 22, 21–34.

Yoshida, A., Shinkawa, T., Aoki, K., 1983. Periodical arrangement on lepidopteran (butterfly and moth) wings. Proc. Jpn. Acad. 59B, 236–239.

Yoshida, A., 1988. Scale arrangement on lepidopteran wings. Special Bull. Lepidopterol. Soc. Jpn. 6, 447–464. (In Japanese).

Yoshida, A., Aoki, K., 1989a. Scale arrangement pattern in a lepidopteran wing. 1. Periodic cellular pattern in the pupal wing of *Pieris rapae*. Dev. Growth Differ. 31, 601–609.

Yoshida, A., Aoki, K., 1989b. Scale arrangement pattern along the wing margin of a small white cabbage butterfly (Lepidoptera: Pieridae). Morph. Histol. Fine Struct. 94, 467–470.

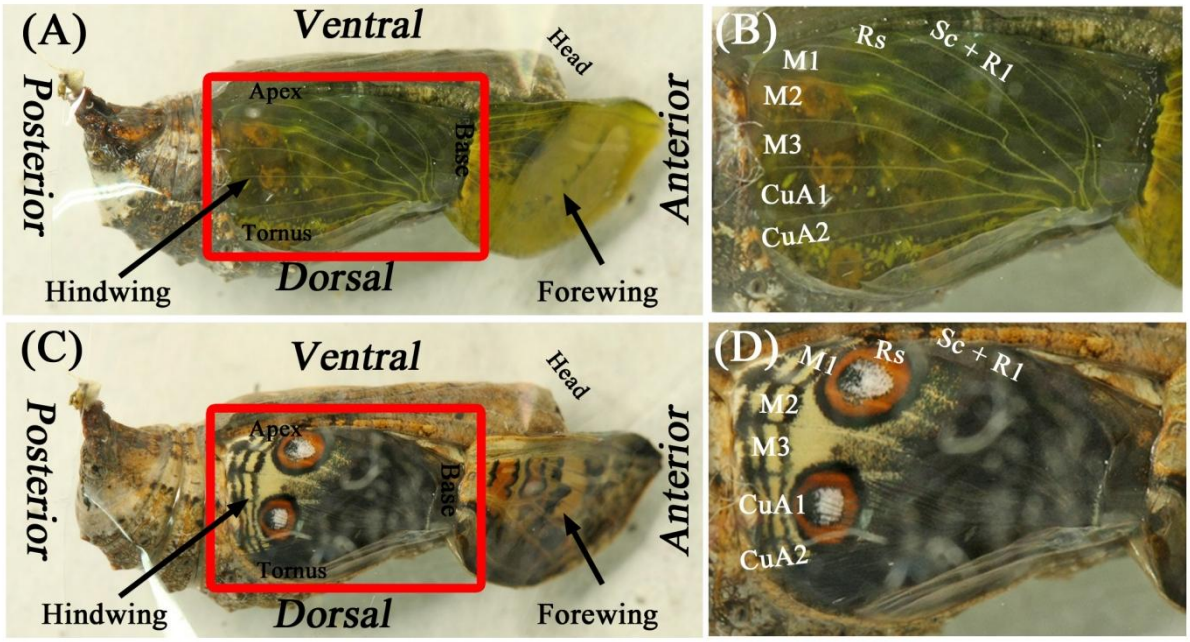

Fig. 1-1. Surgical configuration for observing developing pupal wing tissues *in vivo*. For the complete developmental process over time, refer to Movie S1. **(A)** A pupa immediately after the operation of curling up the pupal forewing. The exposed hindwing is boxed. **(B)** The exposed hindwing from (A), with identification of the compartments. **(C)** A pupa immediately before eclosion with fully developed color patterns on the hindwing. Note that the ventral forewing also display a fully developed color pattern in this individual. This individual is identical to that shown in (A). **(D)** The hindwing of (C), with identification of the compartments, which can be compared to (B). Note that compartment CuA_1 exhibits a large eyespot.

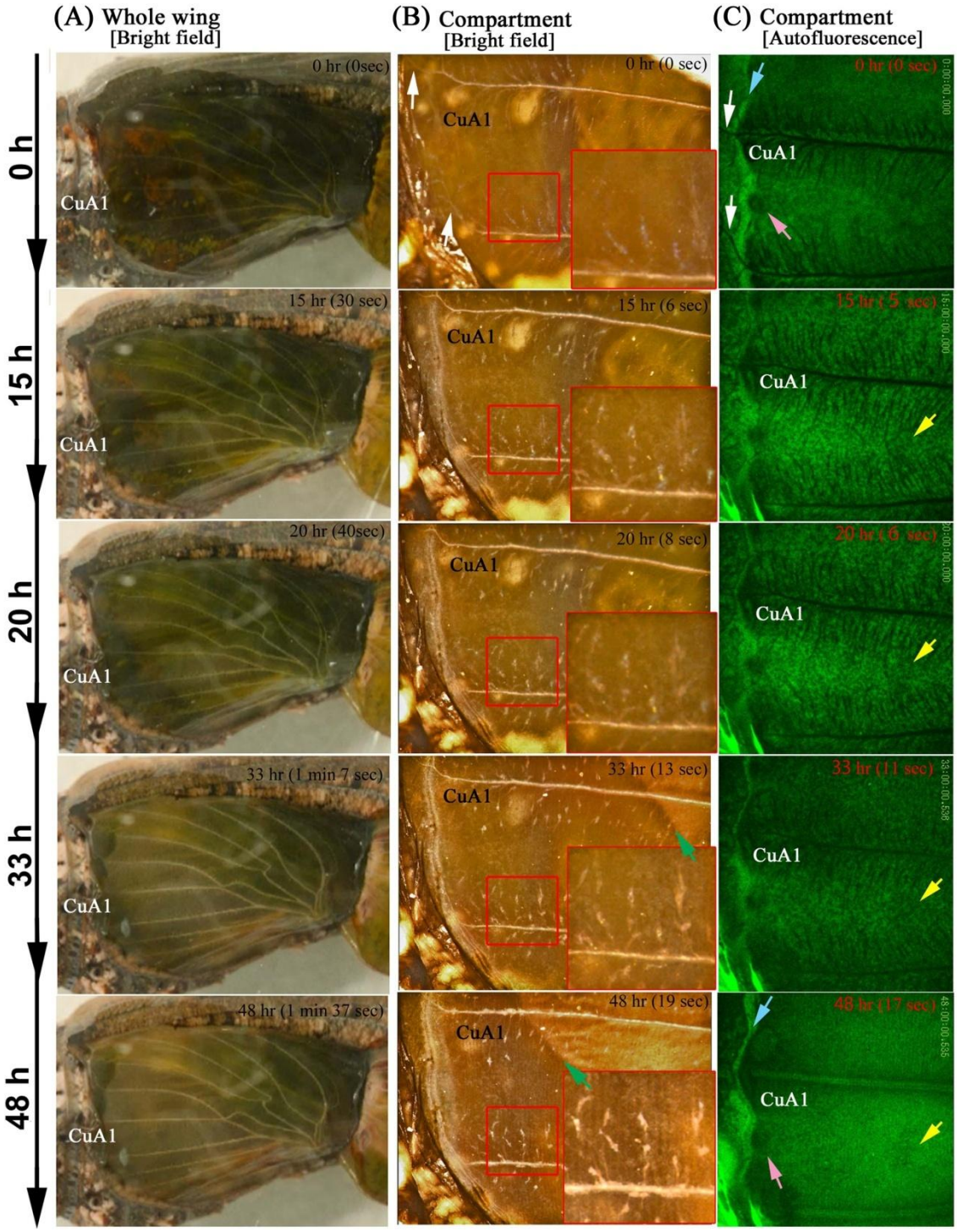

Fig. 1-2. The changes in the pupal wing tissue in the first two days. The hours indicate real developmental time (i.e., the postpupation time), and the minutes and seconds in parentheses indicate time points in the playing movies. **(A)** Whole-wing bright-field images. The transparent tissue is becoming gray-white. Also refer to Movie S1. **(B)** Bright-field images of compartment CuA_1. The small boxed areas are

enlarged in the adjacent large boxes. The elaboration and movement of the tracheal branches are notable. Regular arrays of epithelial cells are observed by 48 h postpupation. The possible appression front moving from the basal to the distal region is indicated by green arrows. White arrows indicate the major tracheae that run off the wing edge at the early stage. Also refer to Movie S2. **(C)** Autofluorescent images of compartment CuA_1 under blue light. Blue arrows indicate the bordering lacuna, which corresponds to the wing edge. White arrows indicate the major tracheae that run off the wing edge at the early stage. The pink arrows indicate the marginal focus (edge spot), which is the possible organizing center for the marginal band system. The yellow arrows indicate the location of the organizing center for a border symmetry system including an eyespot. The extension of tracheal branches, especially toward the organizing centers, is detectable. Moving hemocytes are observed in a relatively early stage, some of which are most likely macrophages. In the later stages, hemocytes are confined to the bordering lacuna, which may promote degradation of the peripheral tissue. Also refer to Movie S3.

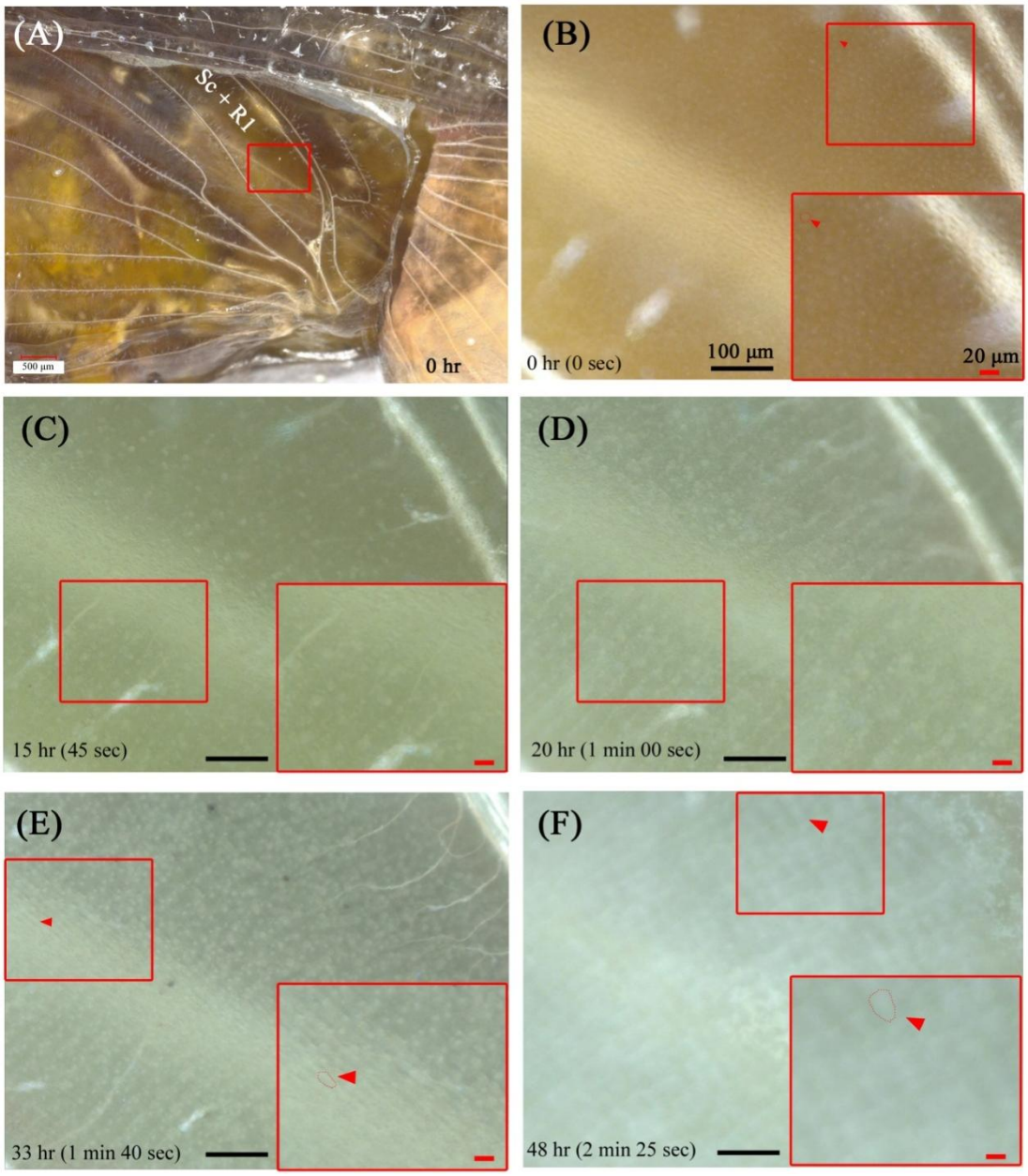

Fig. 1-3. Array and scale formation. Also refer to Movie S4. **(A)** The hindwing basal region after the curling operation. The magnified area of compartment $Sc+R_1$ in the subsequent panels is boxed. **(B-F)** Cellular changes over time. The small boxed areas are enlarged in the adjacent large boxes. Transparent non-aligned epithelial cells are observed in the early stage in (B). Vigorously moving tracheal branches are notable in (C), together with moving hemocytes, some of which are most likely macrophages. Later, the epithelial cells are regularly arranged, and scales grow, as shown in (D) and (E), which are seen as white objects that are increasing in size. Scale growth

accompanies the increase in wing area in (F), which appears to be driven by the contraction pulses of the wing tissue. Red arrowheads indicate single cells or scales that are circled with dots. All panels (B-F) are shown at the same magnification.

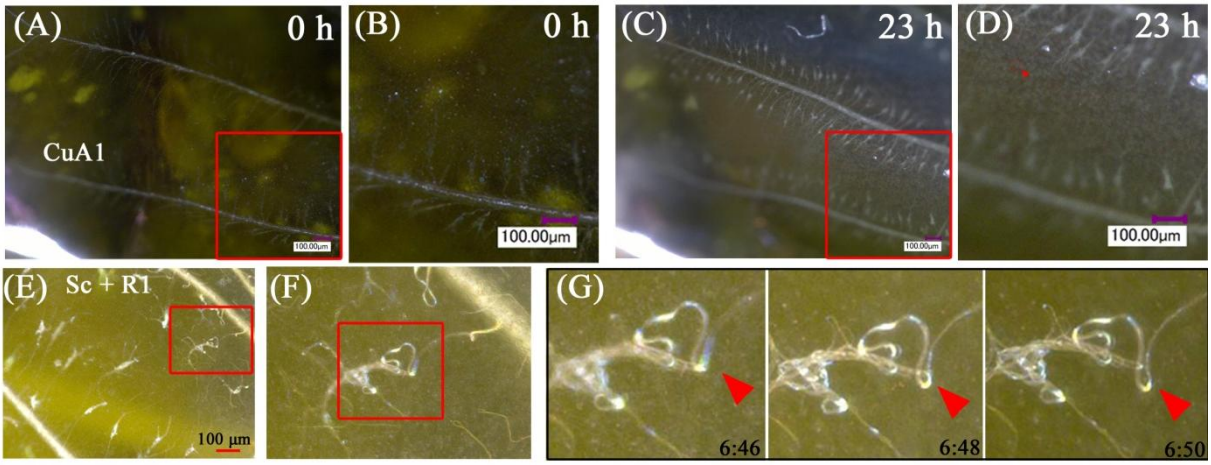

Fig. 1-4. Behavior of tracheal branches and hemocytes. (A, B) Bright-field image of compartment CuA_1 immediately after pupation (0 h postpupation). The boxed region is magnified in (B). Many tracheal branches are already observed at this point, but they are most likely immature and cannot be seen clearly under our observation conditions. They also do not move vigorously. **(C, D)** The identical CuA_1 region 23 h postpupation. Many tracheal branches are observed as white crinoid-like objects, with one side attached to the major trachea. They move relatively vigorously. A single branch exhibits a white knob, from which many thin branches (i.e., tracheoles) radiate. Also note the free-moving hemocytes (indicated by a red arrowhead). **(E-G)** Tracheal branches in compartment $Sc+R_1$. The boxed region in (E) is magnified in (F), and the boxed region in (F) is further magnified in (G), showing the dynamics of the branch, knob, and tracheoles. The red arrowheads in (G) indicate the identical position in the images over time. The postpupation time is indicated in (G).

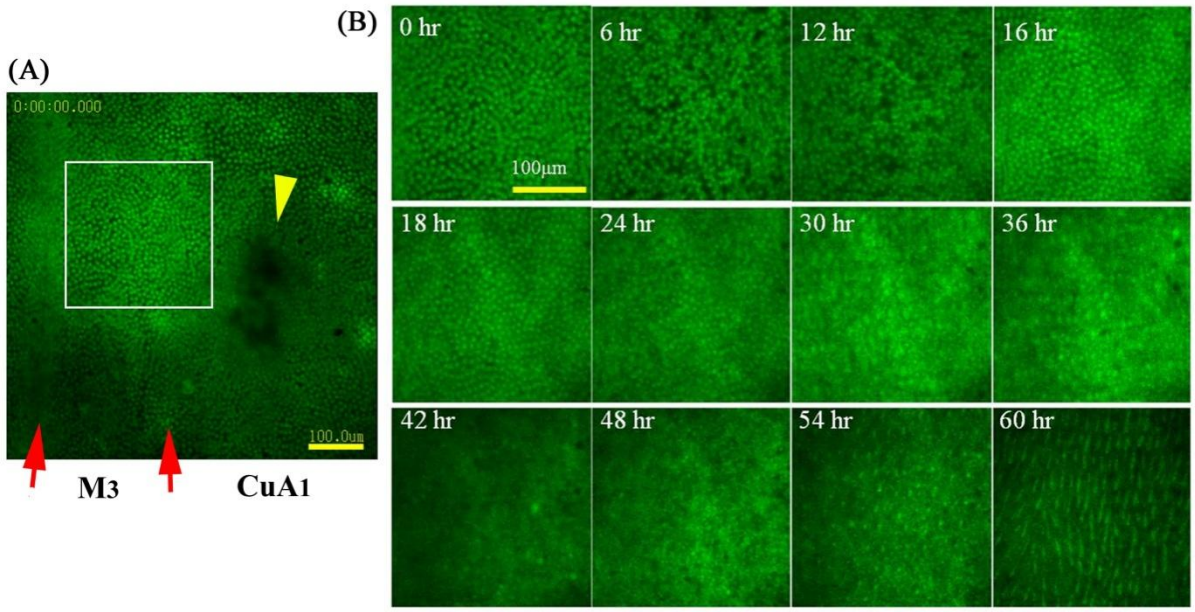

Fig. 1-5. Fluorescent images of array and scale formation. Wing tissue was stained with CFSE. **(A)** Stained M_3 and CuA_1 compartments. Compartment CuA_1 exhibits an organizing center, indicated by a yellow arrowhead. The organizing center appears to be resistant to staining. Note that the adjacent M_3compartment does not have this non-stained black area, probably because the M_3compartment does not have an eyespot in adult wings. Also see Fig. 1-6A. Red arrows indicate the major tracheae. The boxed region is enlarged in the subsequent panels. Also refer to Movie S5. **(B)** Cellular changes over time. At 6 h, the cellular density appears to decrease, and by 16 h the tissue is occupied by densely packed epithelial cells. After 24 h, the cells gradually become arranged, and the wing area increases, which appears to be driven by the contraction pulses that become frequent after 30 h. Scale growth is observed immediately after the cellular row arrangement occurs. All panels are shown at the same magnification.

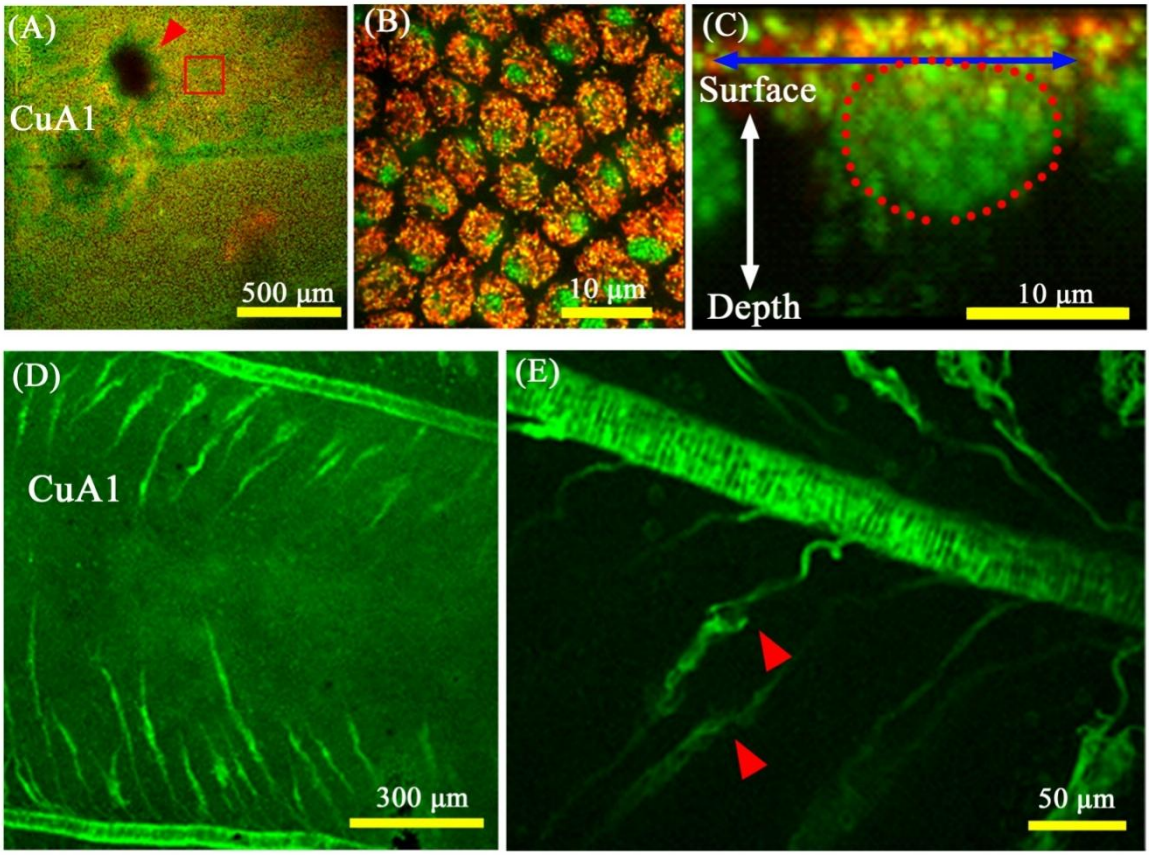

Fig. 1-6. Fluorescent images of epithelial cells and tracheal branches. (A) Low-magnification image of compartments CuA_1 and M_3 stained with MitoTracker Orange for mitochondria (in red) and SYBR Green-1 for nuclei (in green), immediately after pupation. The red arrowhead indicates the organizing center for the border symmetry system, which is resistant to staining. This non-stained black area was not detected in the adjacent compartment where no eyespot exists in adult wings. Also see Fig. 1-5A. The boxed region is magnified in (B). **(B)** High-magnification image of the epithelial cells boxed in (A). Yellow dots indicate mitochondrial DNA. **(C)** Optical cross section of the stained epithelial cells. The diameter of a single cell is indicated by a double-headed arrow. Cellular nucleus is encircled by red dots. Note the mitochondrial distribution on the dorsal surface of the cell. Yellow regions indicate mitochondrial DNA. **(D, E)** Compartment CuA_1 stained with $DiBAC_4(3)$. Tracheae are stained well, and the epithelial cells are weakly stained. A portion of a tracheal knob is indicated by red arrowheads to demonstrate its vigorous movement.

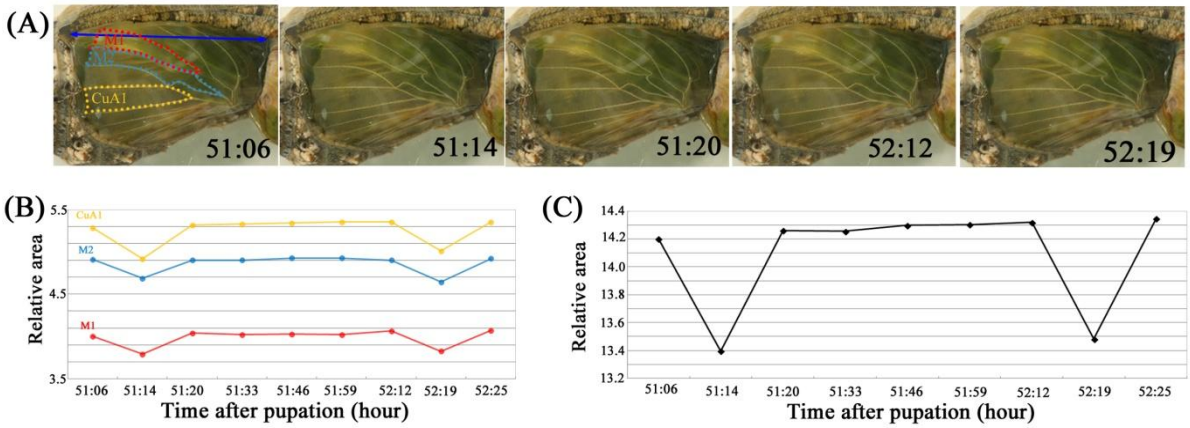

Fig. 1-7. Areal changes associated with the wing-tissue contraction pulses. (A) Bright-field images of the hindwing over time. The postpupation time is indicated in each panel. The areas of the three different compartments (M_1, M_2, and CuA_1), encircled with red, blue, and yellow dotted lines, were measured and normalized according to the hindwing span indicated by the double-headed blue arrow. Note that the hindwing is most contracted at 51∶14 h and at 52∶19 h postpupation. These are static images from Movie S1. **(B)** Relative areal changes over time in compartments M_1, M_2, and CuA_1. The time points correspond to the images shown in (A). These measurements were performed using Movie S1. **(C)** Summation of the three compartment areas.

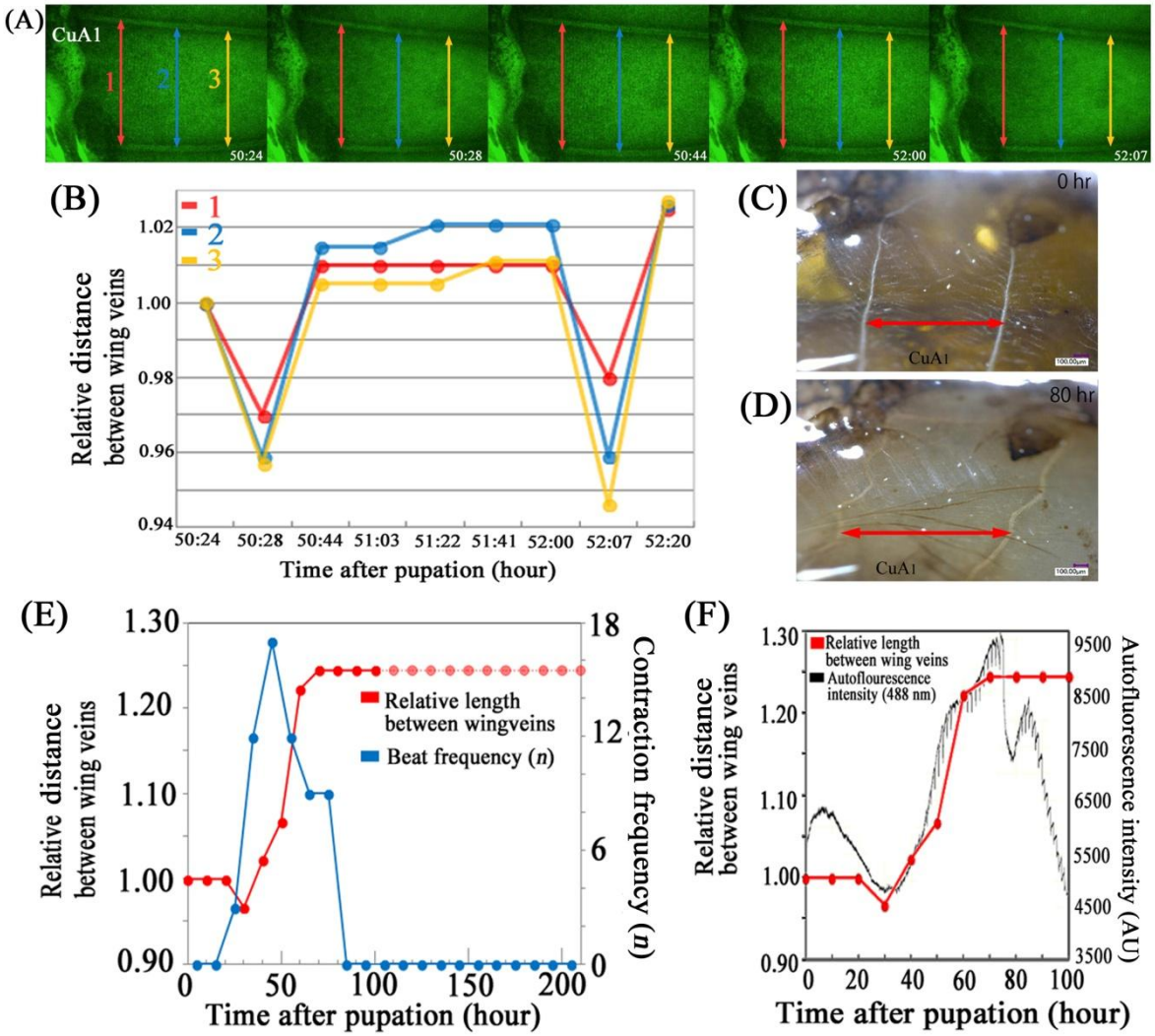

Fig. 1-8. Distance changes associated with the wing-tissue contraction pulses and autofluorescence intensity. (A) Three distance measurements (red, blue, and yellow double-headed arrows, designated 1, 2, and 3, respectively) between the two veins that define compartment CuA_1. The postpupation time is also indicated. All panels are shown at the same magnification. These are static images from Movie S3. **(B)** Changes in length (distance) between the two wing veins over time. The measured distances are indicated in (A). These measurements were conducted using Movie S3. **(C, D)** Images of the distances between the wing veins at 0 h and 80 h postpupation in compartment CuA_1. These panels are at the same magnification, showing static images from Movie S6. These images of the wing of a physically fixed pupa were taken at the same position at different time points, and the distances were measured between the two

points despite the tilting of the wing veins relative to the double-headed red arrows as the wing grows. **(E)** Relative distance between the wing veins in compartment CuA_1, as shown in (C, D) (indicated with red dots and lines), and the contraction frequency (shown in blue dots and lines). The distance at 0 h was considered to be 1.00, and other values were normalized accordingly. The broken lines indicate difficulty in measuring the distance, but no change appeared to occur afterwards. Note that an increase of the contraction frequency is followed by an increase in this distance in the early phase, and a decrease of the beat frequency is followed by the distance plateauing. These measurements were conducted using images from Movie S6. **(F)** The relative distance between the wing veins, as shown in (E) (measured from Movie S6), and the autofluorescence intensity (measured from Movie S3). The autofluorescence intensity increases together with the relative length between the wing veins.

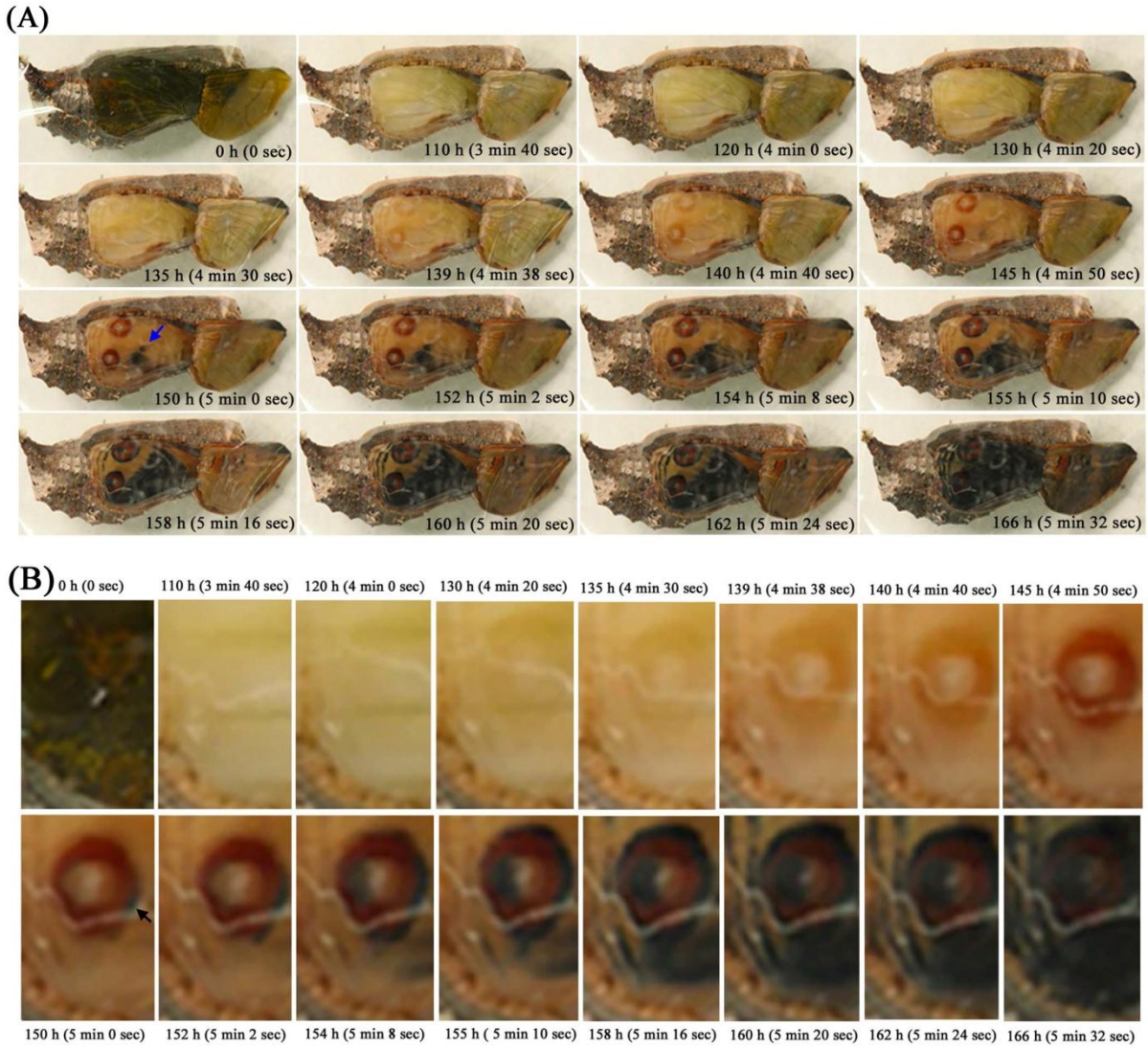

Fig. 1-9. Ontogeny of the pigment deposition process at the whole-wing level. Real time points are shown along with the playing time points from Movie S1 (in parentheses). **(A)** Changes in the whole wing. The background black coloration emerges at the center of the wing (indicated by an arrow at 150 h). **(B)** High-magnification images of the eyespot. The red ring is produced first, and the black ring is produced at a single location at 150 h (indicated by an arrow). The black ring then develops around the red ring. Later, the width of the black ring expands considerably.

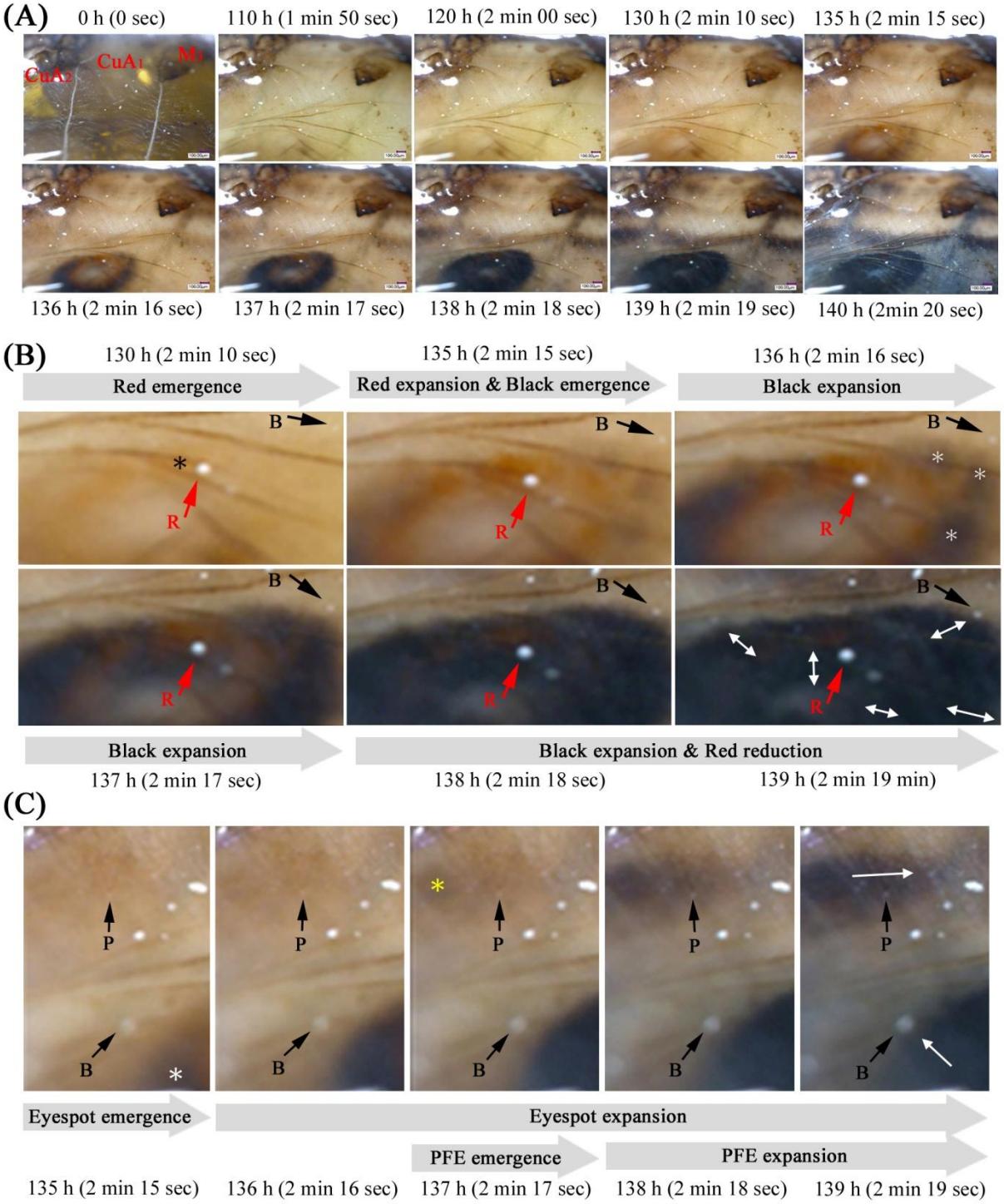

Fig. 1-10. Ontogeny of the pigment deposition process at the compartmental level. Real time points are shown along with the playing time points from Movie S6 (in parentheses). **(A)** The changes in CuA_1 and its adjacent compartments. **(B)** High-magnification images of CuA_1 compartment. The eyespot red ring develops first.

A possible red fragment is indicated by a black asterisk at 130 h. Black fragments are indicated by white asterisks at 136 h. Black and red arrows indicate artifactual objects that can be used as physical reference points. Reference point R is located in the middle of the red ring at 135 h but is gradually invaded by the black ring. Reference point B is located far from the black ring at 136 h, but the black ring reaches it at 139 h. The directions of black ring expansion are indicated by double-headed white arrows in the image from 139 h. **(C)** Another high-magnification image. Reference point B is located far from the black fragment (indicated by a white asterisk) at 135 h, but the black region reaches it at 139 h. Reference point P is located far from the black region at the center of the prospective parafocal element (indicated by a yellow asterisk), but the black region later expands laterally to cover the reference point P entirely. The directions of expansion of the black pigment are indicated by white arrows in the image from 139 h.

Chapter 2: Spatial patterns of scale size in relation to color pattern elements

2.1. Introduction

Introduction

Complex and diverse butterfly wing color patterns are believed to arise through modifications of a basic color pattern model called the nymphalid groundplan (Schwanwitsch, 1924; Süffert, 1927; Nijhout, 1991, 2001; Otaki, 2009, 2012a). The nymphalid groundplan comprises 3 major symmetry systems (the central, basal, and border symmetry systems) and 2 additional peripheral systems (the wing root and marginal band systems) (Otaki, 2012a). Each unit of a single symmetry system has a core element at the center and a pair of paracore elements on both the proximal and distal sides of a core element (Otaki, 2012a). The developmental mechanisms of these 5 systems are likely similar (Otaki, 2012a; Taira et al., 2015).

Among color pattern elements, eyespots are perhaps most conspicuous; they are the core elements of the border symmetry system. Transplantation and physical damage experiments have shown that a prospective eyespot focus functions as a source of morphogen for the eyespot (French and Brakefield, 1992, 1995; Nijhout, 1980a, 1985, 1991; Brakefield et al., 1996; Otaki et al., 2005; Otaki, 2011c). The prospective eyespot foci correspond to the areas of expression of some genes such as *Distal-less*, *Notch*, *engrailed*, and *spalt* during late larval wing development (Carroll et al., 1994; Keys et al., 1999; Monteiro et al., 2006, 2013), although the function of these genes in the context of eyespot development is not well understood.

According to the concentration gradient model for positional information, a putative morphogen diffuses from an organizing center and forms eyespot patterns based on the concentration gradient of morphogen molecules and based on thresholds for morphogen concentration that are predetermined in immature scalebuilding cells (or simply, scale cells) (Nijhout, 1978, 1981, 1991). However, this model is intended

to explain an ideal concentric eyespot ring, and actual butterfly eyespots are too complex to be explained by this simple model (Otaki, 2011a). As an alternative model, the induction model has been proposed based on observations of actual diverse butterfly eyespot patterns (Otaki, 2011b). Thus, the induction model is more capable of explaining actual diverse butterfly wing color patterns and damage-induced and temperature-induced color pattern changes than is the gradient model (Otaki, 2011c, 2012a,b; Taira et al., 2015; Iwata et al., 2013, 2015). The induction model is mechanistically based on repetitive and nested pattern generators that enhance a nearby signal and inhibit a distant signal simultaneously, similar to a reaction–diffusion model (Otaki, 2011b, 2012b).

Although it is difficult to identify a morphogen for color patterns by simple observational studies, a hint of the mechanisms of color pattern determination may be obtained by examining scale size distribution patterns. A few studies have shown the proximodistal size gradient of scales in lepidopteran insects (Kristensen and Simonsen, 2003; Simonsen and Kristensen, 2003) and a correspondence between scale color and scale microstructure (Jansen et al., 2001). The proximodistal size gradient of scales is likely generally observed in Lepidoptera (Kristensen and Simonsen, 2003; Simonsen and Kristensen, 2003). However, spatial scale color–size relationships on a single wing were first discovered by Kusaba and Otaki (2009), in which a reasonable correspondence between scale color and scale size was detected in *J. orithya* and *J. oenone*. Scale size distribution analyses have revealed a size gap between the black and non-black rings of a single eyespot and that eyespot foci have scales that are larger than their surroundings (Kusaba and Otaki, 2009). We also found a proximodistal size gradient in *Vanessa cardui* and *Danaus chrysippus*, although the gradient of the latter species was small (Dhungel and Otaki, 2014). On the basis of these data, we proposed that a morphogenic signal that is released from a prospective eyespot focus determines scale size as well as color (Kusaba and Otaki, 2009) and that this signal is a train of wave-like pulses, as described in the induction model (Otaki, 2011a–c). Because scale

size is probably determined by the size of scale cells, and because cell size can be altered by cell ploidy, we speculated that morphogenic signals for scale size and color may be identical to ploidy signals (Kusaba and Otaki, 2009; Dhungel and Otaki, 2014). From this perspective, the characterization of scale cell development is required to understand the nature of the putative morphogenic signal. Although scale cell development has been observed in some studies (Nardi and Magee-Adams, 1986; Cho and Nijhout, 2013; Ohno and Otaki, 2015a) (see Chapter 1), basic information on developmental morphological changes remains scarce, and exact relationships and interactions between scale size and scale color have been reported only in *J. orithy*a and partially in *J. oenone* (Kusaba and Otaki, 2009).

To test if the scale color–size relationship is a general feature in butterflies and to understand the relationship more deeply, in the present study, we mainly focused on scale size distribution on the hindwings of the peacock pansy butterfly *J. almana* (Nymphalidae, Nymphalinae). This butterfly provides us with an excellent system to investigate wing color pattern determination for the following reasons: (1) it has distinct large eyespots with sharp color boundaries, (2) it has a relatively large orange background area without a color pattern element, (3) it is useful for physiological and damage experiments (Otaki, 2007, 2011c), (4) it has a relatively large wing size resulting in high-resolution analysis (Otaki, 2007, 2011c), and (5) its scale size can easily be measured under a digital microscope because its wing surface is not hairy. For comparison, we also used the dorsal hindwings of other 2 nymphalid species, *V. indica* and *D. chrysippus*, which do not have eyespots. We establish here the relationship between scale color and scale size in nymphalid butterflies, which is probably applicable to other butterflies in general. We also discuss the nature of morphogenic signal for scale color and scale size based on the present and previous results.

2.2. Materials and Methods

Butterflies

Three species of nymphalid butterflies were used for scale size measurements in this study: *J. almana* (Nymphalinae), *V. indica* (Nymphalinae), and *D. chrysippus* (Danainae). Adults or larvae were collected on Okinawa-jima Island or Ishigaki-jima Island of the Ryukyu Archipelago, Japan. Eggs were obtained from field-caught adult females. Larvae were fed their natural host plants at approximately 27 °C. Adults were frozen immediately after eclosion to avoid physical damage to their wings.

We mainly focused on the hindwing of *J. almana* (Fig. 2-1), which is phylogenetically related to *J. orithya* (Kodandaramaiah and Wahlberg, 2007). This species has a relatively large eyespot called the major eyespot in the Rs and M_1 compartments. The scale size of *V. indica* and *D. chrysippus* was also measured for comparison; these species do not have any eyespot. Color pattern elements and their components were defined as shown in Figs. 2-1 and 2-3, based on the terminology of Nijhout (1991), Scott (1986) and Otaki (2007).

Scale observations and measurements

We observed scales under a Keyence VHX-1000 digital microscope with or without a polarization illumination adaptor (Osaka, Japan). Scale measurements on hindwings were made following the protocol established by our previous study (Kusaba and Otaki, 2009). Briefly, we measured the maximum width of cover scales as scale size (see Fig. 2-1A). In some exceptional regions where identification of cover scales from ground scales was difficult, scales that were measurable in our system were considered cover scales. For the wing-wide measurements, 5 scales were selected to measure the scale size every 1 mm from wing base to wing margin along straight lines. The raw datasets of 5 scales were averaged as the scale size of that particular location. These measurements were made from 3 individuals per species. To examine a general size

distribution pattern for each species, the data from 3 individuals were combined and normalized to 1.0 at 0 mm (at the wing base). In addition, 5 scales were selected for measurements of every scale row within the eyespot and marginal areas. For this analysis, 2 individuals were used per species.

Physical damage experiment

Only one side of the wings of *J. almana* was damaged with a stainless needle (0.50 or 0.65 mm in diameter) within 18 h postpupation to induce an ectopic eyespot. The contralateral wing was left untouched and used as an internal control. The operated pupae were kept at approximately 27 °C. The operated adults were readily frozen immediately after eclosion, and 11 individuals that had ectopic color patterns were subjected to morphological analyses for scale shape, color, and size using the digital microscope described above. A quantitative comparison of scale size between the treated and non-treated dorsal hindwings (right and left wings) in the same individual was made every 1 mm from the wing base to the wing margin along straight lines, as mentioned above, using 3 individuals. To make it easier to compare scale size distribution patterns between the right and left wings, these raw data were normalized so that the scale size at the starting point for measurements at 0 mm (at the wing base) was 1.0. We also examined 4 individuals that showed no or small color pattern changes. For this purpose, physical damage was applied to the basal location where ectopic induction of color patterns is known to be difficult (Brakefield and French, 1995).

2.3. Results

Scale color distribution in eyespots

We first observed the scale color distribution pattern of *J. almana* on the dorsal hindwing, which has major and minor eyespots (Fig. 2-1). An eyespot was divided into three components: a black ring, a yellow ring, and an eyespot core (EC) (Fig. 2-1). The dorsal major eyespot core comprised red, black and blue areas and two foci (Fig. 2-1A), indicating that the major eyespot is a fusion of two eyespots. The red area was located on the proximal side, and the black area and the blue area were located on the distal side. The blue scales that characterize the blue area were found mainly in the Rs compartment, while fewer were found in the M_1 compartment.

Similarly, the ventral major eyespot core consisted of orange, black and blue areas and two foci (Fig. 2-1B). The orange area was located on the proximal side, the black area on the distal side, and the blue area on both sides. The blue scales that characterize the blue area were found mainly in the Rs compartment, similar to the dorsal side.

All of the scales of the eyespot foci on the dorsal and ventral hindwings were white and semi-transparent (Fig. 2-1). When a polarization illumination adaptor was used on the microscope, the blue scales of the blue area became semi-transparent, indicating that the blue color is structural but not pigment-based (Fig. 2-2). These observations suggest that the blue scales in the blue area are a focal expression that is essentially similar to that of focal white scales.

Scale size distribution along proximodistal lines

Scale size measurements were made along 3 lines (lines a, b and c) from the wing base to the outer margin in *J. almana* (n = 3 for each line) (Fig. 2-3A and B). On the dorsal and ventral sides of the hindwings, all 3 lines showed an overall similar tendency: the size gradually decreased toward the wing margin (Fig. 2-3A and B). However, 2 lines

(lines a and b) passing through the major eyespot also showed a few size peaks at the eyespot core (EC) and at the parafocal element (PFE) (Fig. 2-3A and B). These results are consistent with the previous results of *J. orithya* (Kusaba and Otaki, 2009). In contrast, line c, passing through a non-eyespot area on the dorsal side, did not show such size peaks, except for possible small peaks at the PFE and at the submarginal band (SMB) (Fig. 2-3A). Line c on the ventral side showed a large size peak at the central band (CB) as well as at the SMB (Fig. 2-3B). It is to be noted that the white band in this species is the distal band of the central symmetry system (dBC) (Otaki, 2012a), that the PFE is a paracore element of the border symmetry system (Dhungel and Otaki, 2009; Otaki, 2009, 2012a), and that the SMB belongs to the marginal band system (Otaki, 2012a; Taira et al., 2015).

If these size peaks depend on color pattern elements, there would be no peak in other species that have few color pattern elements. To test this hypothesis, *V. indica* (n = 3) and *D. chrysippus* (n = 3) were subjected to the scale size measurements along a line from the wing base to the wing margin, passing through the M_1 compartment, where *J. almana* has a major eyespot. As expected, unlike *J. almana* and *J. orithya*, neither *V. indica* nor *D. chrysippus* showed any conspicuous size peaks; both species showed a decreasing tendency in scale size from the beginning of the basal area to the end of the margin (Fig. 2-3C and D), although this tendency in *D. chrysippus* was relatively small.

Scale size distribution within an eyespot

If the putative morphogenic signal for eyespot coloration also codes for scale size directly, the peak scale size would correspond to the organizing position that releases the signal. Alternatively but not mutually exclusively, as the induction model predicts, scale size may correspond to the peaks of the released signal itself. However, if the signal is coded by a concentration gradient that covers an entire eyespot, as the gradient model predicts, the size distribution could show gradual changes throughout

an eyespot despite color gaps. To examine these possibilities, scale size measurements were performed every scale row from the proximal to distal areas that cover the entire major eyespots on the dorsal and ventral sides of the *J. almana* hindwings (*n* = 2 for each line) (Fig. 2-4).

On both the dorsal and ventral sides, scale size fluctuated at every row, indicating that the final size is partially determined stochastically. Interestingly, in the Rs compartment on the dorsal side, the focal white area did not show any size peak but showed a gradual increase from the focal white area to the end of the blue area of the eyespot core (Fig. 2-4A). In contrast, in the M_1 compartments, the focal white area showed a size peak (Fig. 2-4B). Importantly, in both compartments, scale size suddenly decreased at the end of the eyespot core (EC), where the color changes from black (or blue) to yellow. Additionally, the outermost black ring had a small size peak at the distal side in an individual (Fig. 2-4B, right).

Essentially, similar results were obtained in the ventral eyespots, except that the positional discrepancy between the focal white area and the size peak was not observed in the ventral eyespots (Fig. 2-4C and D).

Scale size distribution in the peripheral area

To examine size changes at the peripheral black elements such as PFE, SMB, and MB (marginal band), we measured scale size every row along a line from a given point of the proximal side to the wing margin in the Rs and M_1 compartments on the ventral and dorsal sides of the *J. almana* hindwings (*n* = 2 for each line) (Fig. 2-5). In every case, the size peak was detected at the PFE (Fig. 2-5A–D). Ventrally, one of the two individuals that were examined showed a clear size peak at the SMB in the Rs and M_1 compartments (Fig. 2-5C and D, right). The peak at the MB was not clearly distinguishable from the fluctuation in scale size.

Similar measurements were performed in the M_1 compartment of *V. indica* and *D. chrysippus* on the dorsal side (*n* = 2 for each species) (Fig. 2-6). In *V. indica*,

both of the individuals showed a size peak at both the black spot (BS) and the PFE (Fig. 2-6A). In *D. chrysippus*, both of the individuals showed a small size peak at the marginal black region (MBR), with no other peak in the orange background area (Fig. 2-6B).

Scale color, size, and shape in an ectopic eyespot

To examine the morphological features of ectopic eyespots, we inflicted physical damage to the right or left side of the *J. almana* hindwings at the early pupal stage with a needle and induced an ectopic eyespot in a non-elemental background area (in the M_3 compartment) (n = 11) (Fig. 2-7). On both treated and non-treated dorsal hindwings of the same individual, the scale size was measured every 1 mm along a line from the basal to marginal areas (n = 3). This line spanned the area between the major and minor eyespots. All of the treated wings clearly showed a large size peak at the ectopic eyespot. In contrast, all of the non-treated wings did not show any size peak in the orange background area corresponding to the ectopic eyespot of the treated side (Fig. 2-7).

In addition, we observed morphological structures of scales that constitute an ectopic eyespot in the treated wing, which were compared with those of scales that constitute a background area in the non-treated wing at the same location in the same individual (n = 11). In the non-elemental background area of the non-treated wing in the M_3 and CuA_1 compartments, almost all of the scales were jagged with an orange background color (Fig. 2-8A–F). In contrast, the ectopic eyespot that was induced by physical damage at the same location had smooth scales with a yellow or black color in addition to jagged scales (Fig. 2-8G–L). In both the ectopic and natural minor eyespots, the eyespot core area that was surrounded by the yellow ring was almost exclusively composed of jagged scales, but the outermost black ring and the yellow ring were composed of jagged and smooth scales (Fig. 2-8D–L). Importantly, in the ectopic eyespot, the focal scales were much larger than the surrounding scales (Fig. 2-8G–I).

These observations suggest that a physically induced putative signal that specifies an ectopic eyespot alters the cellular fate not only for scale color but also for scale size and scale shape. Thus, the patterns of color, size, and shape become similar to those of a natural eyespot. However, the focal white or blue scales with a structural color, as observed in a natural eyespot, were not induced by physical damage.

Physical damaged with no or small color changes

To investigate whether physical damage that does not induce ectopic color patterns still causes scale size changes, we observed a sample that happened to fail to induce color patterns at the position where other individual had color pattern induction. In addition, we performed physical damage at the basal position where color pattern induction is highly difficult (Fig. 2-9A–E). In the two cases examined in which damage was completely healed, there were no size changes detected (Fig. 2-9B and C). In other two cases, individuals had small color pattern changes near the damage sites that were easily identifiable (Fig. 2-9D and E). A possible increase of scale size was observed, mostly in ground scales, which was associated with the damage sites (Fig. 2-9D and E). Only a single scale that was relatively large was found in one individual (Fig. 2-9D).

Dislocation of the focal white area

In the Rs compartment of the dorsal major eyespot, the focal white area was located proximally from the location of the largest scales (see Fig. 2-4A). This positional discrepancy was not clearly observed in the other compartments of this species, although small degrees of discrepancy may exist in other compartments (see Fig. 2-4B–D). To obtain insight into this discrepancy, we compared the locations of the major eyespots of the dorsal and ventral sides in a single individual (Fig. 2-10). Because the ventral major eyespot had the focal white area and the largest scales at the same location (see Fig. 2-4C), the corresponding location of the dorsal side may

indicate the original focal location.

The superimposition of the dorsal and ventral images readily showed that the ventral focus was located at the distal side from the focal white area of the dorsal side (Fig. 2-10). That is, the ventral focus (VF) and its associated blue area (BA) corresponded to the dorsal size peak more closely (also see Fig. 2-4A). It is likely that the focal white area on the dorsal side is dislocated toward the basal side from the original position that is indicated by the largest scales.

To support this idea, we found similar cases of focal white dislocation in other nymphalid butterflies, where the focal white area is likely dislocated proximally, distally, or anteriorly (Fig. 2-11A and B). Furthermore, the focal area can be deformed (Fig. 2-11C). It is likely that the dislocation and deformation of the focal white area are occasionally observed in nymphalid butterflies.

2.4. Discussion

Color-size correspondence in elements

In the present study, a reasonable correspondence between the scale size and color pattern element on wings was demonstrated in the nymphalid butterflies *J. almana*, *V. indica* and *D. chrysippus*. Within a major eyespot on the *J. almana* hindwing, a size peak was observed in the eyespot focal area or nearby. Importantly, not only a focal area but also the outermost black rings of an eyespot and peripheral elements, including PFE and SMB, exhibited size peaks when the size was scanned along a proximodistal line, probably indicating the developmentally homologous status of these rings to an eyespot core. Even in *V. indica* and *D. chrysippus*, which have few color pattern elements on their dorsal hindwings, a small but detectable increase in scale size was observed at color pattern elements of the peripheral area, but the scale size did not increase in a non-elemental area. Furthermore, a central band on the ventral side had a scale size peak, demonstrating that this band is an element that is similar to the focal white area in an eyespot (Otaki, 2012a).

These findings suggest that an increase in scale size at the center of an element is likely a general rule in nymphalid butterflies and that an increase in scale size in the peripheral area is induced by an organizing center for each peripheral color pattern element, being consistent with the nested nature of the symmetry system (Otaki, 2012a). This color–size correspondence seems to be conserved in the dorsal and ventral wings; we did not detect any qualitative difference between the dorsal and ventral sides of the hindwing in terms of spatial patterns of scale size. Because correspondence between color and size has also been demonstrated in *J. orithya* and *J. oenone* (Kusaba and Otaki, 2009), it is possible that this correspondence may be conserved in many nymphalid butterflies.

On the basis of the size peak that corresponds to the outermost black ring of the major eyespot, we believe that the black ring is equivalent to the PFE, a physically

separate entity of the border symmetry system (Otaki, 2012a). This interpretation is consistent with the results of color pattern analysis (Otaki, 2009, 2011a), pharmacological color pattern modifications (Dhungel and Otaki, 2009), and simulations based on the induction model (Otaki, 2011b, 2012b).

Color-size correspondence in background

In addition to the elemental peaks, our morphometric analyses in *J. almana*, *V. indica*, and *D. chrysippus* showed a basal peak, after which a decreasing tendency of scale size from the basal to peripheral background area was observed. In the case of *J. orithya*, the blue ‘‘background” area is likely equivalent to an expanded element (Kusaba and Otaki, 2009). Interestingly, the blue coloration that covers a wide wing area in *J. orithya* emerges from the postbasal area and expands toward the distal areas during development (Kusaba and Otaki, 2009). Within a blue area, scale size is graded: scales are larger on the basal side than on the distal side. Moreover, the blue area is confined at the basal side when treated with heat shock or thapsigargin, a general stress inducer (Mahdi et al., 2011). The confinement of the blue area can also be made by physical damage that blocks expansion of the putative signal from the postbasal to distal areas (Mahdi et al., 2011). Interestingly, phylogenetically related species such as *J. oenone*, *J. hierta*, and *J. westermanni* have a small blue area at the postbasal position (Kusaba and Otaki, 2009; Mahdi et al., 2011).

These results suggest that a morphogenic signal for color and size for the blue area is released from an organizing center in the postbasal area. In this sense, the blue area that is usually considered background in *J. orithya* (because it covers a wide wing area) may be an expanded element. The morphogenic signal for the blue area is probably graded, as suggested by the graded scale size. The graded scale size was also observed in the eyespot core in this study (see Fig. 2-4). In the induction model, this gradation may be explained by a gradual deceleration of the signal after being released with a given initial velocity (Otaki, 2011b, 2012b; Iwata et al., 2015).

At first glance, the orange background area of *J. almana* does not have morphological similarity to the blue area of *J. orithya*. However, the posterior orange area in *J. almana* may be equivalent to the expanded element. The fact that we observed similar graded size changes in the ‘‘background” area may suggest that the ‘‘background” formation mechanism may be similar to the elemental formation mechanism. These results further suggest the existence of a long-range signal by which the wing-wide coloration is organized along the proximodistal axis of the hindwing.

Dislocation of the focal white area

A clear positional discrepancy between the size peak and the focal white area in the Rs compartment of *J. almana* requires some explanation. We believe that the location of the size peak (not of white scales) corresponds to the location of an eyespot organizing center because the dorsal major eyespots are distorted proximally, as shown by the corresponding location of the ventral eyespot (see Fig. 2-10). Interestingly, the blue scales are found in the location of the scale size peak (i.e., in the blue area), which may indicate that an organizing center is located in that area. Furthermore, similar cases of dislocation of the focal white area were observed in other butterflies. The focal white area appeared to be flexibly positioned in relation to the whole eyespot. Focal scales may be specified by a unique mechanism beyond the induction model.

In the pupal forewings, the prospective eyespot foci were marked by pupal focal cuticle spots and marks on the surface of pupae in many nymphalid butterflies (Otaki et al., 2005). The cellular size peak probably corresponds to these external structures. Furthermore, in the pupal hindwings, scale cells at the prospective eyespots have a character that is optically different from the rest of the scale cells in fluorescent microscopy (Ohno and Otaki, 2015a,b) (see Chapter 1). These facts are probably a reflection of the large cell size at an organizing center.

Thus, it is likely that the size was determined first and that the focal white coloration was determined secondarily. The coloration decision for immature scale

cells is indeed influenced by surrounding factors such as ecdysteroid (Sawada et al., 2002; Koch et al., 2003; Otaki et al., 2005; Otaki, 2007), temperature shock and cold-shock hormone (CSH) (Otaki, 2007, 2008), adjacent eyespots and other elements (Otaki, 2011c), and the putative proximodistal gradient that covers the entire wing for the ‘‘background” size gradient (Nijhout, 1981; Kusaba and Otaki, 2009; present study). The dislocation and distortion of coloration (but not size) may be a common feature that may be used for color pattern evolution (Otaki, 2008, 2011a; Hiyama et al., 2012). One of the most important features of the color pattern modifications of the temperatureshock (TS) type is indeed a proximal displacement of PFEs (Otaki, 2008). Considering the nested nature of color pattern constructions in butterflies, we speculate that a mechanism that is similar to the TS-type modifications operates in focal (and eyespot) displacement.

Ectopic eyespot

The scale size distribution pattern within an ectopic eyespot that was induced by physical damage was examined for the first time in the present study and was similar to the pattern within a natural eyespot. In both ectopic and natural eyespots, scales at the center were larger than those in the surroundings. Physical damage certainly affected scale size in addition to color, suggesting that the putative organizing signals for color patterns that were experimentally induced by physical damage can also determine scale size. We also examined whether physical damage that does not induce color patterns can induce size changes or not. Our observations prefer an interpretation that size changes of cover scales occur most often in association with color changes. These results, in turn, support the idea that ectopically induced eyespots by physical damage are produced in a manner that is identical to natural eyespot development. It will be interesting to examine ploidy state in damage-associated scale cells in the future (see below).

Color, scale size, cell size, and ploidy

How is the color–size relationship produced? One possibility is that color and size may be regulated by two independent molecular mechanisms despite their mutual interactions. A more simple explanation is that the color and size of scales may be regulated together by a single signal from the organizing center. Butterfly wing scales have many functions (Yoshida, 2014), but because it is difficult to imagine any phenotypic functional advantage for the scale size variation, we believe that the size difference is a byproduct or an unavoidable consequence that is associated with the color pattern determination process during development. Considering that a single scale is produced by a single cell (Nijhout, 1991), it is likely that large and small scales are produced by large and small scale cells, respectively.

Henke (1946) demonstrated that in the wing of the flour moth *Ephestia kühniella*, there are 4 scale types: cover scales (largest in size), middle scales, ground scales, and lower ground scales (Sondhi, 1963). It is reported that the larger a scale is, the larger the number of ploidy is among the 4 scale types. That is, cover scales have the highest number of ploidy than the other types of scales. However, spatial distribution patterns of scale size was not studied well in Henke (1946). The present study used a butterfly *J. almana*, focusing on spatial distribution patterns of cover scale size. We also focused on spatial relationship between size and color pattern at the level of single scale. Although *J. almana* provides us with a system much simpler and clearer than *E. kühniella*, we believe that our results can be applicable to other butterflies and moths including *E. kühniella* and vice versa.

Henke (1946) and Henke and Pohley (1952) further posited so-called Henke's law of compensation or Henke's compensation principle, which states that the number of endomitotic divisions of presumptive scale cells and the number of mitotic divisions of nonscale-forming epithelial cells from a single lineage add up to a constant number in any scale types (Sondhi, 1963; Cho and Nijhout, 2013). We speculate that a group of cells from a single stem cell may be physically connected with each other with

epidermal feet and with cytonemes or nanotubes, forming a cluster of cells (Ohno and Otaki, 2015a) to regulate the total number of genomic amplifications.

Ploidy hypothesis

It has been demonstrated that polyploidization causes a cellular volume increase in scale cells in *Manduca sexta* (Cho and Nijhout, 2013). Except *E. kühniella* and *M. sexta*, polyploidy has not been demonstrated in lepidopteran wings. However, we have already reported emergence of large cells with large nuclei in pupal developing wings in *J. orithya in vivo* (Ohno and Otaki, 2015a). Thus, we believe that polyploidization could be widespread in butterflies and moths. In this line of discussion, the degrees of polyploidy could influence scale size and scale color (Fig. 2-12). We propose the ploidy (gene dosage or genome amplification) hypothesis, which states that gene dosage determines scale size through cell size. This hypothesis may be reasonable in that high gene dosage produces high levels of cuticle synthetases for scale production, simply because of a high copy number of genes. The large cell size also means that a large amount of materials for scale production are available. This ploidy hypothesis further states that gene dosage determines scale color because high levels of gene dosage produce high levels of pigment synthetases to produce dark color. High levels of melanin synthesis may result in black color in elements, whereas low levels may result in orange or yellow colors in *J. almana*. Considering that in insects and other organisms, a cell size increase through polyploidization is utilized for cell growth, high metabolic activity, and gene amplication in many systems (Edgar and Orr-Weaver, 2001), the butterfly wing system may also take advantage of polyploidization for color pattern expression.

We admit that the ploidy hypothesis cannot explain usage of different pigment families. The major butterfly pigments are categorized into a few or more groups, and melanins and ommochromes are two major pigment families in nymphalid butterflies (Nijhout, 1991). According to the binary rule for eyespots (Otaki, 2011a,b), a lightly

colored ring within an eyespot (between darkcolored rings) is equivalent to background, but elaborate eyespots have a complex coloration between dark rings that is different from background color (and thus probably different pigment chemicals), and in that case, the ploidy hypothesis would not be applicable. In the case of *Junonia coenia*, the pigments for the red ring colors are likely ommochromes (Nijhout, 1991), which are regulated differently from melanins.

Moreover, the determination process of the focal white or semitransparent coloration cannot be explained well by the ploidy hypothesis. Focal white scales contain pteridines (Nijhout, 1980b), express structural color, can be dislocated from an organizing center, can be diffused around an organizing center as the blue scales in the blue area, and cannot be induced by physical damage. These aspects of the focal white scales need to be explained beyond the ploidy hypothesis.

Despite these limitations, we believe that the ploidy hypothesis is worth testing further. A switch between pigment families may be dependent on genome dosage. In the eastern tiger swallowtail butterfly *Papilio glaucus*, which has two color pattern forms, yellow wing area (defined by papiliochrome) develops earlier than black wing area (defined by melanin), and this temporal order is recapitulated by dopa decarboxylase expression (Koch et al., 1998). Furthermore, an enzyme called *N*-β-alanyldopamine synthase (BAS) is responsible for directing dopamine away from melanin synthesis and toward papiliochrome synthesis (Koch et al., 2000a–c). Because papiliochrome and melanin share their precursor dopamine, gene dosage may determine which pathway is active if there is a threshold level of gene dosage for this switch. It is interesting to know if cell size (and ploidy) may correspond to wing colors in *P. glaucus* and other butterflies. In *J. orithya*, we demonstrated that color patterns emerge from the basal to peripheral areas and from elements during development (see Chapter 1). This time sequence is in parallel with the scale size (and possibly cell size) distribution patterns in *J. orithya* (Kusaba and Otaki, 2009) (see Chapter 1) and in *J. almana* (the present study), although confirmation of a sequence of color pattern

development with *J. almana* is required. If so, a time sequence of color pattern emergence is a recapitulation of cell size and scale size.

Ploidy and morphogenic signals

The ploidy hypothesis states that a morphogenic signal from an organizing center is a ploidy signal, which may be a train of wavelike pulses as the induction model predicts (Fig. 2-11). We have provided indirect evidence for the induction model by color pattern analysis (Otaki, 2011a,b, 2012b), physical damage experiment (Otaki, 2011c), developmental coloration time course (Kusaba and Otaki, 2009) (see Chapter 1), and morphometric analysis (Kusaba and Otaki, 2009; present study). In the present study, we showed that the size boundary often corresponds to the color boundary, which may be considered supporting evidence for the induction model. This sudden size change at the boundary is consistent with the idea of the induction model that the morphogenic signal for color pattern determination is not smoothly distributed within an eyespot.

However, the nature of the signal is not well understood. To this end, we have devised a method for characterizing epithelial cells *in vivo* in real time (Ohno and Otaki, 2015a,b) (see Chapter 1). We also discovered calcium waves that travel long distance slowly in developing wings (Ohno and Otaki, 2015b). On the basis of the thapsigargin injection experiment, which alters scale color and the size of the blue area in *J. orithya* (Otaki et al., 2005b; Mahdi et al., 2011; Ohno and Otaki, 2015b), calcium waves may play a role in wing-wide phenotypic determination in butterflies. In the future, these aspects should be understood together as a system of wing development.

2.4. References

Brakefield, P.M., French, V., 1995. Eyespot development on butterfly wings: the epidermal response to damage. Dev. Biol. 168, 98–111.

Brakefield, P.M., Gates, J., Keys, D., Kesbeke, F., Wijngaarden, P.J., Monteiro, A., French, V., Carroll, S.B., 1996. Development, plasticity and evolution of butterfly eyespot patterns. Nature 384, 236–242.

Carroll, S.B., Gates, J., Keys, D.N., Paddock, S.W., Panganiban, G.E., Selegue, J.E., Williams, J.A., 1994. Pattern formation and eyespot determination in butterfly wings. Science 265, 109–114.

Cho, E.H., Nijhout, H.F., 2013. Development of polyploidy of scale-building cells in the wings of *Manduca sexta*. Arthropod Struct. Dev. 42, 37–46.

Dhungel, B., Otaki, J.M., 2009. Local pharmacological effects of tungstate on the color-pattern determination of butterfly wings: a possible relationship between the eyespot and parafocal element. Zool. Sci. 26, 758–764.

Dhungel, B., Otaki, J.M., 2014. Morphometric analysis of nymphalid butterfly wings: number, size and arrangement of scales, and their implications for tissue-size determination. Entomol. Sci. 17, 207–218.

Edgar, B.A., Orr-Weaver, T.L., 2001. Endoreplication cell cycles: more for less. Cell 105, 297–306.

French, V., Brakefield, P.M., 1992. The development of eyespot patterns on butterfly wings: morphogen sources or sink? Development 116, 103–109.

French, V., Brakefield, P.M., 1995. Eyespot development on butterfly wings: the focal signal. Dev. Biol. 168, 112–123.

Henke, K., 1946. Über die verschiedenen Zellteilungsvorgänge in der Entwicklungdes des beschuppten Flügelepithels der Mehlmotte *Ephestia kühniella* Z. Biol. Zentralbl. 65, 120–135.

Henke, K., Pohley, H.J., 1952. Differentielle Zellteilungen und Polyploidie bei der

Schuppenbildung der Mehlmotte *Ephestia kühniella* Z. Z. Naturforsch. B 7, 65–79.

Hiyama, A., Taira, W., Otaki, J.M., 2012. Color-pattern evolution in response to environmental stress in butterflies. Front. Genet. 3, 15.

Iwata, M., Hiyama, A., Otaki, J.M., 2013. System-dependent regulations of colourpattern development: a mutagenesis study of the pale grass blue butterfly. Sci. Rep. 3, 2379.

Iwata, M., Taira, W., Hiyama, A., Otaki, J.M., 2015. The lycaenid central symmetry system: color pattern analysis of the pale grass blue butterfly *Zizeeria maha*. Zool. Sci. 32, 233–239.

Jansen, J.M., Monteiro, A., Brakefield, P.M., 2001. Correlations between scale structure and pigmentation in butterfly wings. Evol. Dev. 3, 415–423.

Keys, D.N., Lewis, D.L., Selegue, J.E., Pearson, B.J., Goodrich, L.V., Johnson, R.L., Gates, J., Scott, M.P., Carroll, S.B., 1999. Recruitment of a hedgehog regulatory circuit in butterfly eyespot evolution. Science 283, 532–534.

Koch, P.B., Keys, D.N., Rocheleau, T., Aronstein, K., Blackburn, M., Carroll, S.B., ffrench-Constant, R.H., 1998. Regulation of dopa decarboxylase expression during colour pattern formation in wild-type and melanic tiger swallowtail butterflies. Development 125, 2303–2313.

Koch, P.B., Behnecke, B., ffrench-Constant, R.H., 2000a. The molecular basis of melanism and mimicry in a swallowtail butterfly. Curr. Biol. 10, 591–594.

Koch, P.B., Behnecke, B., Weigmann-Lenz, M., ffrench-Constant, R.H., 2000b. Insect pigmentation: activities of b-alanyldopamine synthase in wing color patterns of wild-type and melanic mutant swallowtail butterfly *Papilio glaucus*. Pigment Cell Res. 13 (Suppl 8), 54–58.

Koch, P.B., Lorenz, U., Brakefield, P.M., ffrench-Constant, R.H., 2000c. Butterfly wing pattern mutants: developmental heterochrony and co-ordinately regulated phenotypes. Dev. Genes Evol. 210, 536–544.

Koch, P.B., Merk, R., Reinhardt, R., Weber, P., 2003. Localization of ecdystone receptor protein during colour pattern formation in wings of the butterfly *Precis coenia* (Lepidoptera: Nymphalidae) and co-expression with Distal-less protein. Dev. Genes. Evol. 212, 571–584.

Kodandaramaiah, U., Wahlberg, N., 2007. Out-of-Africa origin and dispersalmediated diversification of the butterfly genus *Junonia* (Nymphalidae: Nymphalinae). J. Evol. Biol. 20, 2181–2191.

Kristensen, N.P., Simonsen, T.J. 2003. Hairs and scales. In: Kristensen, N.P. (Ed.), Lepidoptera, Moths and Butterflies: Morphology, Physiology, and Development. Handbook of Zoology, Anthropoda: Insecta, vol. IV, Walter de Gruyter, Berlin, pp. 9–22.

Kusaba, K., Otaki, J.M., 2009. Positional dependence of scale size and shape in butterfly wings: wing-wide phenotypic coordination of color-pattern elements and background. J. Insect Physiol. 55, 175–183.

Mahdi, S.H.A., Yamasaki, H., Otaki, J.M., 2011. Heat-shock-induced color-pattern changes of the blue pansy butterfly *Junonia orithya*: Physiological and evolutionary implications. J. Therm. Biol. 36, 312–321.

Monteiro, A., Glaser, G., Stockslagger, S., Glansdrop, N., Ramos, D.M., 2006. Comparative insights into questions of lepidopteran wing pattern homology. BMC Dev. Biol. 6, 52.

Monteiro, A., Chen, B., Ramos, D.M., Oliver, J.C., Tong, X., Guo, M., Wang, W.K., Fazzino, L., Kamal, F., 2013. *Distal-less* regulates eyespot patterns and melanization in Bicyclus butterflies. J. Exp. Zool. 320B, 321–331.

Nardi, J., Magee-Adams, S.M., 1986. Formation of scale spacing patterns in a moth wing, I: epithelial feet may mediate cell rearrangement. Dev. Biol. 116, 278–290.

Nijhout, H.F., 1978. Wing pattern formation in Lepidoptera: a model. J. Exp. Zool. 206, 119–136.

Nijhout, H.F., 1980a. Pattern formation on lepidopteran wings: determination of an eyespot. Dev. Biol. 80, 267–274.

Nijhout, H.F., 1980b. Ontogeny of the color pattern on the wings of *Precis coenia* (Lepidoptera: Nymphalidae). Dev. Biol. 80, 275–288.

Nijhout, H.F., 1981. The color patterns of butterflies and moths. Sci. Am. 245, 104–115.

Nijhout, H.F., 1985. Cautery-induced color patterns in *Precis coenia* (Lepidoptera: Nymphalidae). J. Embryol. Exp. Morphol. 86, 191–203.

Nijhout, H.F., 1991. The Development and Evolution of Butterfly Wing Patterns. Smithsonian Institution Press, Washington, DC.

Nijhout, H.F., 2001. Elements of butterfly wing patterns. J. Exp. Zool. 291, 213–225.

Ohno, Y., Otaki, J.M., 2015a. Live cell imaging of butterfly pupal and larval wings *in vivo*. PLoS ONE 10, e0128332.

Ohno, Y., Otaki, J.M., 2015b. Spontaneous long-range calcium waves in developing butterfly wings. BMC Dev. Biol. 15, 17.

Otaki, J.M., 2007. Reversed type of color-pattern modifications of butterfly wings: a physiological mechanism of wing-wide color-pattern determination. J. Insect Physiol. 53, 526–537.

Otaki, J.M., 2008. Physiologically induced color-pattern changes in butterfly wings: mechanistic and evolutionary implications. J. Insect Physiol. 54, 1099–1112.

Otaki, J.M., 2009. Colour-pattern analysis of parafocal elements in butterfly wings. Entomol. Sci. 12, 74–83. Otaki, J.M., 2011a. Color-pattern analysis of eyespots in butterfly wings: a critical examination of morphogen gradient models. Zool. Sci. 28, 817–827.

Otaki, J.M., 2011b. Generation of butterfly wing eyespot patterns: a model for morphological determination of eyespot and parafocal element. Zool. Sci. 28, 817–827.

Otaki, J.M., 2011c. Artificially induced changes of butterfly wing colour patterns:

dynamic signal interactions in eyespot development. Sci. Rep. 1, 111.

Otaki, J.M., 2012a. Color pattern analysis of nymphalid butterfly wings: revision of the nymphalid groundplan. Zool. Sci. 29, 568–576.

Otaki, J.M., 2012b. Structural analysis of eyespots: dynamics of morphogenic signals that govern elemental positions in butterfly wings. BMC Syst. Biol. 6, 17.

Otaki, J.M., Ogasawara, T., Yamamoto, H., 2005a. Morphological comparison of pupal wing cuticle patterns in butterflies. Zool. Sci. 22, 21–34.

Otaki, J.M., Ogasawara, T., Yamamoto, H., 2005b. Tungstate-induced color-pattern modifications of butterfly wings are independent of stress response and ecdysteroid effect. Zool. Sci. 22, 635–644.

Sawada, H., Nakagoshi, M., Reinhardt, R.K., Ziegler, I., Koch, P.B., 2002. Hormonal control of GTP cyclohydrolase I gene expression and enzyme activity during color pattern development in wing of *Precis coenia*. Insect Biochem. Mol. Biol. 32, 609–615.

Schwanwitsch, B.N., 1924. In the ground plan of wing-pattern in nymphalid and certain other families of rhopalocerous Lepidoptera. Proc. Zool. Soc. Lond. 34, 509–528.

Scott, J.A., 1986. The Butterflies of North America. Stanford University Press, Stanford, CA.

Simonsen, T.J., Kristensen, N.P., 2003. Scale length/wing length correlation in Lepidoptera (Insecta). J. Nat. History 37, 673–679.

Sondhi, K.C., 1963. The biological foundations of animal patterns. Q. Rev. Biol. 38, 289–327.

Süffert, F., 1927. Zur vergleichende Analyse der Schmetterlingsaeinchnung. Biol. Zentralbl. 47, 385–413.

Taira, W., Kinjo, S., Otaki, J.M., 2015. The marginal band system in nymphalid butterfly wings. Zool. Sci. 32, 38–46.

Yoshida, A., 2014. Wing surface of lepidopteran insects (butterflies and moths):

layered structure composed of two kinds of scales. Forma 29, S17–S21.

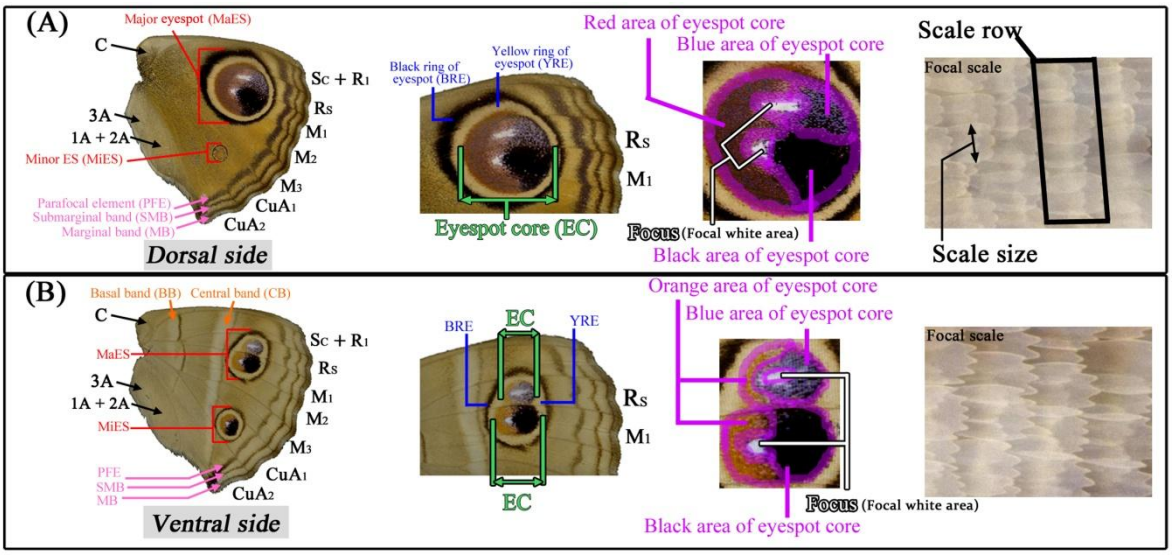

Fig. 2-1. Terminology for color pattern elements on the *J. almana* hindwing. Abbreviations for the elements shown here are used in subsequent figures. Shown are (from left to right) a whole wing, major eyespot, eyespot core of the major eyespot, and scales in the focal white area. **(A)** Dorsal side. Scale size and scale row are defined as shown in the rightmost panel. **(B)** Ventral side.

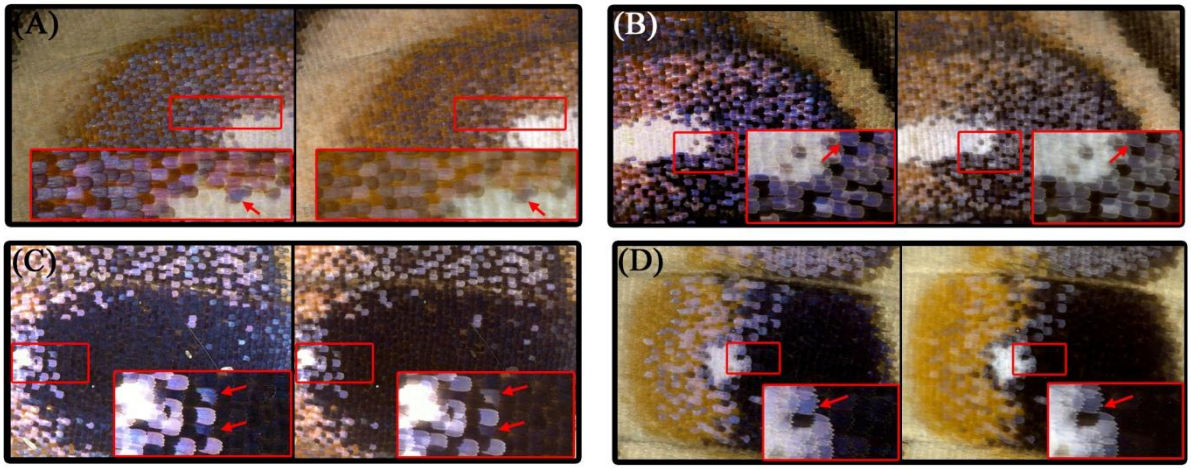

Fig. 2-2. Scales with structural color in the eyespot core of the *J. almana* hindwing. Shown are paired images of the same visual field: a bright field image for pigment color and structural color (left) and a polarized image for pigment color (right). The small boxed areas are enlarged in the adjacent large boxes. Arrows indicate the same scales in the right and left panels. **(A)** Proximal area of the dorsal major eyespot (the Rs compartment). **(B)** Distal area of the dorsal major eyespot (the Rs compartment). **(C)** Distal area of the dorsal major eyespot (the M_1 compartment). **(D)** The ventral major eyespot (the M_1 compartment).

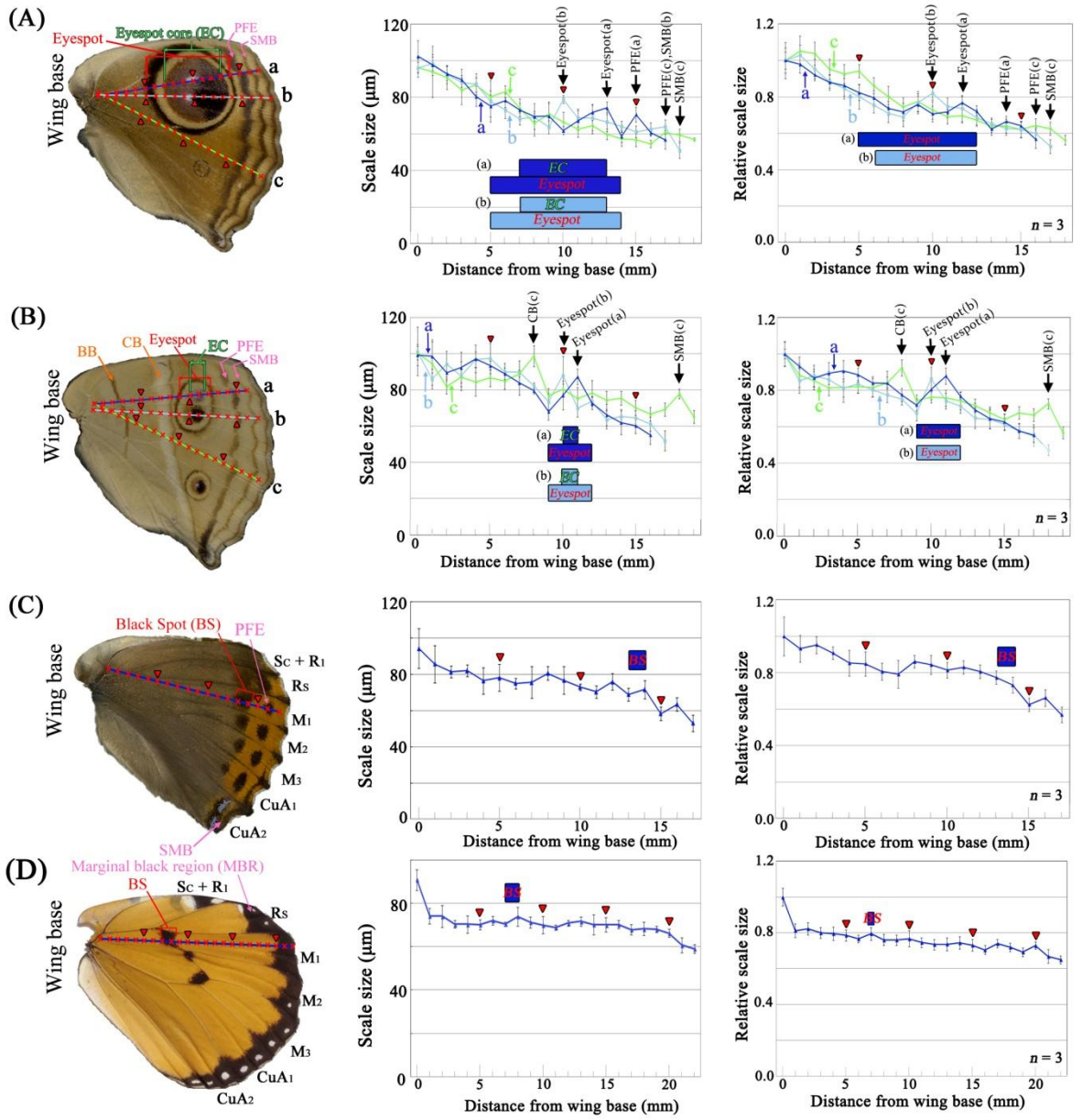

Fig. 2-3. Size distribution of scales on the hindwings of *J. almana*, *V. indica* and *D. chrysippus*. Abbreviations for the elements of *V. indica* and *D. chrysippus* shown here are also used in Fig. 2-6. Shown are (from left to right) a representative hindwing, the representative data from a single wing, and the combined data (n = 3). The representative data (middle) reflect the size distribution of scales on a representative hindwing (left). The size data were obtained from size measurements taken every 1 mm from the basal to distal areas along straight lines, as shown in the left panel. The eyespot and its core areas of *J. almana* and the black spot area of *V. indica* and *D.*

chrysippus are indicated by horizontal bars in graphs. Red arrowheads indicate the points every 5 mm from the starting point (at 0 mm) along a straight line. Error bars in graphs represent standard deviation (SD). Important peaks are indicated by arrows with elemental abbreviations. **(A)** Dorsal side of the *J. almana* female hindwing. **(B)** Ventral side of the *J. almana* female hindwing. **(C)** Dorsal side of the *V. indica* hindwing. **(D)** Dorsal side of the *D. chrysippus* female hindwing.

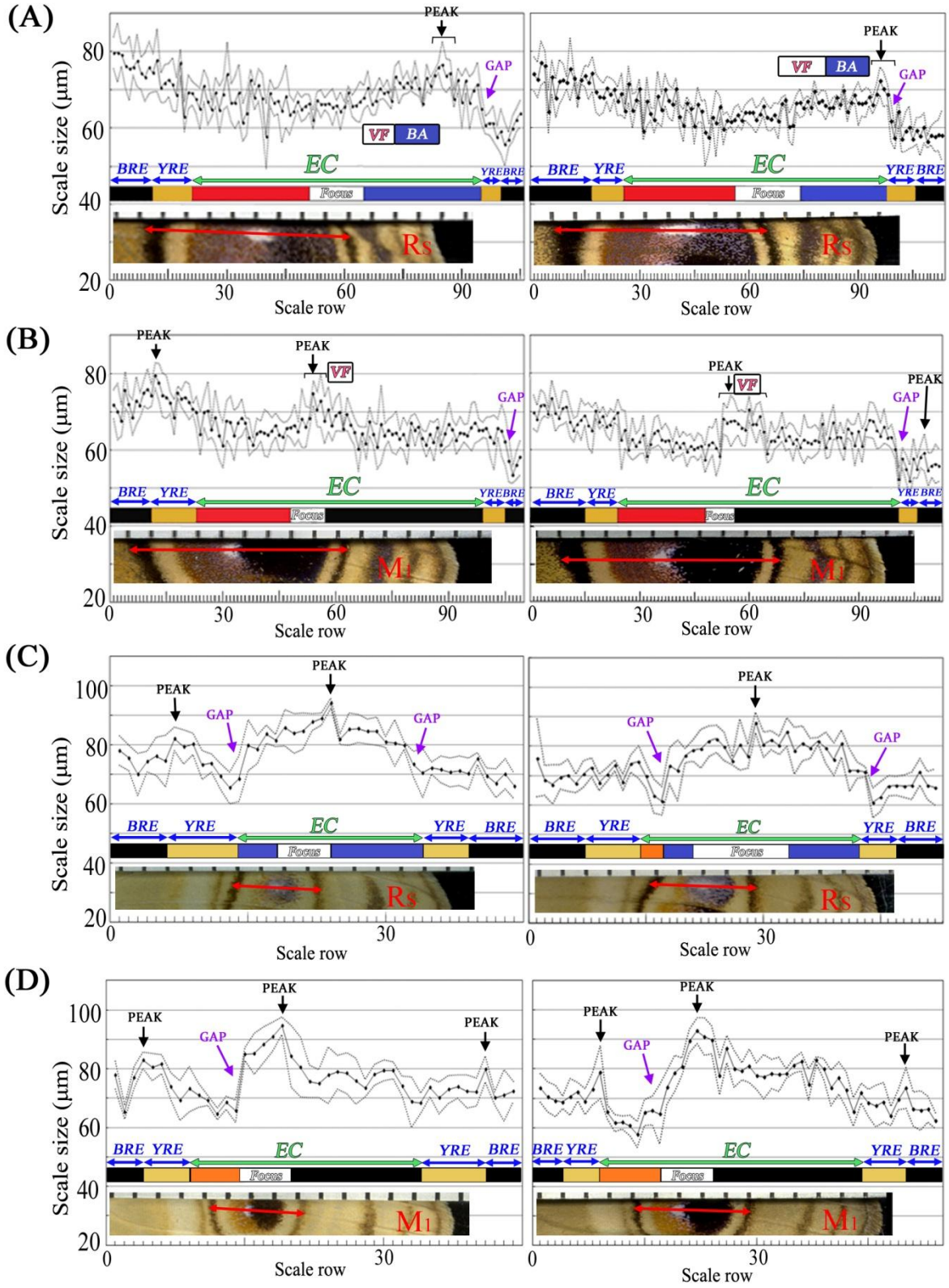

Fig. 2-4. High-resolution size distribution of scales in the major eyespot on the *J. almana* female hindwing. Two individuals were subjected to measurements along a

given proximodistal line, as indicated by double-headed red arrows in insets. Along the line of the double-headed arrowheads, 5 scales were measured every scale row. Horizontal bars indicate areas of an eyespot. Dotted lines indicate standard deviation (SD). Important peaks and gaps are indicated by black and purple arrows, respectively. Corresponding locations of the focal white area of the ventral side (ventral focus; VF) and its associated blue area (BA) are also indicated. **(A)** The Rs compartment of the dorsal major eyespot. **(B)** The M_1 compartment of the dorsal major eyespot. **(C)** The Rs compartment of the ventral major eyespot. **(D)** The M_1 compartment of the ventral major eyespot.

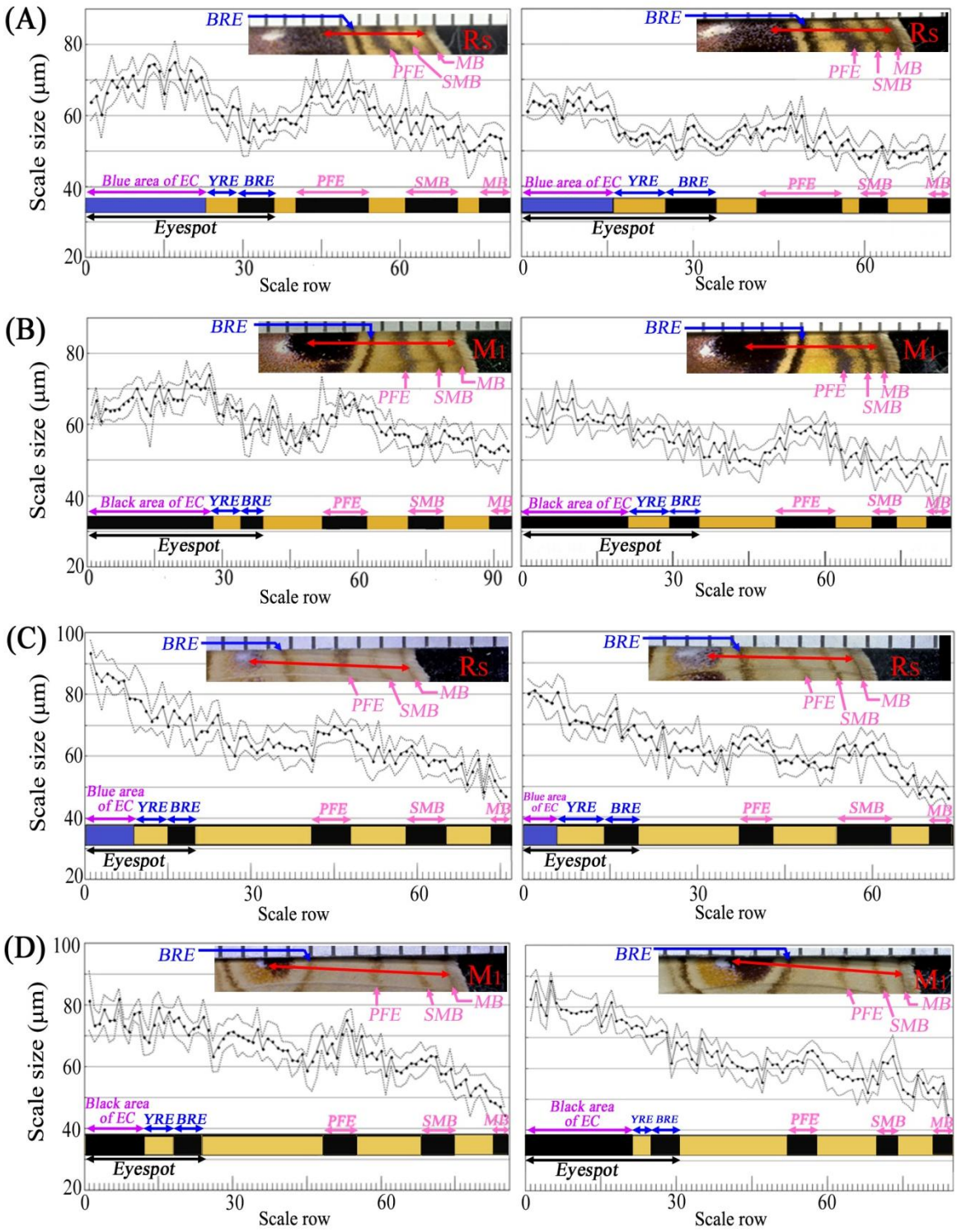

Fig. 2-5. High-resolution size distribution of scales in the marginal area on the *J. almana* female hindwing. Two individuals were subjected to measurements along a given proximodistal line, as indicated by double-headed red arrows in insets. Along the line of the double-headed arrowheads, 5 scales were measured every scale row.

Horizontal bars indicate areas of an eyespot and peripheral elements. Dotted lines indicate standard deviation (SD). **(A)** The Rs compartment of the dorsal marginal area. **(B)** The M_1 compartment of the dorsal marginal area. **(C)** The Rs compartment of the ventral marginal area. **(D)** The M_1 compartment of the ventral marginal area.

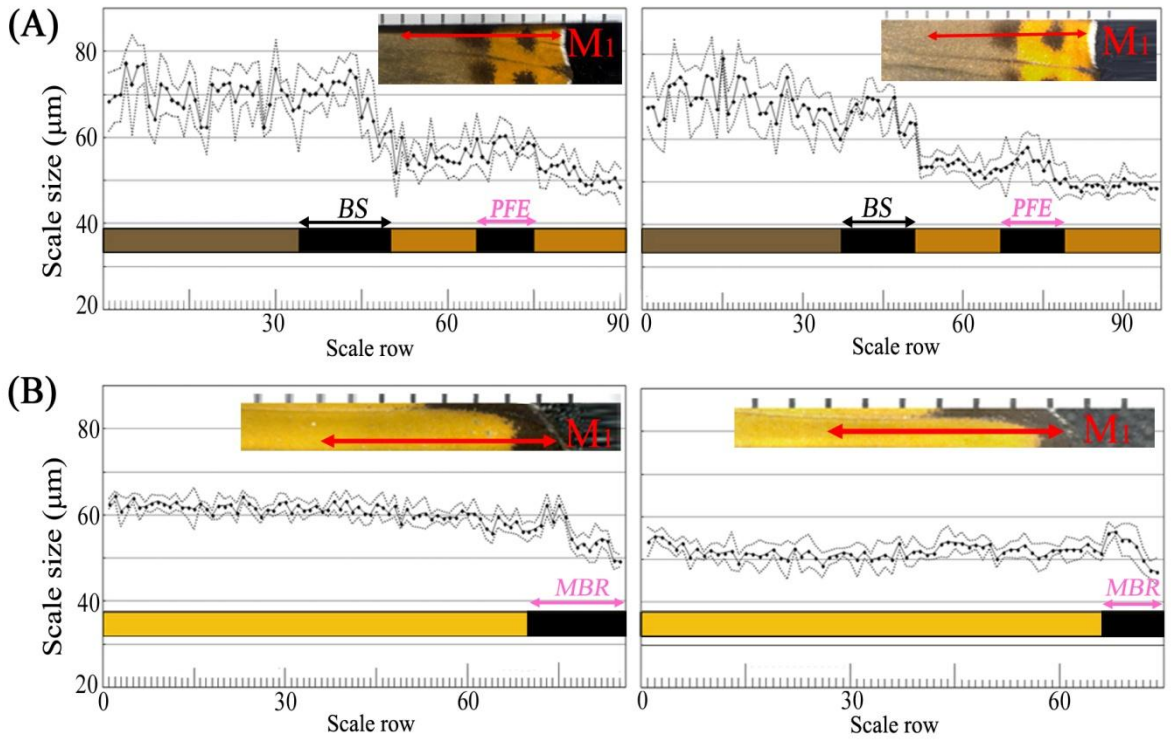

Fig. 2-6. High-resolution size distribution of scales in the marginal area on the hindwings of *V. indica* and *D. chrysippus*. See Fig. 2-3 for abbreviations and Fig. 2-5 for explanations. **(A)** The M_1 compartment of the dorsal marginal area of *V. indica*. **(B)** The M_1 compartment of the female dorsal marginal area of *D. chrysippus*.

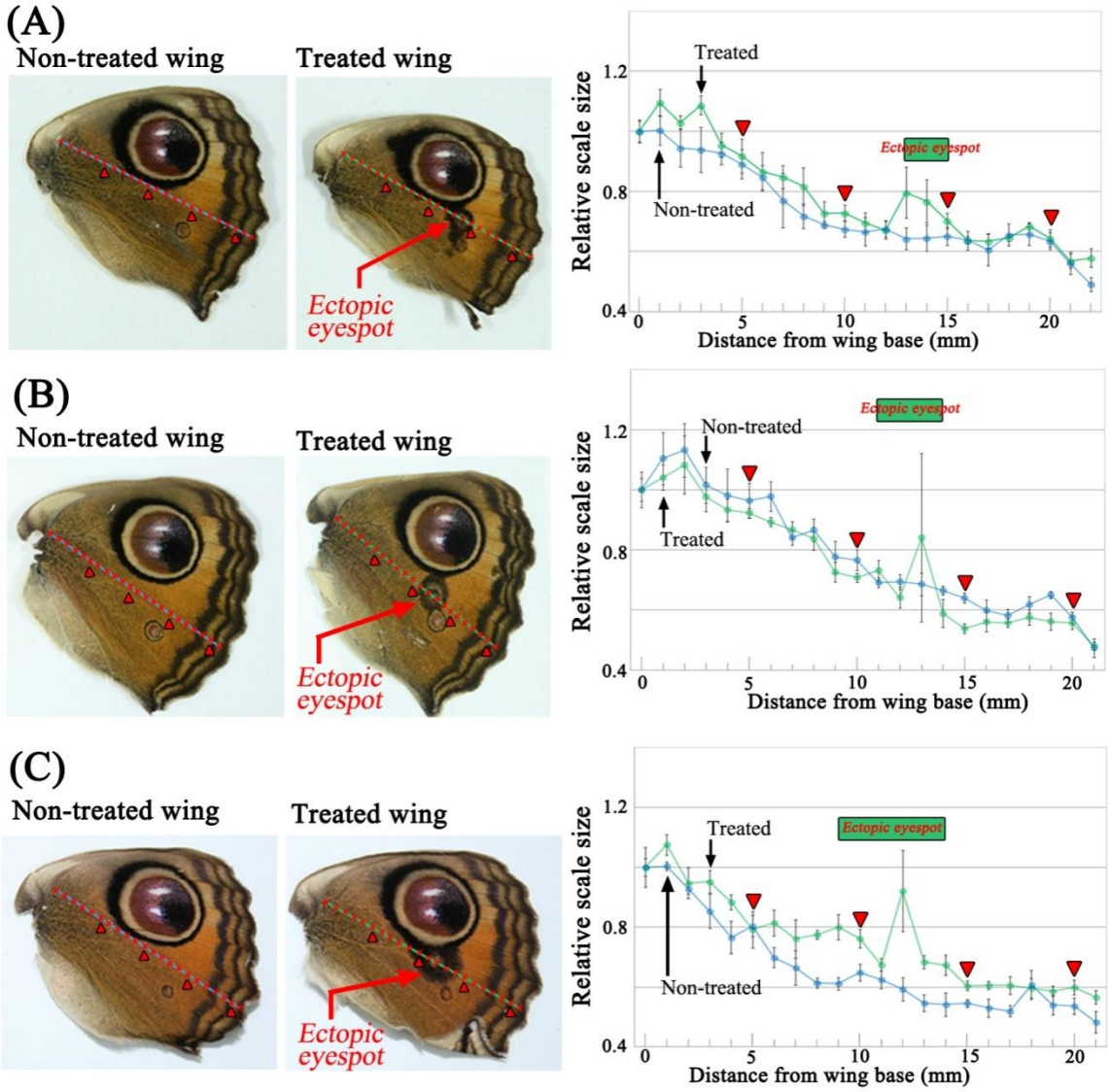

Fig. 2-7. Morphometric comparison of scale size between the non-treated and treated hindwings of the same individual in *J. almana* females. (A–C) Three representative wings with an ectopic eyespot. Shown are (from left to right) non-treated wings, treated wings, and their size data. The size data were obtained from the size measurements every 1 mm from the basal to distal areas along a straight line shown in the wing panels. The line was set to span the area between the major and minor eyespots. The ectopic eyespot area on the line is indicated by a horizontal bar in the rightmost panel. Red arrowheads indicate the points every 5 mm from the starting point (at 0 mm) along the line. Error bars represent standard deviation (SD). The

images of the left wings (non-treated wings) were horizontally flipped for comparison.

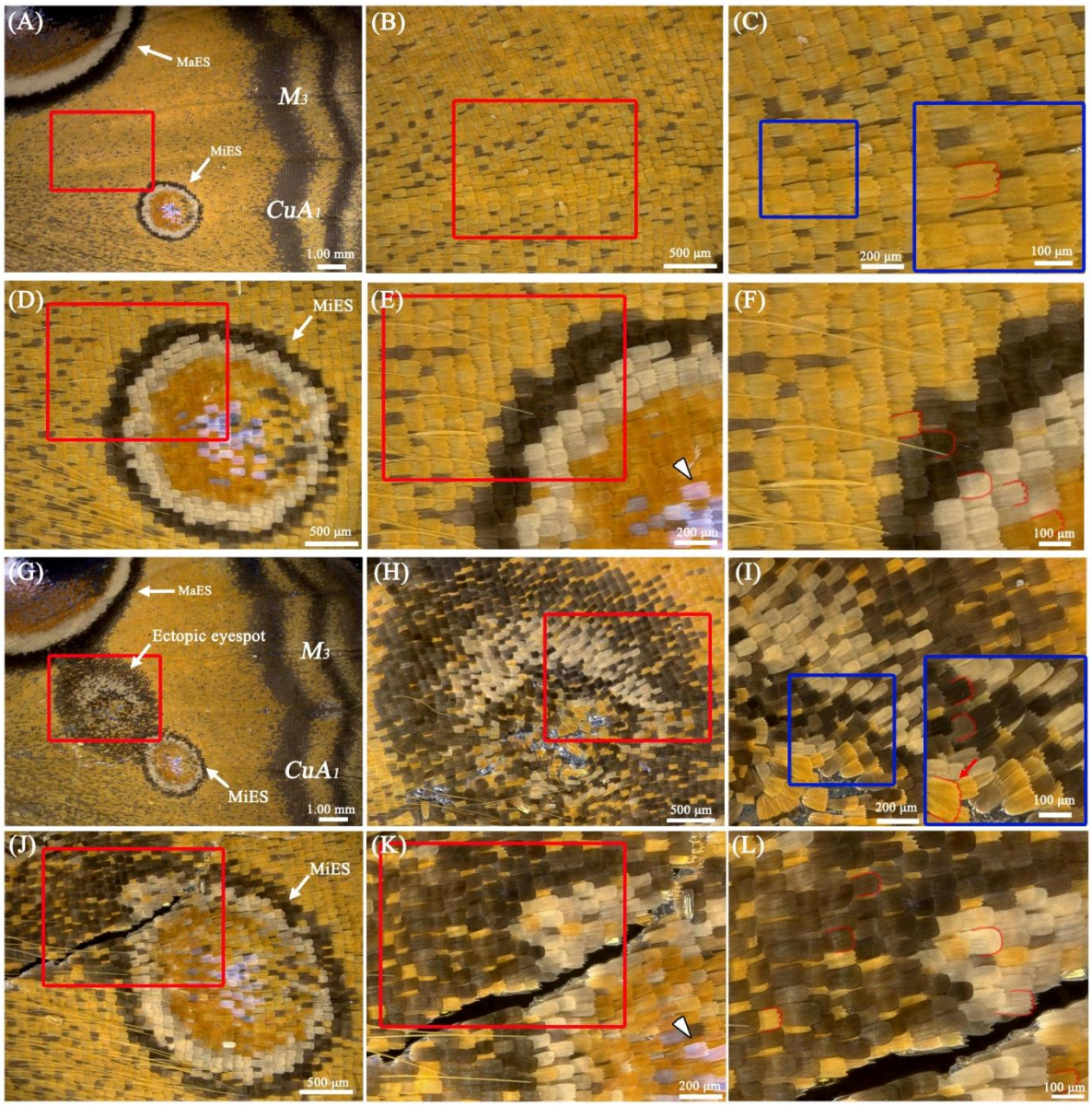

Fig. 2-8. Morphological comparison between the non-treated and treated hindwings of the same individual in *J. almana* females. (A–F) Dorsal side of the non-treated hindwing. The images of the left wing (non-treated wing) were horizontally flipped for comparison. **(A)** Non-treated area between the major and minor eyespots. **(B)** Higher magnification of the boxed region shown in (A). **(C)** Higher magnification of the boxed region shown in (B). The small boxed region is enlarged in the adjacent large box. A representative scale with a jagged edge is shown in red outline. **(D)** High magnification of the minor eyespot shown in (A). **(E)** Higher magnification of the boxed region shown in (D). White arrowheads indicate a focal

scale with structural color. **(F)** Higher magnification of the boxed region shown in (E). Representative scales with jagged edge or with smooth edge are shown in red outlines. **(G–L)** Dorsal side of the treated hindwing with an ectopic eyespot between the major and minor eyespots. **(G)** Ectopic eyespot. **(H)** Higher magnification of the boxed region shown in (G). **(I)** Higher magnification of the boxed region shown in (H). The small boxed region is enlarged in the adjacent large box. A red arrow indicates a large scale at the center of the ectopic eyespot. Jagged and smooth scales are shown in red outlines. **(J)** Higher magnification of the minor eyespot shown in (G). **(K)** Higher magnification of the red boxed region shown in (J). White arrowhead indicates focal scales with structural color. **(L)** Higher magnification of the boxed region shown in (K). Jagged and smooth outlines of representative scales are shown.

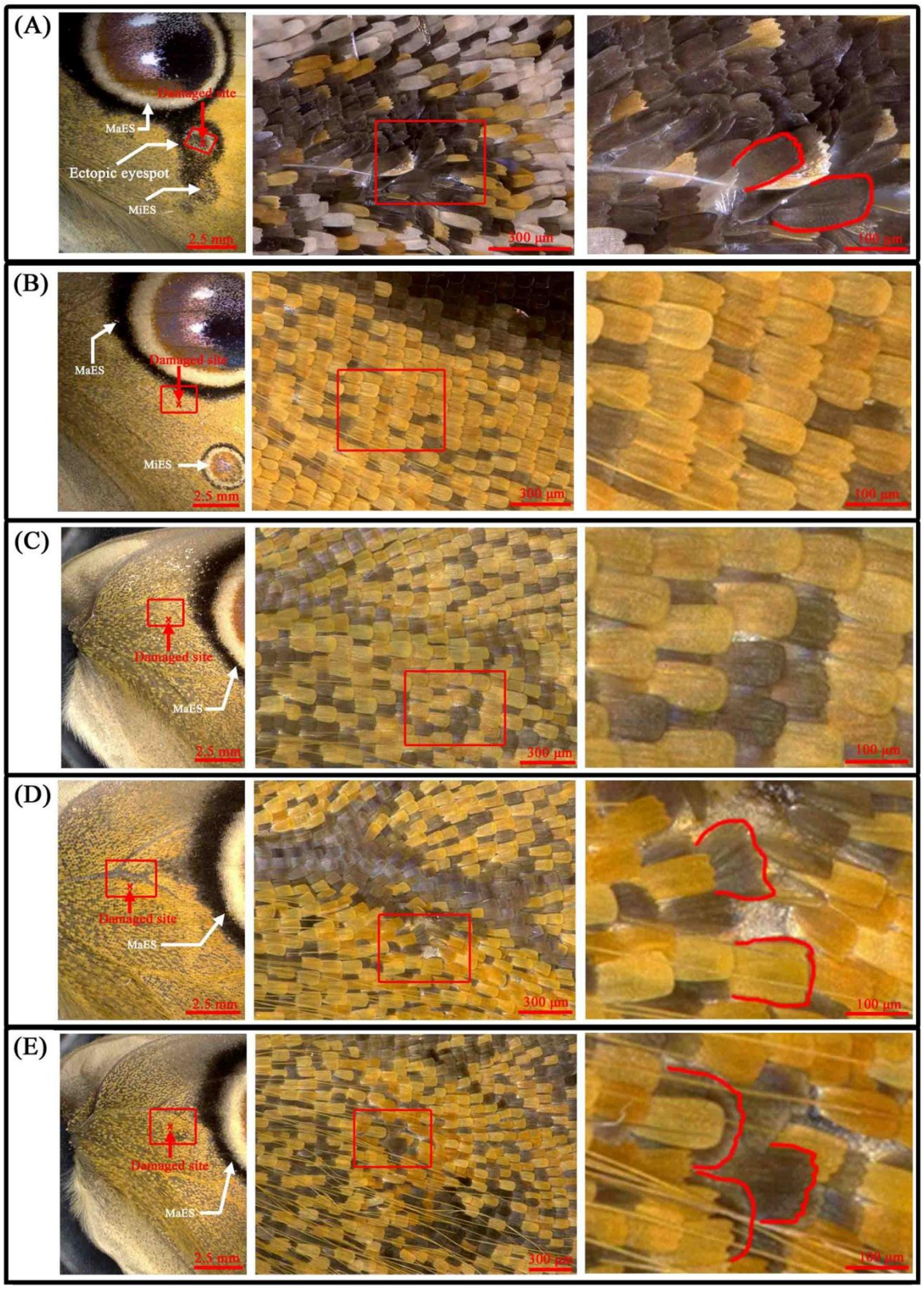

Fig. 2-9. Effects of physical damage that induced no or small color pattern changes. (A) A case of color pattern induction by physical damage for comparison.

This is one of the treated individuals mentioned previously in association with Figs. 7 and 8. Ectopic black spot contains large scales. **(B–E)** Four cases of physical treatment that induced no or small color pattern changes. In three cases, damage was applied to the basal area, where color pattern inducing ability may be low. **(B, C)** No color pattern induction was observed. Damage was completely healed. Scale size change was not observed. **(D, E)** Possible small changes in color patterns were observed. Some large scales, mostly ground scales, were observed at the damage sites that were easily identifiable.

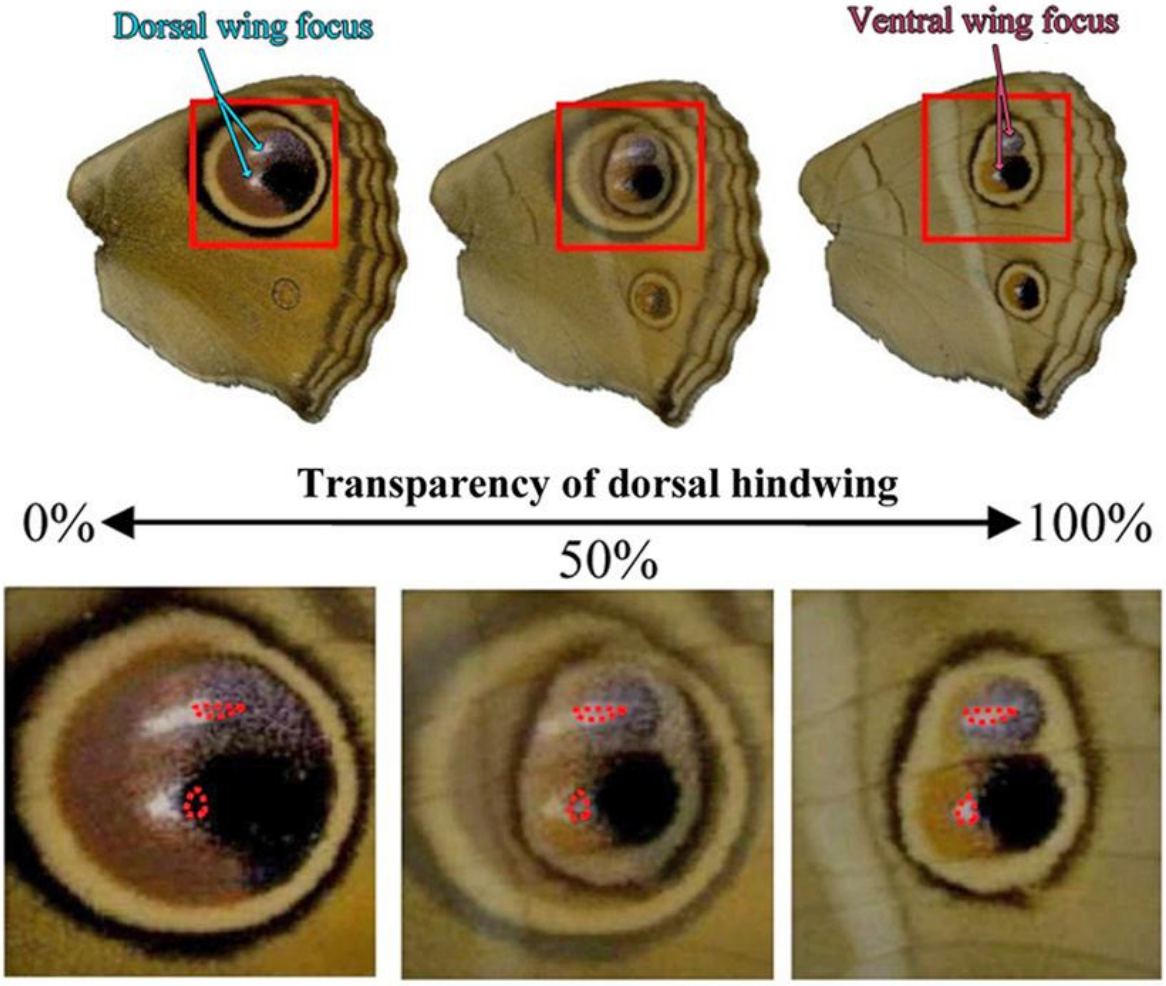

Fig. 2-10. Focal dislocation of the dorsal major eyespot in *J. almana*. The image of the ventral side was flipped so that both the dorsal and ventral images can be superimposed together. Then, the transparency of the dorsal wing image on the ventral wing image was adjusted so that the corresponding locations of the focal white areas can be observed through. The ventral focal white areas are surrounded by red dotted lines. A similar examination using a light box for transparent images showed the same result (not shown).

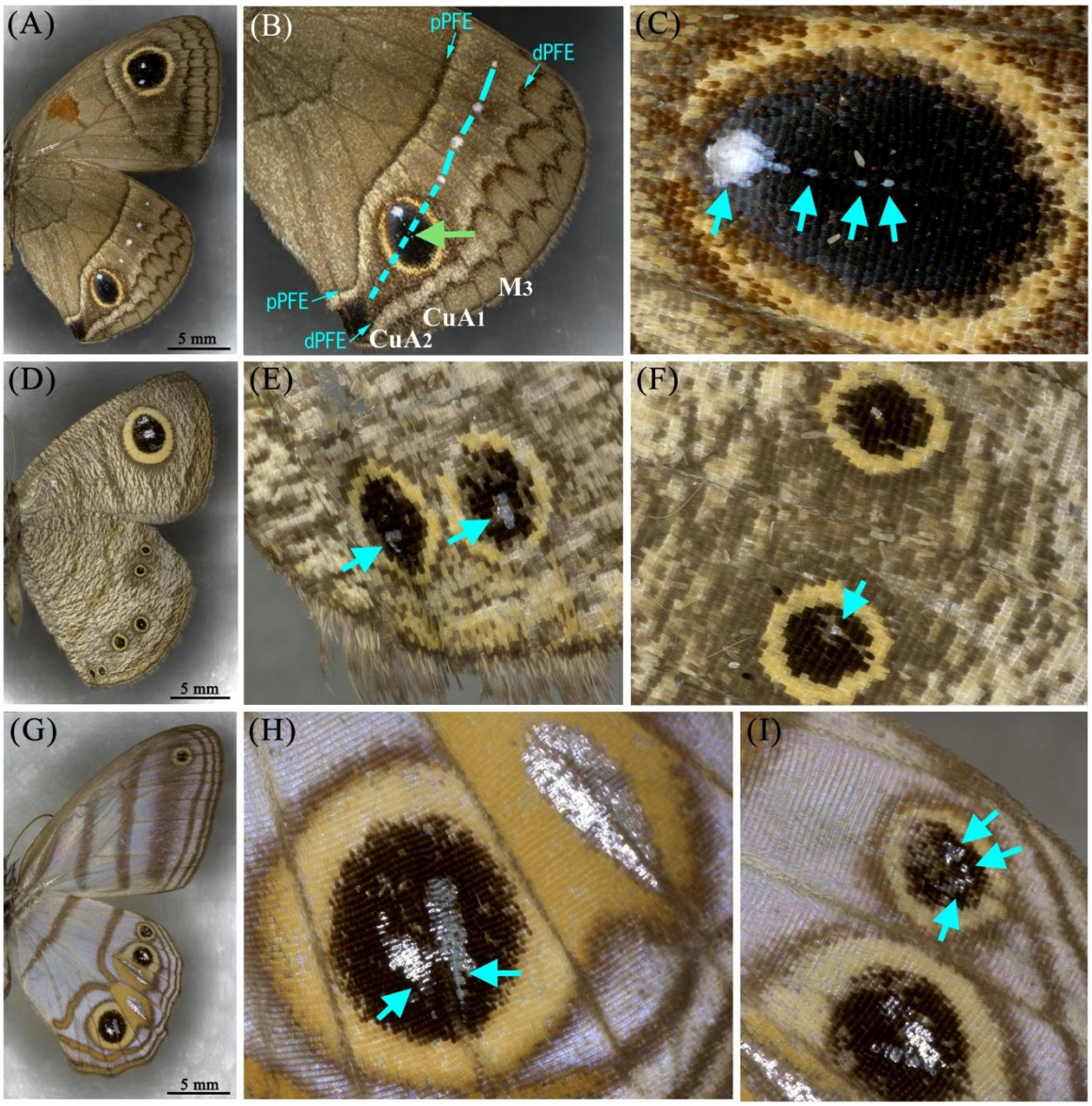

Fig. 2-11. Examples of focal dislocation in nymphalid butterflies. Scale bars, 5 mm. **(A–C)** *Calisto herophile*. The ventral eyespot contains a ‘‘focal” white area but is dislocated proximally from the physical center of the eyespot. White dots are positioned in the middle of the border symmetry system between pPFE (proximal parafocal element) and dPFE (distal parafocal element) in most compartments, except for CuA_1, where a full eyespot exists. The middle position between pPFE and dPFE from the M_3 to CuA_2 compartments is shown in a broken line, and the possible physical center of the eyespot in CuA_1 is indicated by a light green arrow in (B). The focal white area is not on the broken line. In the high-magnification image shown in

(C), white scales (indicated by arrows) are found along a possible displacement line, which is the midline of this compartment. **(D–F)** *Ypthima* sp. Boxed areas in (D) are enlarged in (E) and (F). Dislocated focal white areas are indicated by arrows. In (E), the focal white areas are dislocated distally. In (F), one of the focal white areas is dislocated anteriorly. **(G–I)** *Chloreuptychia herse*. Boxed areas in (G) are enlarged in (H) and (I). Deformed (split and elongated) focal areas are indicated by arrows.

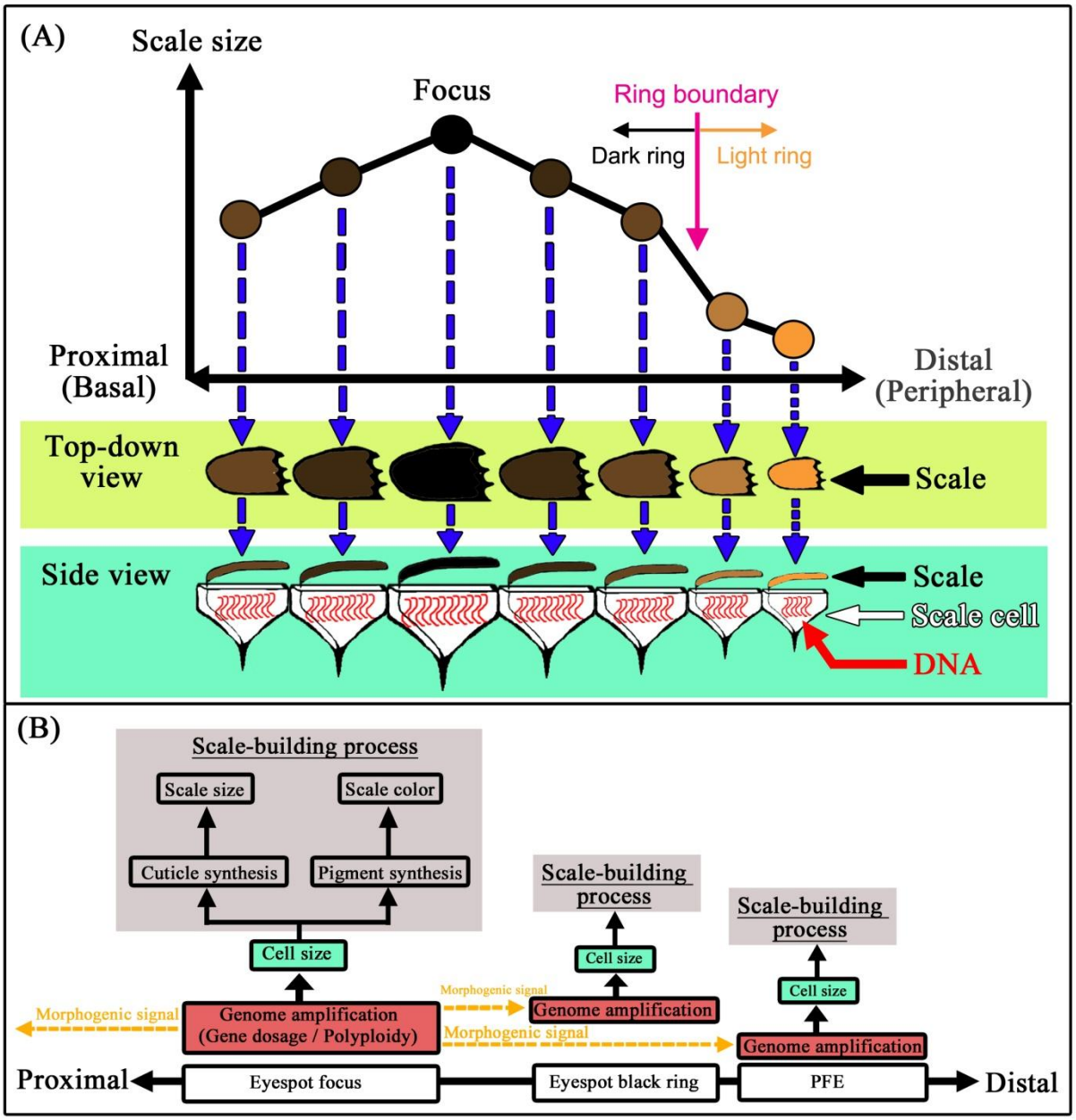

Fig. 2-12. Ploidy hypothesis. (A) Scale size distribution and its possible relationship to cell size. The larger the scale-building cells, the larger the scales that are produced. This pattern occurs probably simply because more enzymes and materials for scale construction are available for larger cells. Additionally, the larger the scale-building cells, the darker the scale color. This trend occurs also probably because more pigment synthetases are available for larger cells. The cell size is proportional to the number of the genome duplication; thus, larger cells have more genes for cuticle and pigment synthesis. In this schematic illustration, the focal scales are shown in black (not in

white). **(B)** A hypothetical determination process for scale color and size. Scale-building cells at the prospective eyespot foci undergo genome amplification (an increase in gene dosage or polyploidization), leading to cell size increase. Increased levels of cuticle synthesis and pigment synthesis result in larger scales and darker color, respectively. Morphogenic signals are released laterally to form the secondary organizing centers, which repeat genome amplification and the scale-building process to form PFE (parafocal element) and eyespot black ring.

Chapter 3: Uncoupling of white spots from eyespot bodies

3.1. Introduction

Introduction

Butterflies and moths are a large group of insects called Lepidoptera. Lepidopteran insects are characterized by wings covered with scales and bristles. These scales are variously colored, and a single scale serves as an image unit (or "pixel"). These scales form diverse mosaic color patterns on wings. One group of butterflies that shows highly diverse color patterns is the family Nymphalidae, from which a common overall color pattern was derived as the nymphalid groundplan (Nijhout, 1978, 1991, 2001; Otaki, 2009, 2012a; Taira et al., 2015). The nymphalid groundplan is composed of three major symmetry systems (the border, central, and basal symmetry systems) and two peripheral systems (wing root and marginal systems), and all five systems are thought to be produced based on the same mechanism (Otaki, 2012a; Taira et al., 2015). A unit of a symmetry system in a single wing compartment is composed of a single core element and a pair of paracore elements located at the distal and proximal sides of the core element (Otaki, 2012a).

Among the symmetry systems, the border symmetry system is probably the most conspicuous in many nymphalid butterflies. It is composed of a border ocellus (an eyespot) as a core element and a pair of parafocal elements (distal and proximal parafocal elements) as paracore elements (Nijhout, 1991, 2001; Dhungel and Otaki, 2009; Otaki, 2009, 2012a). Moving from the center to the peripheral area, a typical eyespot is composed of a white focal spot at the center (often called a "focus"), an inner black disk, a light-colored ring, and an outer black ring. A typical eyespot can be found in the African satyrine butterfly, *Bicyclus anynana*, one of the most popular species in butterfly biology (Beldade and Brakefield, 2002; Carroll et al., 2004). Physical damage at the prospective eyespot focus in *Junonia coenia* (Nijhout, 1980a,

1991), *B. anynana* (French and Brakefield, 1992), *Ypthima argus* (Otaki et al., 2005a), *J. orithya* (Otaki et al., 2005a), and *Junonia almana* (Otaki, 2011a), together with transplantation experiments (Nijhout, 1980a, 1991; French and Brakefield, 1995; Brakefield et al., 1996; Beldade et al., 2008), demonstrated that the center of the prospective eyespot behaves as an organizing center for the eyespot during the pupal stage. However, actual eyespots are highly diverse, and various deformations from the typical eyespot pattern occur (Nijhout, 1990, 1991; Otaki, 2011b). For example, the white focal spot is often missing, and the various rings are often distorted differently in a single eyespot.

Since the last decade of the twentieth century, many candidate genes that could specify eyespots have been identified based on their expression patterns (Carroll et al., 1994; Brakefield et al., 1996; Keys et al., 1999; Brunetti et al., 2001; Reed et al., 2004; Monteiro et al., 2006; Saenko et al., 2011; Tong et al., 2012). These genes are expressed during the late larval to the early pupal stages in the wing tissues, which is when the color pattern determination takes place (Nijhout, 1980a). Among them, the most notable gene is probably *Distal-less* (*Dll*). It has been shown that *Dll* expression recapitulates the locations of organizing centers that were predicted by a reaction-diffusion model (Carroll et al., 1994; Nijhout, 1990, 1991, 1994, 1996), which has often been interpreted as meaning that *Dll* expression defines an organizing center and that *Dll* is a master gene for eyespot determination. In addition to the eyespot focal determination, it has also been suggested that *Dll* determines eyespot size (Brakefield et al., 1996; Beldade et al., 2002).

However, functional tests for *Dll* were not performed until recently. One study using transgenic *B. anynana* butterflies showed that *Dll* plays a role in eyespot size regulation as well as in black spot induction (Monteiro et al, 2013). One study using the blue pansy butterfly, *Junonia orithya*, together with a novel surgical technique, showed a weak but significant correlation of the individual *Dll* expression level with the individual eyespot size (Adhikari and Otaki, 2016). Subsequently, using *J. orithya*

with a baculovirus gene transfer method (Dhungel et al., 2013), it has been shown that *Dll* can induce fragmentary patterns of an eyespot but not an entire eyespot (Dhungel et al., 2016). Taken together, although *Dll* is unlikely to be sufficient for the entire eyespot pattern formation, it plays an important role in eyespot development.

Morphological studies also advanced. Butterfly wings exhibit coordinated scale size distributions in addition to coordinated scale color distributions (Kusaba and Otaki, 2009; Dhungel and Otaki, 2013) (see Chapter 2). The largest scales in an eyespot are often at the center in *J. orithya* (Kusaba and Otaki, 2009) and *J. almana* (see Chapter 2). This finding, together with the observation that scale size is proportional to the size of scale-building cells (Henke, 1946; Sondhi, 1963), led us to propose the ploidy hypothesis that morphogen signals for color patterns are identical to ploidy signals (see Chapter 2).

Additionally, the pupal surface has cuticle focal spots that correspond to adult eyespots in various butterfly species (Nijhout, 1980a; Otaki et al., 2005a). Two *Junonia* species that have large eyespots in adult wings, *J. orithya* and *J. almana*, indeed have large and distinct pupal cuticle focal spots, whereas a *Junonia* species that has small eyespots in adult wings, *J. hedonia*, has small ones (Taira and Otaki, 2016). Interestingly, the size of the cuticle spot is correlated with the size of the corresponding eyespots in *J. orithya* and *Ypthima argus* (Otaki et al., 2005a). Similar correlations were also obtained among serial eyespots on a single wing in *J. orithya* (Taira and Otaki, 2016). The three-dimensional structures of pupal cuticle focal spots as well as adult wings were revealed recently (Taira and Otaki, 2016).

Moreover, physiologically induced changes of color patterns, which are typically considered positional and morphological changes of elements, have been investigated in detail (Nijhout, 1984; Otaki, 1998, 2007, 2008a, b; Otaki and Yamamoto, 2004a, b; Serfas and Carroll, 2005; Otaki et al., 2005b, 2010; Mahdi et al., 2010, 2011; Hiyama et al., 2012). Meanwhile, an invention of a real-time *in vivo* observation system made it possible to record how wing tissues develop inside the

pupal case (see Chapter 1). Developing epithelial cells are elongated vertically as well as horizontally (Ohno and Otaki, 2015a), confirming a century-old histological study (Mayer, 1896). Long-range slow calcium waves have been discovered in pupal wing tissues, which may function as signals to coordinate development throughout a wing (Ohno and Otaki, 2015b).

This information should collectively evaluate the feasibility of mechanistic models for color pattern determination. Historically, morphogen gradient models have been proposed and used to explain various experimental results (Nijhout, 1978, 1980a, 1981, 1990, 1991; French and Brakefield, 1992, 1995; Brakefield and French, 1995; Monteiro et al., 2001; Serfas and Carroll, 2005; Otaki, 2008a). Nijhout (1990) examined the diverse eyespot patterns of nymphalid butterflies and identified 36 pattern categories, which were used to construct a gradient-based model. These models are based on the simple diffusion of a putative morphogen that forms a gradient, together with differentiation thresholds inherently programmed into immature scale cells. Abrupt changes of the cellular interpretation of a smooth gradient were attained mathematically by a sigmoidal curve, resulting in two thresholds and three colors (Nijhout, 1991).

However, Otaki (2011b, c) pointed out several difficulties of the gradient models to explain actual butterfly wing color patterns. For example, an “archetypical” butterfly eyespot is likely composed of a series of repetitions of an inductive signal for black (or dark) area (Otaki, 2011c). In other words, a non-black (i.e., light-colored) area between the black areas is equivalent to background (Otaki, 2011c). This binary rule (stating that a series of repetitions of dark areas with light-area intervals is the basic expression of an eyespot) alone makes threshold-based diffusion models unrealistic because the black rings or disks are equivalent to each other in actual butterflies. Moreover, not just two but three or more repetitive black rings are observed in many butterflies (Otaki, 2011b). Indeed, one of the “black rings” of an eyespot is a pair of discontinued elements called parafocal elements (Otaki, 2009, 2011c, 2012a, b).

Moreover, color pattern analysis of neighboring or serial eyespots with different structures on the same wing surface pointed out that thresholds for gradient interpretation, if exist according to the gradient models, do not vary among neighboring compartments and that these eyespots should be produced by different levels of a morphogen to reflect their morphological differences (Otaki, 2011b). But it is theoretically difficult to satisfy these two points simultaneously in gradient models (Otaki, 2011b). In fact, the dynamic responses of eyespots to physical damage requires flexible models that can accommodate signals from damage sites and from neighboring organizing centers (Otaki, 2011a).

As an alternative model, the induction model has been proposed (Otaki, 2011b, c; 2012b). The induction model is based on many case analyses of normal and experimentally induced color patterns (Otaki, 2011b, c; 2012b), incorporating the principle of "short-range activation and long-range inhibition" that have been found in many biological patterns (Gierer and Meinhardt, 1972; Meinhardt, 1982; Meinhardt and Gierer, 1974, 2000).

In either model, the status of the white focal area has not been explained well in the literature. Nijhout (1978, 1980a) proposed that a "focus" at the center of an eyespot releases a morphogen at the late larval and early pupal stages, based on which a gradient model was formulated. Since then, one tends to assume that the white focal spot directly corresponds to an organizing center for the entire eyespot. In many instances, this assumption seems to be valid; a white spot is located at the physical centers of eyespots in many nymphalid butterflies. However, this is not always the case. Nijhout (1980a) indeed pointed out that the white scales at the eyespot center do not precisely correspond to the "focus". Likewise, there is a discrepancy between the location of the largest scales and the location of the white spots in a particular eyespot of *J. almana* (see Chapter 2). Similar cases have been pointed out in *Calisto herophile* and other butterflies (see Chapter 2). Moreover, the white coloration is structural rather than pigment-based (Nijhout, 1980b, 1991) (see Chapter 2). In a gradient model, the

area of the highest morphogen concentration above a certain threshold is supposed to become the white spot. But molecular pathways for structural color production are probably qualitatively different from those for pigment-based color production. Thus, one could think that these two production lines may be distinctly specified. In any case, the relationships between white spots and their corresponding eyespot bodies (defined as all the eyespot portions except white spots) should be clarified to understand how butterfly eyespots are constructed during development.

Lepidopterists in Asian (and probably in many other) countries are not familiar with the genus *Calisto* because they are endemic to the West Indian regions (mainly in Hispaniola, which is occupied by Haiti and Dominican Republic). Indeed, *Calisto*-type pear-shaped eyespot patterns were not incorporated in the pattern analysis of Nijhout (1990). However, we had an opportunity to examine specimens of *Calisto* butterflies. The genus *Calisto* is an exclusive group of satyrine butterflies in the West Indies that constitutes more than 40 species (Smith et al., 1994; Miller and Miller, 2001; Askew and Stafford, 2008). Among them, we here focused on eyespots of *Calisto tasajera* González, Schwartz & Wetherbee, 1991 (González et al., 1991; Hedges and Johnson, 1994) because it has unique pear-shaped eyespots that have two or more white "focal" spots. Molecular phylogenetic analysis and historical biogeography of *Calisto* have been reported (Sourakov and Zakharov, 2011; Matos-Maraví et al., 2014). We also examined eyespots of other nymphalid butterflies to support our findings with *C. tasajera*. The present study argues for an uncoupling of white spots from the rest of the eyespots (i.e., eyespot bodies).

3.2. Material and Methods

Butterflies

We primarily analyzed 17 specimens of *C. tasajera* owned by Nariaki Yamada (The Butterfly Science Society of Japan), Tokyo, Japan (Fig. 3-1A). These butterflies were collected in the Dominican Republic on July 17, 2002, by Haruo Takizawa (Fig. 3-1B). Sex of these individuals was not identified; this species is not sexually dimorphic. We focused on three wing regions of the ventral side that contain eyespots and/or white spots: the anterior forewing, the anterior hindwing, and the posterior hindwing (Fig. 3-1C). The ventral side of the left wings was examined in all cases except for one individual which had left wing damage; in this case, the ventral side of the right wings was examined. Other *Calisto* butterflies other than *C. herophile* were also owned by N. Yamada. Other butterfly specimens were owned by J.M. Otaki.

Images and morphometry

Images of specimens were taken by an Olympus digital camera STYLUS TG-4 Tough (Tokyo, Japan) using its microscope mode. Areas of white spots and black disks of eyespots in *C. tasajera* were measured using ImageJ v. 1.48 image analysis software (Schneider et al., 2012). Because we were not allowed to measure absolute values, which potentially damages the specimens, relative values within a single image were used for comparison in this study.

Basic assumptions

We assumed that a basic molecular mechanism for color pattern formation is shared in all compartments of a single wing surface or at least in two adjacent wing compartments. This is the very basic assumption that is required for this type of color pattern analysis.

In analyzing color patterns, we assumed that morphogenic signals are released

from an organizing center and that the signals move equally well in all directions. These assumptions led to the following interpretations. (1) If an eyespot is close to an exact circle, its signals were released from its physical center. (2) If an eyespot is clearly distorted from an exact circle as observed in an oval or pear-shaped eyespot, its signals were released from two or multiple sites, unless there is a nearby element that blocks the propagation of the morphogenic signals. That is, a morphogenic gradient is made as a merge of two or multiple signals.

In discussing a diffusion-based gradient model, it has often been assumed implicitly that a white spot at the center of an eyespot corresponds to an organizing center for the entire eyespot (see Introduction). We do not believe that this assumption is always correct; however, because this assumption is associated with the gradient models, it was used as a starting point of color pattern analysis in the present study. Furthermore, the simplest form of a conventional diffusion-based gradient model predicts that the eyespot focus had the highest concentration of a morphogen in the larval and pupal wings. Accordingly, the area of the highest morphogen concentration corresponds to a white spot. If the threshold level is fixed and not changeable, the higher the level of morphogen that is released, the wider the area of the white spot that is specified by the morphogen.

In making models for color pattern formation, it is often assumed that adult wing color patterns is directly determined by their pre-patterns in pupal wings. For simplicity, this assumption is also followed in the present study. If one considers that color patterns are finalized through a four-step process (signaling, reception, interpretation, and expression) (Otaki, 2008a), a pre-pattern may not be realized solely by the signaling step without the subsequent steps of reception, interpretation, and expression. A direct determination of adult color patterns by pre-patterns thus means that these subsequent steps are all normally executed without positional bias. In reality, however, it has been known that the proximal and distal wing surfaces have different sensitivities to morphogenic signals (Nijhout, 1978, 1980a, 1985; Brakefield and

French, 1995; French and Brakefield, 1995).

Statistics

Numerical values were recorded in Microsoft Excel and analyzed with R statistical software, version 3.2.1 (The R Foundation for Statistical Computing, Vienna, Austria). For each dataset, normality was checked with a Shapiro-Wilk test, based on which nonparametric tests were performed. Mean and standard deviation (SD) values were calculated, and Mann-Whitney *U* tests (pairwise comparison using Wilcoxon rank sum tests) were performed to compare two samples. When multiple pairwise comparisons were made, *p*-values were adjusted by Holm correction. The Spearman rank correlation coefficient ρ was obtained to examine the possible correlation between two variables.

3.3. Results

Anterior forewing spots in *C. tasajera*

We first analyzed the color patterns of the anterior forewing spots in *C. tasajera*. A relatively large eyespot was present in the anterior forewing (Fig. 3-2A–F). The white spot ("focus") of this eyespot was located in the M_1 compartment, but this eyespot was not confined to the M_1 compartment; it also occupied two adjacent compartments, R_5 and M_2 (Fig. 3-2). This invading eyespot suggests that immature scale cells in these three compartments were equally receptive to morphogenic signals from the M_1 organizing center during the late larval and early pupal stages.

In the M_2 compartment, a white spot was present, the size of which was similar to that of the M_1 compartment. This white spot was located just on the yellow ring or on the edge of the inner black disk, without a significant distortion of the M_1 eyespot, in 6 individuals out of 17 (Fig. 3-2A, E, F). In these cases, the M_1 eyespot was almost an exact circle. According to a conventional understanding (see Materials and Methods), the central positioning of the white spot within this eyespot suggests that the M_1 white spot corresponds to the organizing center from which morphogenic signals for the eyespot body were released during development in this particular eyespot. On the other hand, 11 individuals showed a distortion of the M_1 eyespot; in these cases, the M_2 white spot was located completely inside the eyespot (Fig. 3-2B–D). This likely occurs from a fusion of the smaller M_2 eyespot and the larger M_1 eyespot. Thus, the M_1 white spot appears to have corresponded to a highly active organizing center and the M_2 white spot to either an inactive or less active organizing center.

A close examination of an M_1 eyespot revealed that there was an outermost weak black ring located outside a yellow ring (Fig. 3-2E, F). This weak black ring existed all around the yellow ring including the immediate vicinity of the M_2 white spot in all 6 cases when there was no distortion of the M_1 eyespot (Fig. 3-2E, F), suggesting that the M_2 white spot in these cases was completely inactive as an

organizing center for the eyespot body despite a clear expression of the white scales.

Anterior hindwing spots in *C. tasajera*

The anterior hindwing in *C. tasajera* had two solitary white spots, one in the M_1 compartment and the other in the M_2 compartment (Fig. 3-3). In all 17 individuals, the M_2 white spot was much larger than the M_1 white spot (Fig. 3-3A). Moreover, the M_2 white spot showed a "sparse pattern" *sensu* Nijhout (1991). Some of these sparse scales were not white but light brown (Fig. 3-3B). These scales probably contained relatively small amount of brown pigment and developed white structural color simultaneously, suggesting that a decision-making process for differentiation is not all or nothing. Neither the M_1 nor the M_2 white spot accompanied any eyespot structure, suggesting that the organizing cells that differentiated into these white spots did not have any eyespot-inducing activity.

Posterior hindwing spots in *C. tasajera*

The posterior hindwings of *C. tasajera* had two eyespots, one in the CuA_1 compartment and the other in the CuA_2 compartment (Fig. 3-4). Most of the CuA_1 eyespots (and the CuA_2 eyespots to a similar degree) were pear-shaped (Fig. 3-4A–H). These pear-shaped eyespots suggest that morphogenic signals were released from two or more sites within a single compartment. This pear-shaped eyespot morphology can be considered as a merger of two (or more) eyespots: a main eyespot and a sub eyespot (Fig. 3-4M). In all 17 individuals, the most distinct white spot in these compartments was located at the proximal edge of the eyespot, often with a few small white spots along the midline. The organizing cells for the most proximal white spot did not seem to have been highly active to induce the eyespot body, but the organizing cells for black scales (or the small white dot) at the physical center of the eyespot were probably highly active to induce the eyespot body.

The merger of the main and sub eyespots in the CuA_1 and CuA_2 compartments

is comparable to that in the anterior forewing region. In the anterior forewing region, two organizing centers (specified by the white spots) were located in different compartments. In the case of the posterior hindwing region, two (or more) organizing centers were located in the same compartment along the midline. Interestingly, in 4 individuals out of 17, the proximal white spot was located outside the eyespot, forming an independent spot (Fig. 3-4I-L, N).

Quantitative comparisons of white areas

The white area ratios were calculated for the anterior forewing region (M_1/M_2), the anterior hindwing region (M_1/M_2), and the posterior hindwing region (CuA_1/CuA_2) of *C. tasajera* (Fig. 3-5A). Although the anterior forewing and hindwing regions are homologous, the ratios were significantly different between them ($p = 2.1 \times 10^{-6}$); in the anterior forewing region, the two white dots were similar in size, showing a ratio of 0.83 ± 0.29 (mean ± SD; also hereafter), but in the anterior hindwing region, the ratio was 0.16 ± 0.10. The ratio of the posterior hindwing region was also close to one, 1.09 ± 0.60 and was significantly different from that of the anterior hindwing region ($p = 2.1 \times 10^{-6}$). The ratios between the anterior forewing region and the posterior hindwing regions were not significantly different ($p = 0.23$).

In the posterior hindwing region, the ratio of black area to white area (black/white) in each compartment was calculated to quantitatively understand eyespot constituents. The ratio of the CuA_1 compartment, 18.54 ± 9.49, was significantly larger than that of the CuA_2 compartment, 6.46 ± 3.68 ($p = 7.8 \times 10^{-7}$) (Fig. 3-5B). Then, from a different perspective, the ratio of the white areas between the two compartments and the ratio of the black areas between the two compartments were compared. The white area ratio (1.09 ± 0.60) and the black area ratio (3.21 ± 1.4) were significantly different in these two adjacent compartments ($p = 4.6 \times 10^{-6}$) (Fig. 3-5C). In 17 individuals, the black area ratio and the white area ratio were not correlated significantly in the Spearman correlation analysis ($\rho = 0.29$; $p = 0.27$) (Fig. 3-5D).

White spot diversity in Nymphalidae

Thus far, we have focused on white spot patterns only in *C. tasajera*. To investigate whether similar white spot patterns are present in other species, we examined specimens of other nymphalid butterflies—including other *Calisto* species.

We were able to examine five other *Calisto* species (one specimen per species), all of which showed that the eyespots on the posterior hindwing had a proximal white spot with or without multiple small white spots along the midline. In these five species, we were not able to confirm the morphological features that were found in *C. tasajera* in the anterior forewings (i.e., a full circular eyespot in a compartment and a solitary white spot in the adjacent compartment) and anterior hindwings (i.e., two adjacent white spots, one of which shows sparse pattern) (Fig. 3-6).

A white spot on the proximal side (or even outside) of the main eyespot body, as observed in the posterior hindwings of all the *Calisto* species examined here, is probably not found frequently, but many examples of "focus-less" eyespots were found in other nymphalid butterflies. In the forewings of *J. orithya*, eyespots both on the dorsal and ventral sides were similar in size and structure, but interestingly, the dorsal eyespots had bluish-white spots at the center, whereas the ventral eyespots did not (Fig. 3-7A). The opposite was true in *Protogoniomorpha temora*: the dorsal eyespots had no white spot, whereas most of the ventral eyespots (not all) had white spots (Fig. 3-7B).

Many other examples of focus-less eyespots on the dorsal side but not in the ventral side were found in satyrine butterflies, including *Zophoessa callipteris* (Fig. 3-7C), *Kirinia fentoni*, *Erebia ligea*, *Neope goschkevitschii*, *Neope niphonica*, and *Lopinga achine* (Fig. 3-8A). Among these, *L. achine* is a noteworthy case: some individuals of this species had focus-less eyespots on both sides of the wings (Fig. 3-8B). The presence or absence of the white spot did not seem to affect the eyespot size in this species.

3.4. Discussion

Uncoupling of white spots from eyespot bodies

In this paper, we analyzed the eyespots and white spots of *C. tasajera*. We focused on three regions of ventral wings: the anterior forewing, the anterior hindwing, and the posterior hindwing. In the two adjacent compartments of the anterior forewing, there were a full circular eyespot and a solitary white spot. Also noteworthy is the invasion of the M_1 eyespot to the adjacent R_5 and M_2 compartments, despite the fact that the M_2 compartment harbors a white spot (with no or small eyespot body) that is as large as that in the M_1 eyespot, suggesting that all three compartments had the same sensitivity to morphogenic signals. In the anterior hindwing, we observed different shapes and sizes of the white spots in the two adjacent compartments, neither of which were associated with eyespots. In the posterior hindwing, we observed unique pear-shaped eyespots that contained two or more white spots.

Assuming that color patterns are determined by organizing cells, each cluster of organizing cells for white spots and eyespot bodies appear to have behaved differently during development. We speculate that in the anterior forewing, one cluster of organizing cells was highly active and the other was weakly active or completely inactive for eyespot body determination. This means that completely inactive cells (regarding the inducing activity for an eyespot body) can still induce or differentiate into a white spot. If the area values of white spots represent morphogen levels for eyespot bodies, as a conventional gradient model predicts, both the M_1 and M_2 compartments in the anterior forewing should have comparable levels of morphogens (indeed, the M_1/M_2 ratio of white spots was 0.83, meaning that the M_2 eyespot is slightly larger than the M_1 eyespot). In reality, however, the M_2 white spot is associated with either no or only a small eyespot body (that is, the M_1/M_2 ratio of eyespot bodies was infinitely large, meaning that the M_1 eyespot body is much larger than the M_2 eyespot body). Therefore, the area values of white spots do not indicate the

activity levels of organizing centers for eyespot bodies in the anterior forewing of *C. tasajera*, contrary to the expectation from a conventional gradient model. This conclusion is also relevant for the anterior and posterior hindwing regions in this species (see below).

In the anterior hindwing, there are two different solitary white spots. Interestingly, these two white spots are morphologically different: one is relatively small with clear boundary, and the other is relatively large with diffused boundary, showing the eyespot-independent morphological diversity of white spots. A difference in white patterns in adjacent compartments within the major eyespot of *Junonia almana* (see Chapter 2) is probably a similar phenomenon. Similar white spot patterns were also found in some *Cithaerias* species such as *C. pireta* and in some *Pierella* species such as *P. astyoche* (Otaki, 2011b).

In the posterior hindwing, we observed unique pear-shaped eyespots. For the main eyespots of these pear-shaped eyespots, the actual organizing center may be located at the physical center of the main eyespot and may be marked with a small white spot or not marked at all. The large proximal white spots exhibited little or no activity for inducing eyespot bodies. Quantitatively, the area values of white spots were not correlated with the black area values. These results, together with the results of the other two regions, argue that the white-inducing activity is independent of the eyespot-inducing activity—at least in *C. tasajera*. This conclusion was supported by the eyespot and white spot patterns of other *Calisto* butterflies and other nymphalid butterflies.

Morphological diversity of white spots

Nijhout (1990) examined color patterns of 2208 species (330 genera) of nymphalid butterflies, in which (also in Chapter 7 of Nijhout (1991)) several types of eyespot focal morphology were discussed: arc-shaped foci in *Morpho hecuba*, double foci in *Euptychia*, fragmented foci in *Lethe*, and sparse patterns. Importantly, most of the

white spot diverse patterns are successfully reproducible mathematically by a reaction-diffusion model (Nijhout, 1990, 1991). Although the white spots of *Calisto* (i.e., the pear-shaped *Calisto*-type eyespots) were not specifically discussed, it was concluded that the relationship between the shape of the white area (or "focus") and the surrounding ocellus (i.e., eyespot body) is highly variable (Nijhout, 1990), which is consistent with the present study. Moreover, Nijhout (1990) introduced "two point sources" along the midline as a part of a "toolbox" to produce diverse eyespot patterns, which is reminiscent of the pear-shaped *Calisto*-type eyespots. It is to be noted that the distortions of the pear-shaped eyespots of *Calisto*, which have two or more foci along the midline, are very different from a common distortion of single-focus eyespots, which was explained by the two-gradient model (Nijhout, 1978, 1981).

Mathematical models

In Chapter 7 of the seminal book (Nijhout, 1991) and also in the previous paper (Nijhout, 1990), two mathematical models are presented for color pattern formation, one that determines the location of the organizing centers (source formation model) and a second that determines actual eyespots (eyespot formation model). The latter model is based on a morphogen gradient model as discussed in the Introduction section of this paper, while the former is a model for determining the position of the organizing centers (Nijhout, 1990, 1991). The former model is given by reaction-diffusion equations based on the principle of "short-range activation and long-range inhibition" (Gierer and Meinhardt, 1972; Meinhardt and Gierer, 1974, 2000; Meinhardt, 1982). In this model, activator concentration becomes high along the midline. This high midline region then retracts toward the wing margin, but a few high activation points are left behind. The multiple white spots along the midline found in the posterior hindwing of *C. tasajera* are therefore compatible with this model. The activator dots will then become white spots in *C. tasajera*. However, stable emergence of the white spots with and without eyespot bodies in particular compartments—as

observed in the anterior forewing region in *C. tasajera*—is enigmatic.

Sekimura et al. (2015) recently reported successful simulation of the emergence of an eyespot organizing center in particular compartments but not in other compartments by changing boundary conditions. However, the emerging organizing centers in particular compartments may release morphogenic signals either for an eyespot body or for a white spot or both. In other words, considering the results of the present paper, what is specified in the source formation model (Nijhout, 1990, 1991) is the location of immature cells that could differentiate either (1) into a white spot organizing center, or (2) into an eyespot body organizing center (without white spot), or (3) both. It will be interesting to see whether a model similar to that proposed in Sekimura et al. (2015) can explain these various immature-cell-fate options, as observed in the anterior forewing region of *C. tasajera*. Moreover, sparse patterns such as those observed in the anterior hindwing region of *C. tasajera*, which are common in nymphalid eyespots and white spots, should also be simulated in the future.

Dll expression in eyespot organizing centers

A high *Dll* expression level is found at the center of prospective eyespots in *J. coenia* (see FIG. 4, page 238 in Brakefield et al. (1996) or Figure 6.4, page 167 in Carroll et al. (2004)). The interpretation of this fact has been to consider *Dll* as an important regulatory gene for eyespot formation (Brakefield et al., 1996; Nijhout, 1996). However, one should notice that the adult eyespots of *J. coenia* do not have a discrete white "focus" at the center. White scales are scattered along the proximal side of the eyespot. Thus, *Dll* expression appears to regulate eyespot bodies but not to specify the white area in this instance. This interpretation is likely also applicable to the case of *J. almana*, in which the largest scales are blue/black scales located at the center of the eyespot, while white scales are located proximally (see Chapter 2).

On the other hand, in the case of the forewing eyespots of *J. orithya*, which have distinct white (or strictly, bluish) focal areas; the size of the entire eyespot as well

as the size of these white foci are only weakly correlated with the *Dll* expression level (Adhikari and Otaki, 2016). In this case, *Dll* expression that regulates the size of eyespot bodies probably coincides with the expression of unknown genes that regulate the size of white areas.

Structural versus pigment-based coloration

The white coloration of white spots is structural, rather than pigment-based, in *Junonia* butterflies (Nijhout, 1980b, 1991) (see Chapter 2). Because developmental processes of structural color production and pigment synthesis would be very different, an uncoupling of the white spots (i.e., structural color expression) from the eyespot bodies (i.e., pigment production) may be reasonable. Interestingly, probably because of the different synthetic pathways, it seems that pigment synthesis and structural color expression are able to coexist in a given cell to some extent, because brownish white scales are present in the anterior hindwing region in *C. tasajera*. Furthermore, colored foci are not rare in nymphalid butterflies. A good example is the dorsal forewing eyespots of *J. orithya*, which have bluish white foci. The coexistence of structural and pigment-based coloration in focal spots certainly contributes to the diversity of "white spots" in nymphalid butterflies.

Conclusions

Eyespot body behavior and white spot behavior are different and separable, although the same cells may function to organize both in many instances. The size of white spots in adults does not necessarily reflect the degrees of organizing activity for eyespots. Because it is likely that white coloration of white scales is largely structural rather than pigment-based, the differentiation mechanism for white scales may be independent from that for black or other pigmented scales.

3.5. References

Adhikari, K., Otaki, J.M., 2016. A single-wing removal methods to assess correspondence between gene expression and phenotype in butterflies: a case of *Distal-less*. Zool. Sci. 33, 13-20.

Askew, R.R., Stafford, P.A.V.B., 2008. Butterflies of the Cayman Islands. Apollo Books, Stenstrup.

Beldade, P., Brakefield, P.M., 2002. The genetics and evo-devo of butterfly wing patterns. Nat. Rev. Genet. 3, 442-452.

Beldade, P., Brakefield, P.M., Long, A.D., 2002. Contribution of *Distal-less* to quantitative variation in butterfly eyespots. Nature 415, 315-318.

Beldade, P., French, V., Brakefield, P.M., 2008. Developmental and genetic mechanisms for evolutionary diversification of serial repeats: eyespot size in *Bicyclus anynana* butterflies. J. Exp. Zool. Mol. Dev. Evol. 310B, 191-201.

Brakefield, P.M., French, V., 1995. Eyespot development on butterfly wings: the epidermal response to damage. Dev. Biol. 168, 98-111.

Brakefield, P.M., Gates, J., Keys, D., Kesbeke, F., Wijngaarden, P.J., Monteiro, A., French, V., Carroll, S.B., 1996. Development, plasticity and evolution of butterfly eyespot patterns. Nature 384, 236-242.

Brunetti, C.R., Selegue, J.E., Monteiro, A., French, V., Brakefield, P.M., Carroll, S.B., 2001. The generation and diversification of butterfly eyespot color patterns. Curr. Biol. 11, 1578-1585.

Carroll, S.B., Gates, J., Keys, D.N., Paddock, S.W., Panganiban, G.E., Selegue, J.E., Williams, J.A., 1994. Pattern formation and eyespots determination in butterfly wings. Science 265, 109-114.

Carroll, S.B., Grenier, J.K., Weatherbee, S.D., 2004. From DNA to Diversity. Molecular Genetics and the Evolution of Animal Design. 2nd ed, Wiley-Blackwell, Oxford.

Dhungel, B., Otaki, J.M., 2009. Local pharmacological effects of tungstate on the color-pattern determination of butterfly wings: a possible relationship between the eyespot and parafocal element. Zool. Sci. 26, 758-764.

Dhungel, B., Otaki, J.M., 2013. Morphometric analysis of nymphalid butterfly wings: number, size and arrangement of scales, and their implications for tissue-size determination. Entomol. Sci. 17, 207-218.

Dhungel, B., Ohno, Y., Matayoshi, R., Otaki, J.M., 2013. Baculovirus-mediated gene transfer in butterfly wings *in vivo*: an efficient expression system with an anti-gp64 antibody. BMC Biotechnol. 13, 27.

Dhungel, B., Ohno, Y., Matayoshi, R., Iwasaki, M., Taira, W., Adhikari, K., Gurung, R., Otaki, J.M., 2016. Distal-less induces elemental color patterns in *Junonia* butterfly wings. Zool. Lett. 2, 4.

French, V., Brakefield, P.M., 1992. The development of eyespot patterns on butterfly wings: morphogen sources or sinks? Development 116, 103-109.

French, V., Brakefield, P.M., 1995. Eyespot development on butterfly wings: the focal signal. Dev. Biol. 168, 112-123.

Gierer, A., Meinhardt, H., 1972. A theory of biological pattern formation. Kybernetik 12, 30-39.

González, F.L., Schwartz, A., Wetherbee, D.K., 1991. A new species of Calisto (Lepidoptera: Satyridae) of the lyceia complex on Hispaniola. Milwaukee Public Mus. Contr. Biol. Geol. 80, 1-8.

Hedges, S.B., Johnson, K., 1994. *Calisto tasajera* in the Hispaniolan Cordillera Central (Lepidoptera: Nymphalidae: Satyrinae). Tropical Lepidoptera 5, 93-94.

Henke, K., 1946. Ueber die verschiendenen Zellteilungsvorgänge in der Entwicklung des beschuppten Flügelepithelis der Mehlmotte *Ephestina kühniella* Z. Biol. Zentralbl. 65, 120-135. (in German)

Hiyama, A., Taira, W., Otaki, J.M., 2012. Color-pattern evolution in response to environmental stress in butterflies. Front. Genet. 3, 15.

Keys, D.N., Lewis, D.L., Selegue, J.E., Pearson, B.J., Goodrich, L.V., Johnson, R.L., Gates, J., Scott, M.P., Carroll, S.B., 1999. Recruitment of a *hedgehog* regulatory circuit in butterfly eyespot evolution. Science 283, 532-534.

Kusaba, K., Otaki, J.M., 2009. Positional dependence of scale size and shape in butterfly wings: wing-wide phenotypic coordination of color-pattern elements and background. J. Insect Physiol. 55, 174-182.

Mahdi, S.H.A, Gima, S., Tomita, Y., Yamasaki, H., Otaki, J.M., 2010. Physiological characterization of the cold-shock-induced humoral factor for wing color-pattern changes in butterflies. J. Insect Physiol. 56, 1022-1031.

Mahdi, S.H.A., Yamasaki, H., Otaki, J.M., 2011. Heat-shock-induced color-pattern changes of the blue pansy butterfly *Junonia orithya*: Physiological and evolutionary implications. J. Therm. Biol. 36, 312-321.

Matos-Maraví, P., Águila, R.N., Peña, C., Miller, J.Y., Sourakov, A., Wahlberg, N., 2014. Causes of endemic radiation in the Caribbean: evidence from the historical biogeography and diversification of the butterfly genus *Calisto* (Nymphalidae: Satyrinae: Satyrini). BMC Evol. Biol. 14, 199.

Mayer, A.G., 1896. The development of the wing scales and their pigment in butterflies and moths. Bull. Mus. Comp. Zoöl. Harvard College XXIX (5), 219-236.

Meinhardt, H., 1982. Models of biological pattern formation. Academic Press, London

Meinhardt, H., Gierer, A., 1974. Applications of a theory of biological pattern formation based on lateral inhibition. J. Cell Sci. 15, 321-346.

Meinhardt, H., Gierer, A., 2000. Pattern formation by local self-activation and lateral inhibition. BioEssays 22, 753-760.

Miller, J.Y., Miller, L.D., 2001. The biogeography of the West Indian butterflies (Lepidoptera): An application of a vicariance/dispersalist model. In: “Biogeography of the West Indies: Patterns and Perspectives” 2nd ed, Ed by CA Woods, FE Sergile, CRC Press, Boca Raton, pp 127-155.

Monteiro, A., Chen, B., Ramos, D., Oliver, J.C., Tong, X., Guo, M., Wang, W-K., Fazzino, L., Kamal, F., 2013. *Distal-less* regulates eyespot patterns and melanization in *Bicyclus* butterflies. J. Exp. Zool. B Mol. Dev. Evol. 320, 321-331.

Monteiro, A., French, V., Smit, G., Brakefield, P.M., Metz, J.A., 2001. Butterfly eyespot patterns: evidence for specification by a morphogen diffusion gradient. Acta Biotheor. 49, 77-88.

Monteiro, A., Glaser, G., Stockslager, S., Glansdorp, N., Ramos, D., 2006. Comparative insights into questions of lepidopteran wing pattern homology. BMC Dev. Biol. 6, 52.

Nijhout, H.F., 1978. Wing pattern formation in lepidoptera: a model. J. Exp. Zool. 206, 119-136.

Nijhout, H.F., 1980a. Pattern formation on lepidopteran wings: Determination of an eyespot. Dev. Biol. 80, 267-274.

Nijhout, H.F., 1980b. Ontogeny of the color pattern on the wings of *Precis coenia* (Lepidoptera: Nymphalidae). Dev. Biol. 80, 275-288.

Nijhout HF (1981) The color patterns of butterflies and moths. Sci Am 254: 145-151.

Nijhout, H.F., 1984. Colour pattern modification by coldshock in Lepidoptera. J. Embryol. Exp. Morphol. 81, 287-305.

Nijhout, H.F., 1985. Cautery-induced colour patterns in *Precis coenia* (Lepidoptera: Nymphalidae). J. Embryol. Exp. Morphol. 86, 191-203.

Nijhout, H.F., 1990. A comprehensive model for color pattern formation in butterflies. Proc. R. Soc. London B. 239, 81-113.

Nijhout, H.F., 1991. The Development and Evolution of Butterfly Wing Patterns. Smithsonian Institution Press, Washington

Nijhout, H.F., 1994. Genes on the wing. Science 265, 44-45.

Nijhout, H.F., 1996. Focus on butterfly eyespot development. Nature 384, 209-210.

Nijhout, H.F., 2001. Elements of butterfly wing patterns. J. Exp. Zool. 291, 213-225.

Ohno, Y., Otaki, J.M., 2015a. Live cell imaging of butterfly pupal and larval wings *in vivo*. PLoS ONE 10, e0128332.

Ohno, Y., Otaki, J.M., 2015b. Spontaneous long-range calcium waves in developing butterfly wings. BMC Dev. Biol. 15, 17.

Otaki, J.M., 1998. Color-pattern modifications of butterfly wings induced by transfusion and oxyanions. J. Insect Physiol. 44, 1181-1190.

Otaki, J.M., 2007. Reversed type of color-pattern modifications of butterfly wings: a physiological mechanisms of wing-wide color-pattern determination. J. Insect Physiol. 53, 526-537.

Otaki, J.M., 2008a. Physiologically induced color-pattern changes in butterfly wings: mechanistic and evolutionary implications. J. Insect Physiol. 54, 1099-1112.

Otaki, J.M., 2008b. Phenotypic plasticity of wing color patterns revealed by temperature and chemical applications in a nymphalid butterfly *Vanessa indica*. J. Therm. Biol. 33, 128-139.

Otaki, J.M., 2009. Color-pattern analysis of parafocal elements in butterfly wings. Entomol. Sci. 12, 74-83.

Otaki, J.M., 2011a. Color-pattern analysis of eyespots in butterfly wings: a critical examination of morphogen gradient models. Zool. Sci. 28, 403-413.

Otaki, J.M., 2011b. Artificially induced changes of butterfly wing colour patterns: dynamic signal interactions in eyespot development. Sci. Rep. 1, 111.

Otaki, J.M., 2011c. Generation of butterfly wing eyespot patterns: a model for morphological determination of eyespot and parafocal element. Zool. Sci. 28, 817-827.

Otaki, J.M., 2012a. Colour pattern analysis of nymphalid butterfly wings: Revision of the nymphalid groundplan. Zool. Sci. 29, 568-576.

Otaki, J.M., 2012b. Structural analysis of eyespots: dynamics of morphogenic signals that govern elemental positions in butterfly wings. BMC Syst. Biol. 6, 17.

Otaki, J.M., Yamamoto, H., 2004a. Species-specific color-pattern modifications of

butterfly wings. Dev. Growth. Differ. 46, 1-14.

Otaki, J.M., Yamamoto, H., 2004b. Color-pattern modifications and speciation in butterflies of the genus *Vanessa* and its related genera *Cynthia* and *Bassaris*. Zool. Sci. 21, 967-976.

Otaki, J.M., Ogasawara T., Yamamoto, H., 2005a. Morphological comparison of pupal wing cuticle patterns in butterflies. Zool. Sci. 22, 21-34.

Otaki, J.M., Ogasawara, T., Yamamoto, H., 2005b. Tungstate-induced color-pattern modifications of butterfly wings are independent of stress response and ecdysteroid effect. Zool. Sci. 22, 635-644.

Otaki, J.M., Hiyama, A., Iwata, M., Kudo, T., 2010. Phenotypic plasticity in the range-margin population of the lycaenid butterfly *Zizeeria maha*. BMC Evol. Biol. 10, 252.

Reed, R.D., Serfas, M.S., 2004. Butterfly wing pattern evolution is associated with changes in a Notch/Distal-less temporal pattern formation process. Curr. Biol. 14, 1159-1166.

Saenko, S.V., Marialva, M.S., Beldade, P., 2011. Involvement of the conserved *Hox* gene *Antennapedia* in the development and evolution of a novel trait. EvoDevo 2, 9.

Schneider, C.A., Rasband, W.S., Eliceiri, K.W., 2012. NIH Image to ImageJ: 25 years of image analysis. Nat. Methods 9, 671-675.

Sekimura, T., Venkataraman, C., Madzvamuse, A., 2015. A model for selection of eyespots on butterfly wings. PLoS One 10, e0141434.

Serfas, M.S., Carroll, S.B., 2005. Pharmacologic approaches to butterfly wing patterning: sulfated polysaccharides mimic or antagonize cold shock and alter the interpretation of gradients of positional information. Dev. Biol. 287, 416-424.

Smith, D.S., Miller, L.D., Miller, J.Y., 1994. The Butterflies of the West Indies and South Florida. Oxford University Press, Oxford

Sondhi, K.H., 1963. The biological foundations of animal patterns. Q. Rev. Biol. 38, 289-327.

Sourakov, A., Zakharov, E.V., 2011. “Darwin’s butterflies”? DNA barcoding and the radiation of the endemic Caribbean butterfly genus *Calisto* (Lepidoptera, Nymphalidae, Satyrinae). Comp. Cytogenet. 5, 191-210.

Taira, W., Kinjo, S., Otaki, J.M., 2015. The marginal band system in the nymphalid butterfly wings. Zool. Sci. 32, 38-46.

Taira, W., Otaki, J.M., 2016. Butterfly wings are three-dimensional: pupal cuticle focal spots and their associated structures in *Junonia* butterflies. PLoS One 11, e0146348.

Tong, X., Lindemann, A., Monteiro, A., 2012. Differential involvement of Hedgehog signaling in butterfly wing and eyespot development. PLoS ONE 7, e51087.

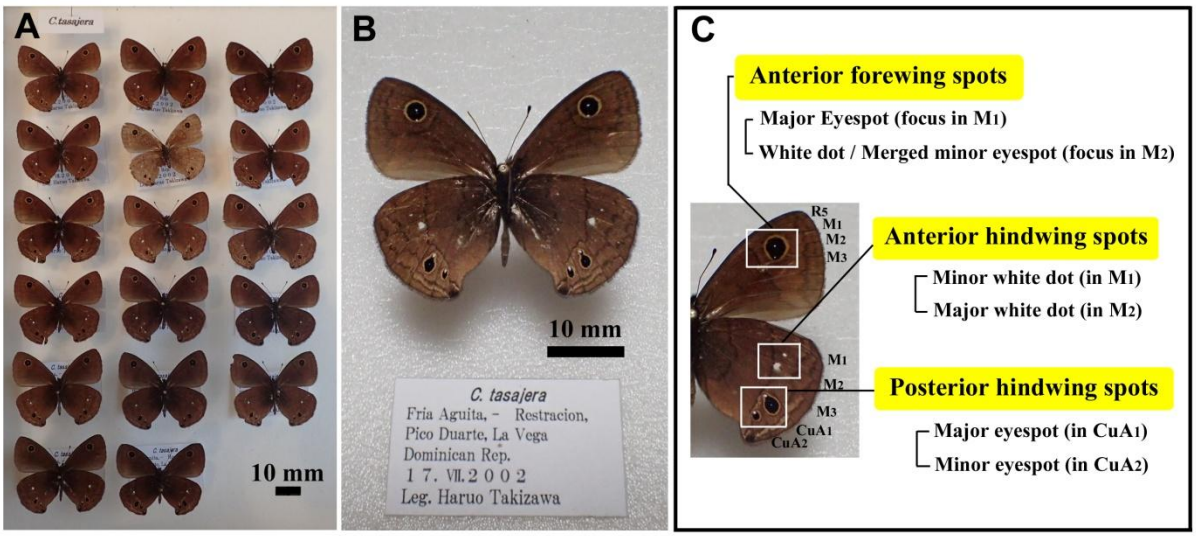

Fig. 3-1. Specimens of *Calisto tasajera*. (A) 17 specimens that were analyzed in this study; **(B)** A specimen (one of 17) showing the ventral side; **(C)** Three regions of analysis on the ventral wings.

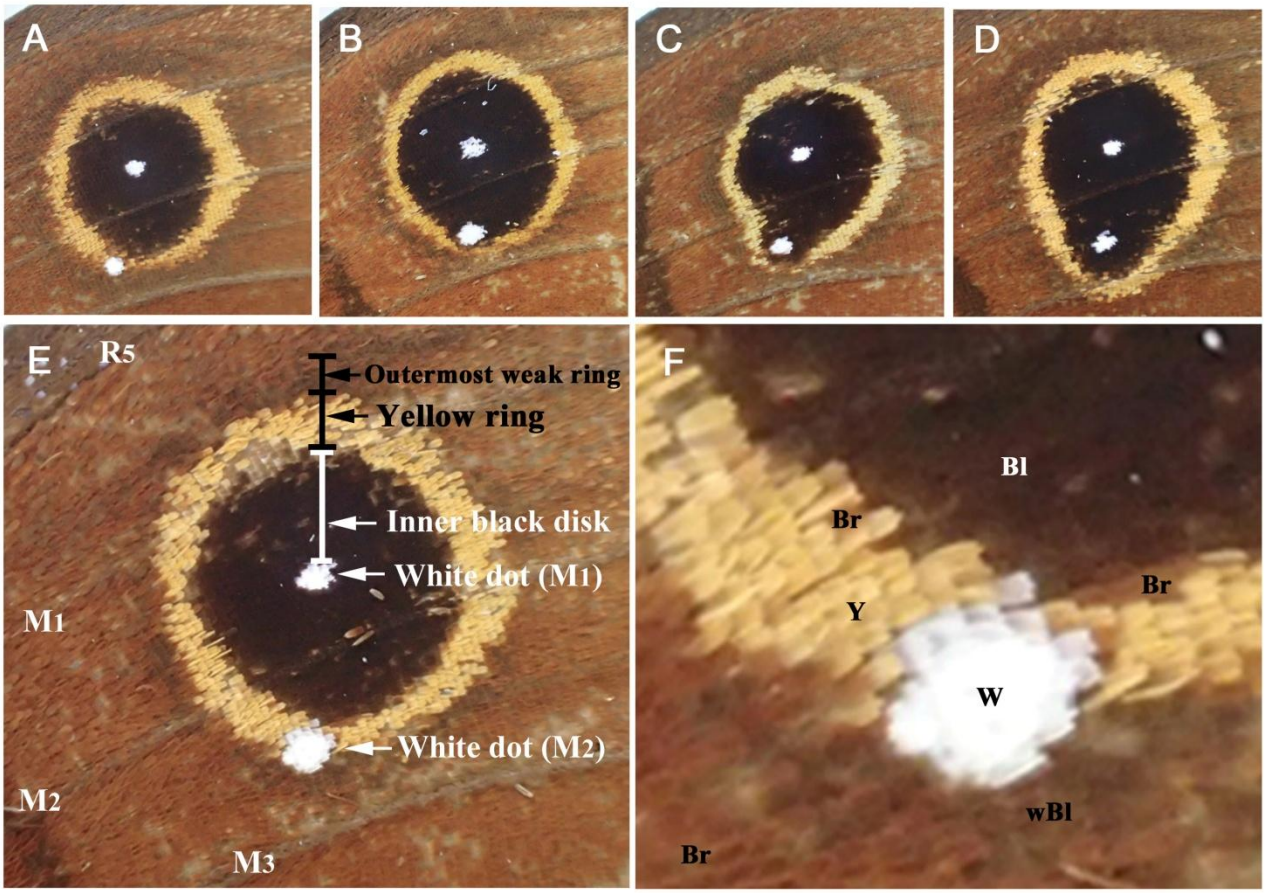

Fig. 3-2. Anterior forewing spots. (A-D) Variations of spots. **(E)** High magnification image of the anterior forewing spots with annotations. Four wing veins, R_5, M_1, M_2, and M_3, are marked. **(F)** Higher magnification image of E. Scale colors are indicated as follows: W (white), Bl (black), Y (yellow), Br (brown), and wBl (weak black).

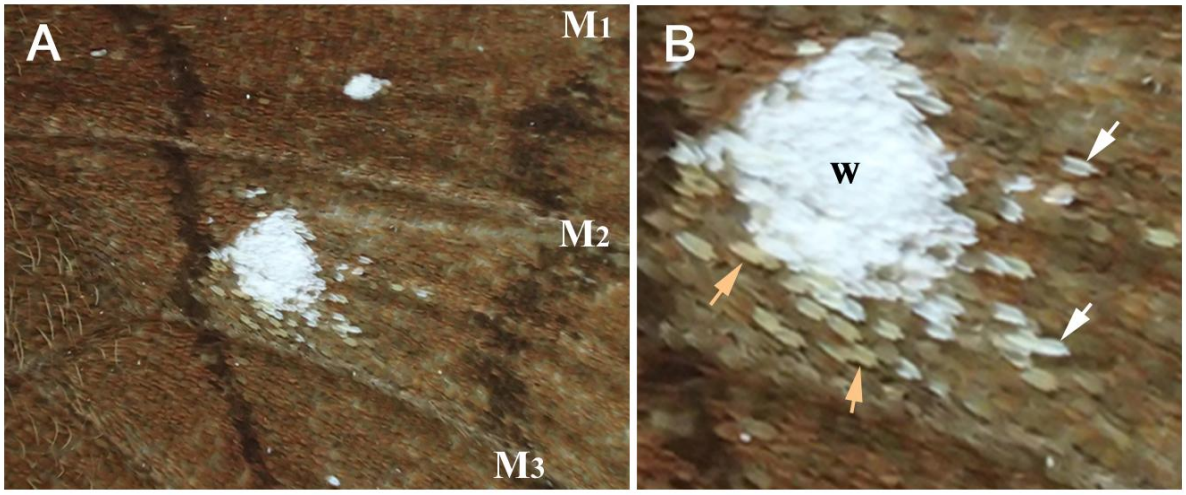

Fig. 3-3. Anterior hindwing spots. (A) White spots in the M_1 and M_2 compartments. Three wing veins, M_1, M_2, and M_3, are marked. **(B)** High magnification of the white spot in the M_2 compartment. The sparse pattern can be clearly observed. Some sparse scales are white (white arrows), and other sparse scales are brown (light brown arrows).

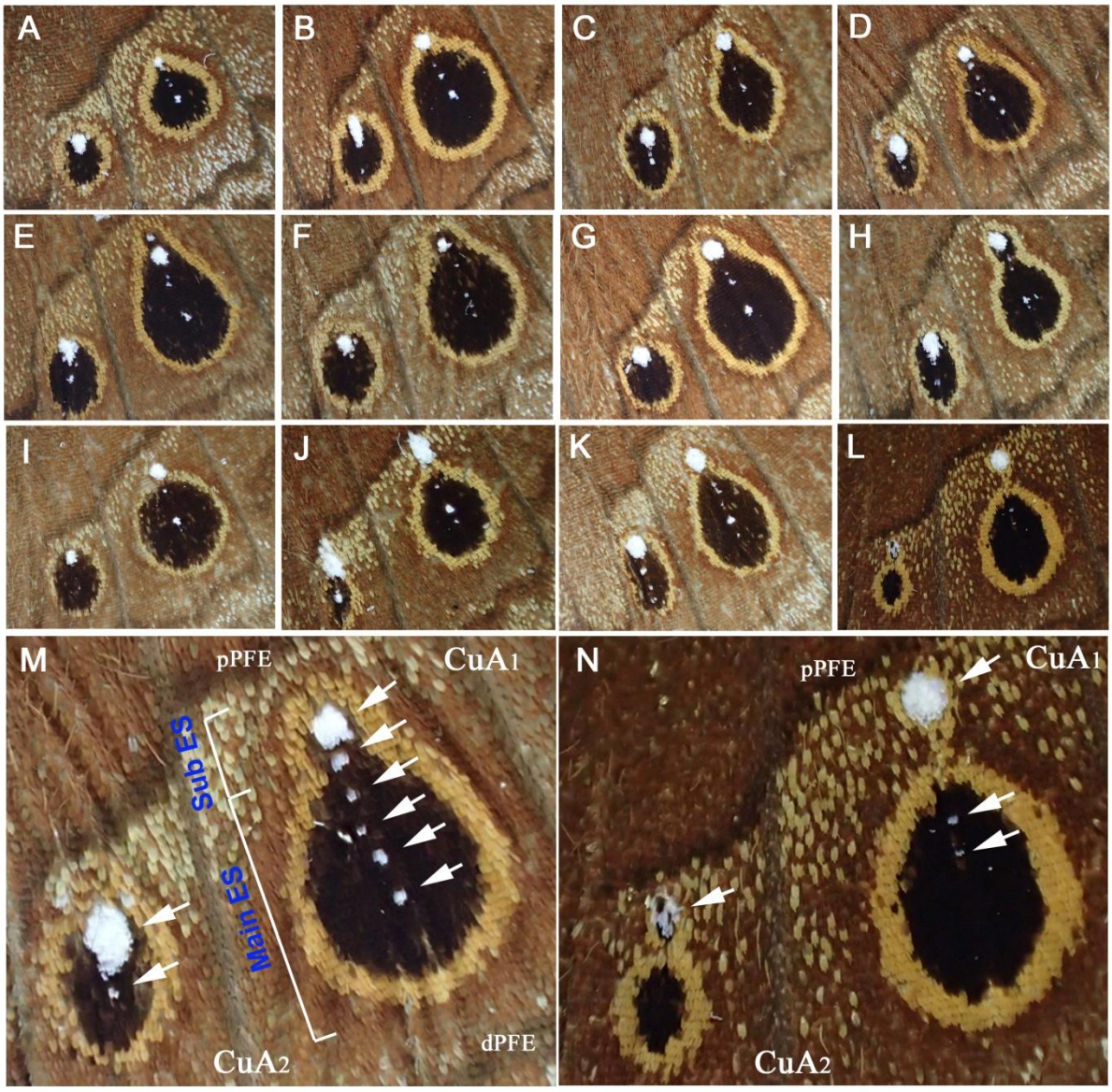

Fig. 3-4. Posterior hindwing spots. (A-L) Variations of spots. **(M)** An example of a high magnification image with annotations. Arrows indicate white dots along the midline. The white dots are located within the merged eyespots. The whole structure may be called a pear-shaped eyespot. The sub eyespot (ES) and the main ES are distinctly named. Wing veins CuA_1 and CuA_2 are marked, and parafocal elements, pPFE (proximal PFE) and dPFE (distal PFE) are also indicated (also in N). **(N)** Another example of a high magnification image. Arrows indicate white dots along the midline. The large white dots are located outside the eyespots in both compartments.

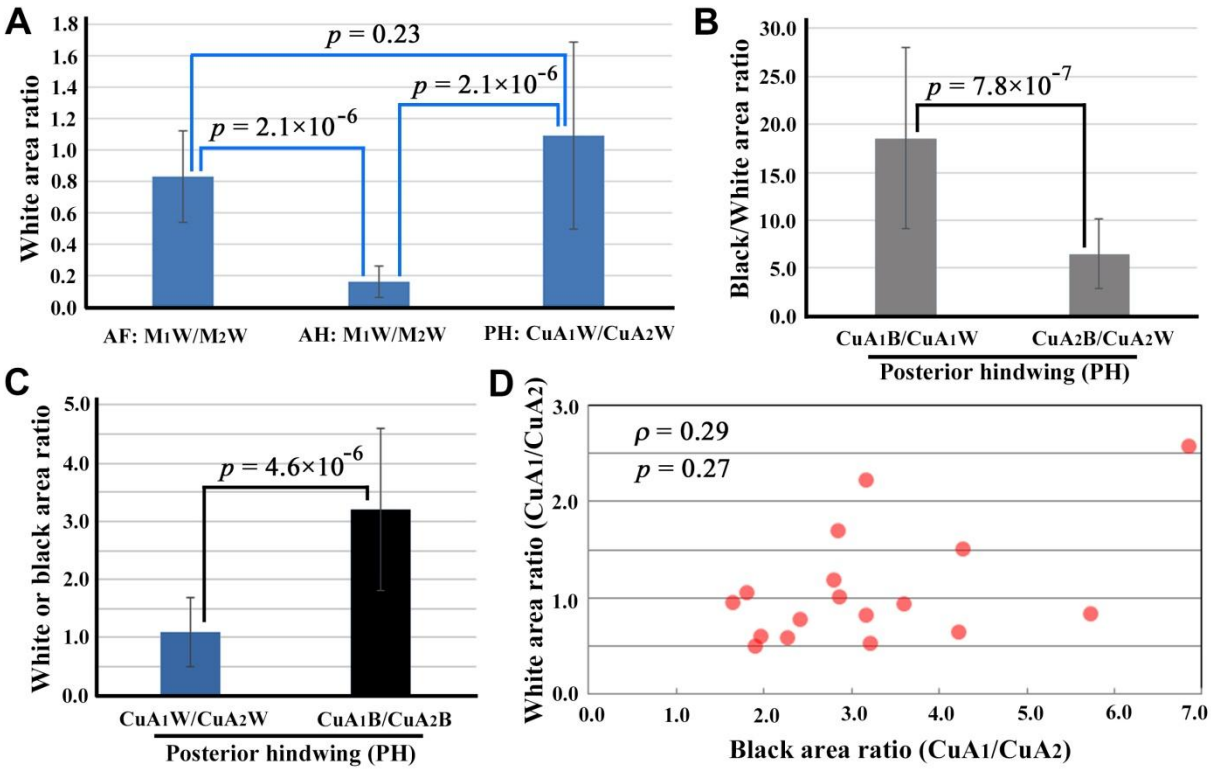

Fig. 3-5. Quantitative comparisons of area ratios in the anterior forewings (AF), anterior hindwings (AH), and posterior hindwings (PH). Compartmental names with W (white) or B (black) at the end are indicated. **(A)** White area ratios among three wing regions. **(B)** Black/white ratios in the posterior hindwing region. **(C)** White area ratio versus black area ratio in the posterior hindwing region. **(D)** Scatter plot of black area ratio versus white area ratio.

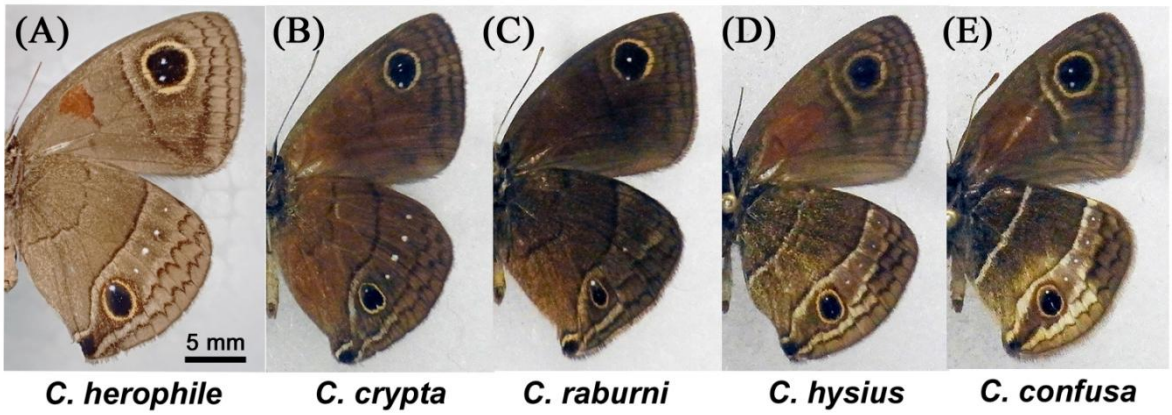

Fig. 3-6. Additional five *Calisto* species. Ventral sides are shown. Images are adjusted so that individuals appear at similar sizes. **(A)** *C. herophile*. Scale bar: 5 mm. This scale bar is not applicable to other panels. **(B)** *C. crypta*. **(C)** *C. raburni*. **(D)** *C. hysius*. **(E)** *C. confusa*.

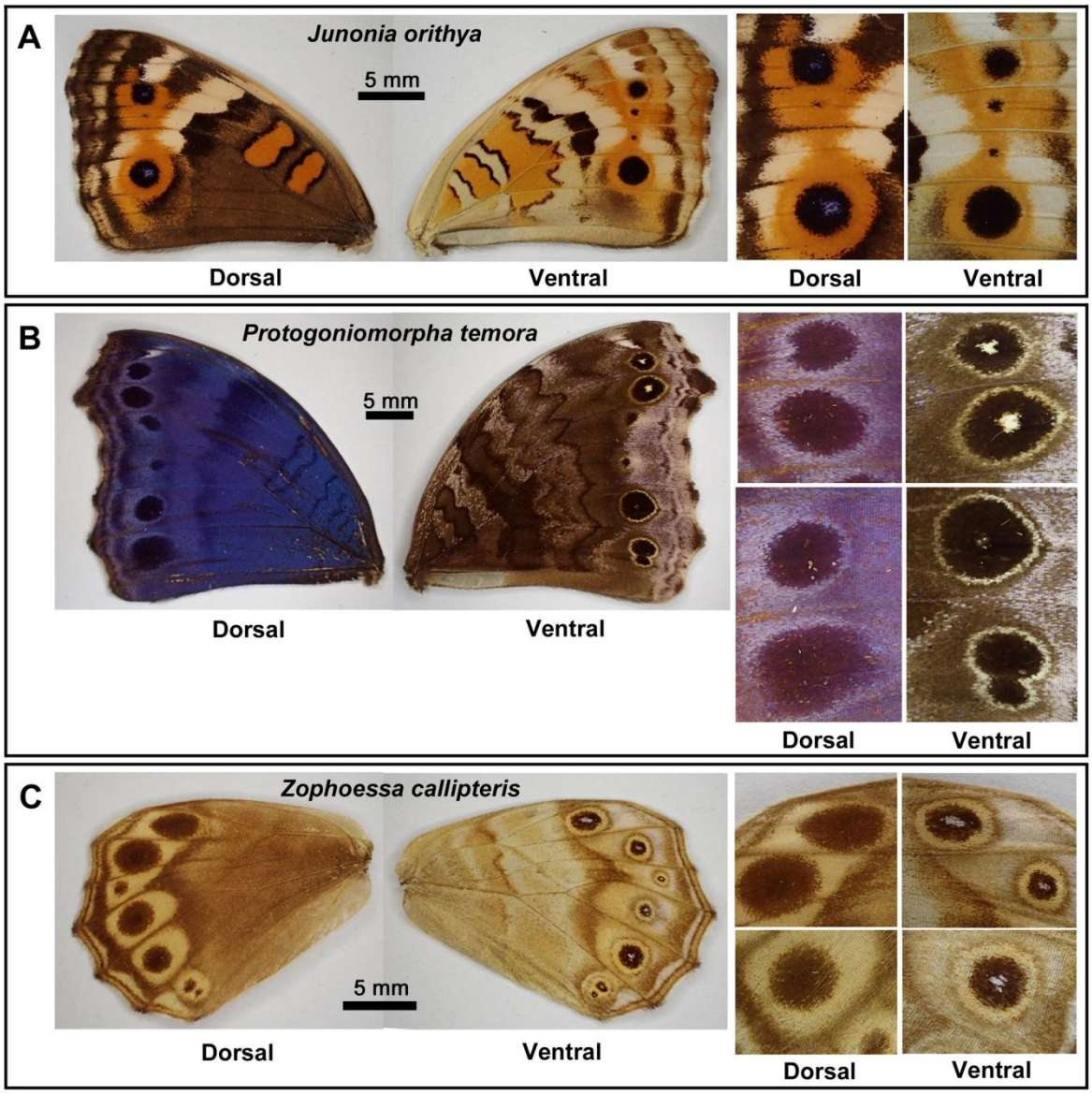

Fig. 3-7. Examples of "focus-less" eyespots. The dorsal and ventral sides are shown. Enlarged eyespot images are shown at the right side. Scale bars: 5 mm. **(A)** *J. orithya*. **(B)** *Protogoniomorpha temora*. **(C)** *Zophoessa callipteris*.

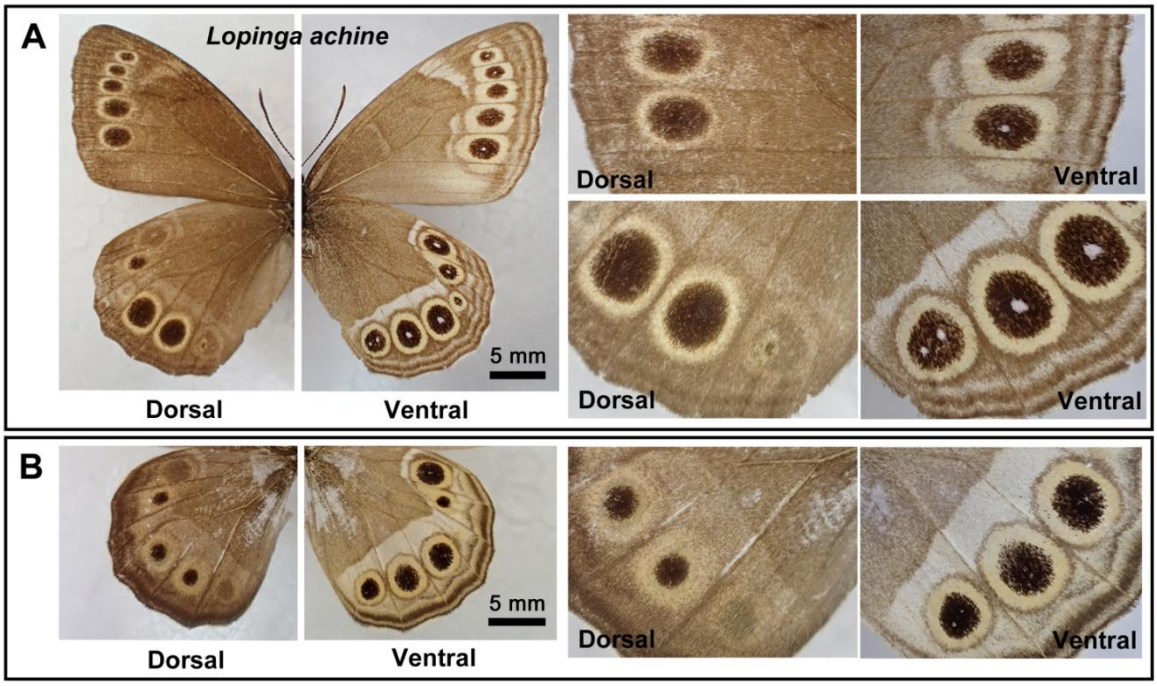

Fig. 3-8. Eyespots of *Lopinga achine*. Scale bars: 5 mm. **(A)** Normal wings. Most eyespots (but not all) on the ventral side have a white spot, but those on the dorsal side do not. **(B)** A mutant wing. The ventral eyespots have no or very small white spots.

General Discussion

A pupal case in some butterflies such as *J. orithya* and *J. almana* is too dark and thick to observe pupal wing development and coloration in real time and to stain a pupal wing tissue with a dye. Curling up a pupal forewing can expose a ventral forewing and dorsal hind wing. This operation allows the observation of living pupal wing development and the *in vio* staining of pupal wing tissues. In the tissues and epithelial cells of the *J. orithya* dorsal hindwings, the techniques have clarified the richness of mitochondria, intracellular networks of endoplasmic reticulum, the denseness of epidermal feet between pupal epithelial cells, and the propagation of intracellular calcium signaling over long distances (Ohno and Otaki, 2015a,b). Although it remains unclear how the distribution patterns of these organisms, the cellular morphology and the calcium signaling in wing tissues contribute to wing development and coloration, these results are important because of the lack of morphological and physiological information on pupal wing tissues. In the future, comparison of quantitative analyses in morphological features and calcium signaling between other butterflies and between their various developmental stages will reveal how the color pattern formation and cellular arrangement of butterfly wings occur. In addition, the long-term observation of living wing tissues during the pupal stage is useful for deciding the sites to apply physical damage on the pupal wings (Fig. 4-1 and 4-2). The real-time imaging of pupal wings provides us with the information on when, where and what color patterns appear on the surface of pupal wings.

Damage-induced color pattern changes in butterfly wings caused the changes of scale size and scale shape (Fig. 2-8 and 2-9). In addition, in *B. anyana*, correlation between scale color and microstructure (the density of cross rib) has been reported (Janssen et al., 2001). These results support the idea that the organizing signals for

color pattern formation on butterfly wings have an effect not only on pigmentation but also on the size, shape and microstructure of butterfly scales.

On butterfly wings, there are scent scales (odorant scales), which release sex pheromones. The scale morphology and/or its pheromones for mating behaviors have been studied in some butterflies such as the genus *Pieris* (Barth, 1949; Bergström and Lundgren, 1973; Hayashi et al., 1978; Honda and Kawatoko, 1982; Kuwahara, 1979; Yata et al., 1986), *B. anyana* (Nymphalidae) (Nieberding, 2008) and *Zizeeria maha* (Lycaenidae) (Wago, 1978). As mentioned above, because color changes in scales can affect various factors, it is likely that wing color pattern changes induced by environmental stress have an effect on odorants of scent scales. If this is true, such odorant changes could result in an alteration of butterfly mating behavior that eventually leads to color pattern evolution or speciation. It is generally known that chemical odorants of scent scales in some butterflies activate their courtship or mating behavior **(**Nieberding, 2008; Pivnick, 1992; Wago, 1978**)**. However, there is neither direct nor indirect evidence to support the color-odor relationship in scales.

Hiyama (2015) reported that changes in the mate choice by *Z. maha* males with wing color pattern modifications induced by temperature shock (cold shock). The mate-choice experiment showed a significant difference between non-modified and modified males (Fig. 4-3) in their mate preferences for different color-pattern females (non-modified and modified females) and suggested that the modified males are attracted by similar modified females (Hiyama, 2015). Interestingly, the above-mentioned modification type that can be induced by cold shock is morphologically similar to a certain modification type (outward type) observed in the field in summer (Fig. 4-3) (Otaki et al., 2010). Moreover, artificial selection for the outward type induced by cold shock for ten generations demonstrated that the outward type starts to appear without cold shock treatment after fifth generations (Otaki et al., 2010). This result supported that the outward type found in the field in summer result from the ongoing process of genetic assimilation (Buckley et al., 2010; Otaki et al.,

2010).

On the basis of these results and speculations, it is reasonable to think that the color pattern modifications induced by exogenous stimulus play an important role in evolution and speciation not only through visual information but also through olfactory information. A further study on the relation between the color modification and the behavioral alteration will clarify how butterfly wing color patterns evolve and have their speciation occurs via phenotypic plasticity such as the color pattern modification of *Z. maha*.

As can be seen from the above description and Chapter 1-3, classical morphological approaches (e.g., size, shape and color) are also necessary to understand the development and evolution of living things although in recent years many researchers are apt to use molecular biological approaches (e.g., gene expression analysis). By linking these two approaches, we can understand how molecular-level dynamics and variation reflect morphorogical traits. Furthermore, to elucidate the common mechanism of color pattern formation that is widely used in butterflies, in the future, the experiment based on these two approaches should be carried out using other butterflies (e.g., *Z. maha*) other than Nymphalidae.

References

Barth, R., 1949. Vergleichend morphologische studien über die duftschuppen der pieriden *Pieris brassicae* and *Pieris rapae* und der satyrine *Coenonympha pamphilus*. Zoologische Jahrbücher (Abteilung für Anatomie und Ontogenie der Tiere) 70, 397-426.

Bergström, G., Lundgren, L., 1973. Androconial secretion of three species of butterflies of the genous *Pieris* (Lep., Pierdae). Zoom Supplement 1, 67-75.

Buckley, J., Bridle, J.R., Promiankowski, A., 2010. Novel variation associated with species expansion. BMC Evol. Biol. 10, 382.

Hayashi, N., Kuwahara, Y., Komae, H., 1978. The scent scale substances of male *Pieris* butterfies (*Pieris melete* and *Pieris napi*). Experientia 34, 684-685.

Hiyama, A., 2015. Causal factors for the outbreak of color-pattern modified individuals in the northern range-margin populations of the pale grass blue butterfly *Zizeeria maha* (Lepidoptera: Lycaenidae). Doctral Thesis in University of the Ryukyus. (In Japanese).

Hiyama, A., Taira, W., Otaki, J.M., 2012. Color-pattern evolution in response to environmental stress in butterflies. Front. Genet. 3, 15.

Honda, K., Kawatoko, M., 1982. Exocrine substances of the white cabbage butterfly, *Pieris rapae crucivora* (Lepidoptra: Pieridae) Appl. Entomol. Zool. 17, 325-331.

Jansen, J.M., Monteiro, A., Brakefield, P.M., 2001. Correlations between scale structure and pigmentation in butterfly wings. Evol. Dev. 3, 415-423.

Kuwahara, Y., 1979. Scent scale substance of male *Pieris melete* MENETRIES (Pieridae: Lepidoptera). Appl. Entomol. and Zool. 14, 350-355.

Nieberding, C.M., Vos, H.D., Schneider, M.V., Lassance J., Estramil, N., Andersson, J., Bång, J., Hedenstrom, E., Löfstedt, C., Brakefield, P.M., 2008. The male sex pheromone of the butterfly *Bicyclus anyana*: Towards an evolutionary analysis. PLoS ONE 3, e2751.

Ohno, Y., Otaki, J.M., 2015a. Live cell imaging of butterfly pupal and larval wings *in vivo*. PLoS ONE 10, e0128332.

Ohno, Y., Otaki, J.M., 2015b. Spontaneous long-range calcium waves in developing butterfly wings. BMC Dev. Biol. 15, 17.

Otaki, J.M., Hiyama, A., Iwata, M., Kudo, T., 2010. Phenotypic plasticity in the range-margin population of the lycaenid butterfly *Zizeeria maha*. BMC Evol. Biol. 10, 252.

Pivnick, K.A., Lavoie, D.J., McNeil, J.N., 1992. The role of the androconia in the mating behaviour of the European skipper, *Thymelicus lienola*, and evidence for a male sex pheromone. Physiol. Entomol. 17, 260-268.

Wago, H., 1978. Studies on the mating behavior of the pale grass blue, *Zizeeria maha argia* (Lepidoptera: Lycaenidae) IV. Experimental analyses of the role of the male odor in male-male interactions. Zool. Mag. 87, 240-246.

Yata, O., Abe, M., Nakai, M., 1986. Relationship between androconial scale and the male wing odour in *Pieris melete Ménétriés* (Lepidoptera, Pieridae). Sieboldia 5, 131-136.

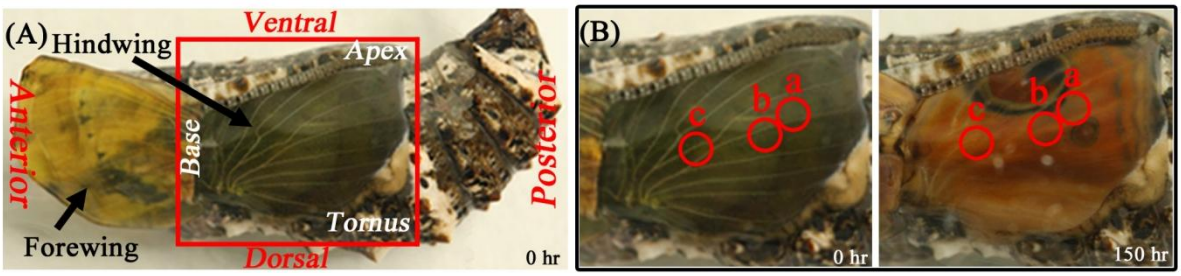

Fig. 4-1. Elemental positions of the dorsal hindwing in the *J. almana* pupal wing tissue. The postpupation time is indicated in each panel. **(A)** A pupal hind wing immediately after the operation of curling up the pupal forewing. **(B)** Higher magnification of the boxed region shown in (A). Circles a-b indicates the physical damage sites shown in **Fig. 2-9A, B and C**, respectively.

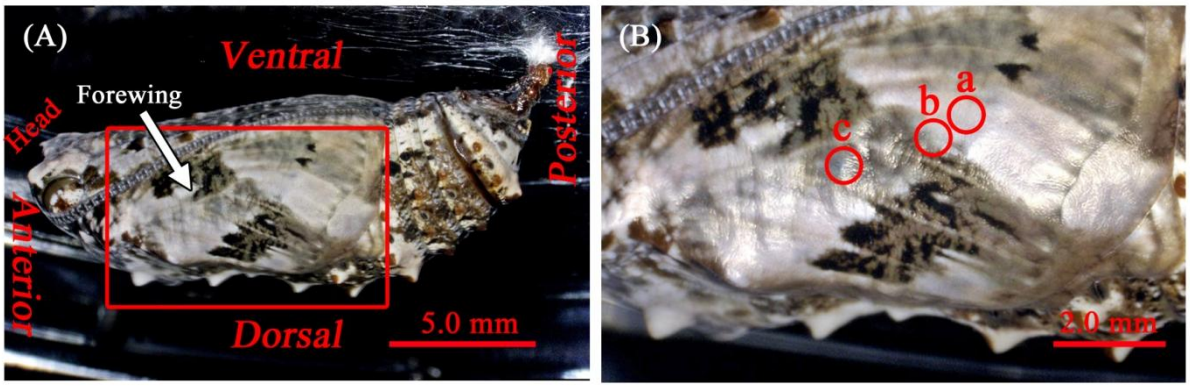

Fig. 4-2. *J. almana* pupa. (A) Pupal forewing. **(B)** Higher magnification of the boxed region shown in (A). Circles a-b on the pupal forewing indicates the physical damage sites shown in **Fig. 2-9A, B and C**, respectively.

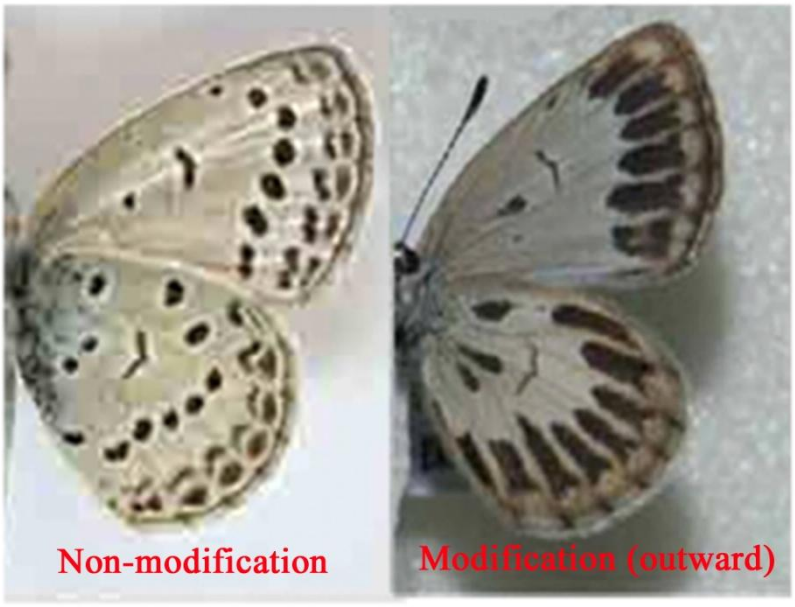

Fig. 4-3. Modified individual in *Z. maha*. Non-modified individual (left) and modified individual (right). Left and right panels were modified from Hiyama et al. (2012) and Otaki et al. (2010), respectively.